

Vertical Vibration of Mass Timber Floors Subjected to Seismic and Footfall Loading

Davis Wright

A thesis

submitted in partial fulfillment of the
requirements for the degree of

Masters of Science in Civil Engineering

University of Washington

2023

Committee:

Jeffrey W. Berman, Chair

Richard Wiebe

Program Authorized to Offer Degree:
Civil and Environmental Engineering

©Copyright 2023

Davis Wright

University of Washington

Abstract

Vertical Vibration of Mass Timber Floors Subjected to Seismic and Footfall Loading

Davis Wright

Chair of the Supervisory Committee:
Jeffrey W. Berman
Civil and Environmental Engineering

With the continued development of mass timber products, use of these products in tall buildings has become more feasible. Previous research has shown that mass timber floors perform well under footfall loading, but no research has been conducted on the response of mass timber floors when subjected to vertical seismic ground motions.

This study aimed to compare the results of numerical models of mass timber floors with the results of the NHERI Tallwood Project's 10-story test, as well as analyze the performance of the mass timber floors when subjected to vertical ground motions during the NHERI Tallwood Project's 10-story test. The numerical models were developed using methods for modeling the vibration in floors due to human-induced footfall loading. The developed numerical models did not prove to produce accurate results due to various factors including, but not limited to, influence from horizontal seismic motions, unknown damping coefficients of the mass timber floors, and high-frequency noise within the data collection.

TABLE OF CONTENTS

	Page
List of Figures	iv
List of Tables	vii
Chapter 1: Introduction	1
1.1 Overview	1
1.2 NHERI TallWood Project	1
1.3 Objectives of Research	2
1.4 Organization of Thesis	2
Chapter 2: Literature Review	4
2.1 Introduction	4
2.2 Mass Timber as a Building Material	4
2.3 Previous Research on Vertical Vibration of Mass Timber Floors	10
2.4 Vertical Vibration Design Guides	23
2.5 Conclusions and Research Needs	26
Chapter 3: Specimen Design and Construction	27
3.1 Introduction	27
3.2 Beam and Gravity Column Design	27
3.3 Floor Design	29
3.4 Diaphragm Construction	42
3.5 Design of Other Building Elements	45
Chapter 4: Instrumentation and Experiment Protocol	47
4.1 Introduction	47
4.2 Instrumentation	47

4.3	Heel Drop Testing	49
4.4	Ground Motions for Seismic Testing	50
Chapter 5:	Numerical Model Development	53
5.1	Introduction	53
5.2	U.S. Mass Timber Floor Vibration Design Guide Recommendations	53
5.3	Isotropic Shell Element Model Development	54
5.4	Layered Shell Element Model Development	65
5.5	10-Story Model Development	76
5.6	Preliminary Analysis Results	77
Chapter 6:	Numerical Model Frequency Calibration	84
6.1	Introduction	84
6.2	Comparison of Footfall and Numerical Model Natural Frequencies	84
6.3	Redistributing Wing Plate Mass	85
6.4	Length Variation Adjustment	87
6.5	Stiffness Adjustments	88
6.6	Exterior Wall Springs	89
6.7	Updated Frequencies	89
Chapter 7:	Data Analysis	91
7.1	Introduction	91
7.2	Data Processing	91
7.3	SAP Model and Data Comparisons	91
7.4	Vertical Response Spectra for Horizontal Ground Motions	101
7.5	Vertical Response Spectra Ratios	114
7.6	Fragility Curve Development	119
Chapter 8:	Summary and Conclusions	122
8.1	Summary	122
8.2	Conclusions	123
8.3	Recommendations for Future Work	124
References	126

Appendix A: 10-Story Test Detailed Drawings	130
Appendix B: Nonstructural Wall Location Drawings	169
Appendix C: 45° Plots	176

LIST OF FIGURES

Figure Number	Page
2.1 CLT Panel Configuration [Karacabeyli and Douglas, 2013]	5
2.2 Straight Glulam Beam [How et al., 2016]	6
2.3 GLT Floor Panel	7
2.4 Nailing Pattern of NLT [Werner, 1997]	8
2.5 Configuration of DLT [StructureCraft, 2021]	8
2.6 Details of MPP [Soti et al., 2021]. Each panel has 7 layers (5 layers in the long-ply and 2 in the cross-ply direction).	10
2.7 CLT Laboratory Setup [Jarnerö et al., 2015]	11
2.8 <i>In Situ</i> Floor Dimensions and Shaker Location [Jarnerö et al., 2015]	12
2.9 <i>In Situ</i> Modes, Frequencies, and Damping Ratios [Jarnerö et al., 2015]	13
2.10 Running Footfall Loads [Huang et al., 2020]	14
2.11 Comparison of Numerically Modelled and Measured Vertical Acceleration [Huang et al., 2020]	15
2.12 Single Surface Spline Connection: a) Actual, b) Equivalent Elastic Strip. [Huang et al., 2020]	18
2.13 Mode Shapes and Associated Natural Frequencies of 6 m × 6 m Square CLT Floor (One-Way Boundary), Considering Different Inter-Panel Connection Types [Milojević et al., 2023]	19
2.14 Mode Shapes and Associated Natural Frequencies of 6 m × 6 m Square CLT Floor (Two-Way Boundary), Considering Different Inter-Panel Connection Types [Milojević et al., 2023]	20
2.15 Mode Shapes and Associated Natural Frequencies of 6 m × 6 m Square CLT Floor (One-Way Boundary), Considering Different Inter-Panel Connection Types [Milojević et al., 2023]	21
2.16 Mode Shapes and Associated Natural Frequencies of 6 m × 6 m Square CLT Floor (Two-Way Boundary), Considering Different Inter-Panel Connection Types [Milojević et al., 2023]	21
3.1 Typical Beam and Column Plan View	28

3.2	Labeled Floor Spans	30
3.3	Weak Axis Support Angle	31
3.4	Typical CLT Layout	32
3.5	Typical GLT Layout	35
3.6	Typical NLT/DLT Layout	38
3.7	Typical VLT Layout	41
3.8	Crane Lifting Panel	43
3.9	Workers Guiding Panel Into Place	44
4.1	Possible Vertical Accelerometer Locations	48
4.2	Vertical Ground Motion Response Spectra	51
5.1	Stiffness Modifier Directions	56
5.2	Time History Function in SAP2000	59
5.3	CLT Model Before Meshing	60
5.4	CLT Model After Automatic Meshing	61
5.5	CLT Model After Manual Meshing	63
5.6	Beam to CLT Connection Detail	64
5.7	Weak Axis Cross Section in Bending	66
5.8	NLT Stress-Strain Curve	67
5.9	Simple Model Shell Element Layers	68
5.10	Cross Section Analysis Illustration	69
5.11	Multiple Layer Model Cross Section	72
5.12	Strap Distribution Floor Section Labels	74
5.13	10-Story Model	77
5.14	Cumulative Mass Participation Ratio	82
5.15	Mode Shape at 12.66 Hz	83
6.1	Area Distribution of Wing Plate Masses	86
7.1	Peak Acceleration Comparison for Ferndale MCE: 10-Story SAP Model vs Measured Data	92
7.2	Peak Acceleration Comparison for Ferndale MCE: Single-Story SAP Model vs Measured Data	93
7.3	Level 4 Measured Data vs 2% Damped SAP Models Response Spectra	95
7.4	Level 4 Measured Data vs 7% Damped SAP Models Response Spectra	96

7.5	Level 8 Measured Data vs 2% Damped SAP Models Response Spectra	97
7.6	Level 8 Measured Data vs 7% Damped SAP Models Response Spectra	98
7.7	Level 11 Measured Data vs 2% Damped SAP Models Response Spectra	99
7.8	Level 11 Measured Data vs 7% Damped SAP Models Response Spectra	100
7.9	Shake Table Vertical Response Spectra for Horizontal-Only and Low-Amplitude Vertical-Only Motions	102
7.10	Level 4 Vertical Response Spectra for Horizontal-Only and Low-Amplitude Vertical-Only Motions	103
7.11	Level 8 Vertical Response Spectra for Horizontal-Only and Low-Amplitude Vertical-Only Motions	104
7.12	Level 11 Vertical Response Spectra for Horizontal-Only and Low-Amplitude Vertical-Only Motions	105
7.13	Shake Table Vertical Response Spectra for Horizontal-Only Motions of Vary- ing Hazard Levels	106
7.14	Level 4 Vertical Response Spectra for Horizontal-Only Motions of Varying Hazard Levels	107
7.15	Level 8 Vertical Response Spectra for Horizontal-Only Motions of Varying Hazard Levels	108
7.16	Level 11 Vertical Response Spectra for Horizontal-Only Motions of Varying Hazard Levels	109
7.17	Shake Table Vertical Response Spectra for Ferndale 975	111
7.18	Level 4 Vertical Response Spectra for Ferndale 975	112
7.19	Level 8 Vertical Response Spectra for Ferndale 975	113
7.20	Level 11 Vertical Response Spectra for Ferndale 975	114
7.21	Spectral Acceleration Ratios of the COM to the Table Input for MCE Motions	115
7.22	Spectral Acceleration Ratios of the COM to the Table Input for 975 Motions	116
7.23	Spectral Acceleration Ratios of the Floor Spectra to the COM Spectra for MCE	118
7.24	Fragility Curves for Mass Timber Floors	120
C.1	Peak Acceleration Comparison for Loma Prieta MCE: 10-Story SAP Model vs Measured Data	176
C.2	Peak Acceleration Comparison for Loma Prieta MCE: Single-Story SAP Model vs Measured Data	177

LIST OF TABLES

Table Number	Page
2.1 Testing Setup [Huang et al., 2020]	16
2.2 First Three Natural Frequencies of the Floor System Under Different Testing Conditions, as Analysed Using OPENSEES Simulated Time-History Data [Huang et al., 2020]	17
2.3 SAP Modifier Equations [Breneman et al., 2021]	24
3.1 Floor Type at Each Level	29
3.2 CLT Material Properties	33
3.3 CLT Section Properties	34
3.4 GLT Material Properties	36
3.5 GLT Section Properties	37
3.6 NLT and DLT Material Properties	39
3.7 NLT and DLT Section Properties	39
3.8 VLT Section Properties	42
4.1 Accelerometer Locations by Level	49
4.2 Heel Drop Test Floor Frequencies (Hz)	50
4.3 Vertical Ground Motion Scale Factors	52
5.1 Floor Weights	55
5.2 Generic Floor Material Properties	55
5.3 Isotropic Shell Element Stiffness Modifiers	56
5.4 Model Validation Deflections (in)	57
5.5 Modal Frequency Validation	58
5.6 Simple Model Shell Element Layer Behaviors	68
5.7 Simple Layered Shell Model Deflection Validation (in)	70
5.8 Orthotropic Material Model Deflection Validation	71
5.9 Multiple Layer Model Deflection Validation	72
5.10 One-Way Mass Timber Layer Definitions	75

5.11 Preliminary Cantilever Results	79
5.12 Preliminary Span Results	80
5.13 10-Story Model Preliminary Results	81
6.1 Numerical Model Natural Frequency Comparison to Footfall Natural Frequencies	85
6.2 Frequency Increases Factors	88
6.3 Material Stiffness Adjustments	88
6.4 Exterior Wall Spring Stiffness	89
6.5 Adjusted Numerical Model Natural Frequencies Comparison to Footfall Nat- ural Frequencies	90
7.1 Sapn to COM Peak Acceleration Ratios	118
7.2 Logarithmic Mean and Deviation for Fragility Curves	119

ACKNOWLEDGMENTS

I would first like to thank my advisor, Professor Jeff Berman. Jeff's support was critical in the completion of this thesis. His guidance helped me to persevere through many road blocks along the way. I would also like to thank Professor Richard Wiebe for taking the time to serve on my committee.

I would like to thank the project team which included, but is not limited to: Professor Shiling Pei of the Colorado school of Mines; Professor John van de Lindt of Colorado State University; Professor Keri Ryan of University of Nevada Reno; Professor Tara Hutchinson of the University of California San Diego; and Reid Zimmerman of KPFF. I would also like to thank the NHERI@UCSD staff for their help in the construction process. Thank you to my fellow research students who made my time San Diego a joy.

I would not have been able to finish up my work without the encouragement of my fellow graduate students. Special thanks to Sarah Wichman for all of her help and willingness to share knowledge. Thank you to my office mates in More 235. Also, thank you to the Sundodgers. Finally – and most importantly – thank you to my family and friends for the constant support.

Chapter 1

INTRODUCTION

1.1 Overview

Mass timber floors are currently used as floor systems in many buildings. There is an increasing demand for long span, sustainable floor systems such as mass timber in retail and commercial buildings. Industry professionals have developed methods to numerically model human-induced footfall vertical vibrations in mass timber floor systems, but there is a lack of methods to model the vertical vibration response of mass timber floors to vertical seismic motion.

Damage to nonstructural elements have made up the majority of damage in recent earthquakes in the United States [ATC, 2012]. Limiting accelerations in the floor systems can help prevent nonstructural element and acceleration-sensitive equipment failure during an earthquake.

The research presented in this thesis aims to apply the methods for modeling human-induced footfall vibrations to model the vibrations induced by vertical seismic ground motions. The modeling techniques used for footfall vibrations are summarized in Section 2.4.1. The research also analyzes vertical vibration acceleration data from the NHERI TallWood Project 10-Story test to review the performance of mass timber floor systems subjected to vertical seismic ground motions.

1.2 NHERI TallWood Project

The research in this thesis compares numerical models to the 10-story building from the NHERI TallWood Project. The 10-story building was a mass timber building featuring mass timber rocking walls, nonstructural walls, steel stairs, and mass timber floors. The

NHERI TallWood project is a collaboration between multiple universities and firms from the industry. The main collaborators included: University of Washington, Colorado School of Mines, Colorado State University, University of California San Diego, University of Nevada Reno, and KPFF Consulting Engineers from Portland, Oregon.

1.3 Objectives of Research

The objectives of this research are outlined here:

- Develop numerical models of the 10-story building to capture the acceleration response of the mass timber floors due to vertical ground motion loading scenarios.
- Measure the frequencies of the 10-story building floor plans using heel drop tests.
- Calibrate the numerical models to best match the measured, human-induced frequencies.
- Analyze data from the dynamic testing of the 10-story building to check the overall performance of the mass timber floors.
- Compare the results from the 10-story test to the numerical models to check the validity of the modeling process.
- Develop fragility curves for mass timber floors subjected to vertical dynamic loading.

1.4 Organization of Thesis

The remaining chapters of this thesis are organized as follows:

- *Chapter 2* contains an overview of previous related research pertaining to the vertical vibration of mass timber floors.

- *Chapter 3* contains a summary of the design and construction of the different elements in the 10-story building. This chapter mainly focuses on the design and construction of the mass timber floors but contains a brief summary of the other building elements.
- *Chapter 4* summarizes the instrumentation employed to record the vertical data during the 10-story dynamic tests. This chapter also contains information on the experimental tests performed on the 10-story building.
- *Chapter 5* summarizes the process of developing the numerical models. This chapter also presents the initial results of the numerical models.
- *Chapter 6* summarizes the process of calibrating the numerical models to the frequencies identified by the heel drop tests.
- *Chapter 7* details the analysis of the data from the 10-story dynamic tests, compares the results to the numerical models, and provides an overview of the development of the mass timber floor fragility curves.
- *Chapter 8* provides a summary of the research and recommends future work.

Chapter 2

LITERATURE REVIEW

2.1 Introduction

Using mass timber for floors in construction is not a new concept. However, as people search for ways to reduce global emissions from the construction industry, mass timber products have gained interest and popularity. One impediment to broader use of mass timber floor systems is a lack of modeling methods for vertical vibration. In high seismic zones this includes the need to model floors under vertical ground motion. This chapter will first review use of several different mass timber products as building materials. Then, research projects that studied vertical vibration in mass timber floors will be summarized. Finally, research need will be identified that will define the scope of the research in this thesis.

2.2 Mass Timber as a Building Material

2.2.1 Cross Laminated Timber

The development of Cross Laminated Timber (CLT) stems from the construction of glue laminated beams which was first patented in 1901. CLT was not developed until the 1990s when sawmills wanted to find higher value use for their side boards. CLT has since become a product of global interest and has been a subject of research, development, production, and standardization across Europe, Canada, United States, Japan, China, and New Zealand [Brandner et al., 2016]. Multiple layers of lumber boards are stacked crosswise to make up a CLT panel. There are typically an odd number of layers (three, five, or seven) and they are attached together most commonly by gluing, but nails or wooden dowels can be used instead. The thickness of each layer varies from 5/8 in to 2 in while the width of the panels vary from 2 ft to 10 ft. The length of a panel can extend up to 60 ft [Karacabeyli and Douglas, 2013].

Figure 2.1 illustrates the configuration a CLT panel.

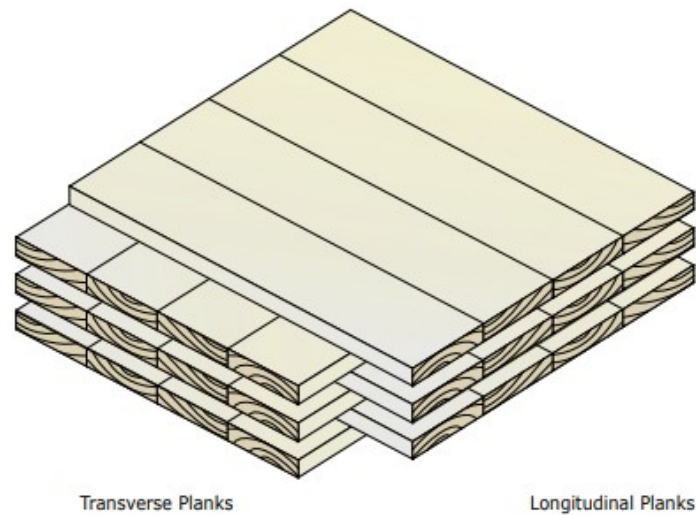


Figure 2.1: CLT Panel Configuration [Karacabeyli and Douglas, 2013]

One of the key advantages of CLT is it has relatively high strength and stiffness in both in-plane directions resulting in the potential use as a two-way floor system. The layering effect also increases the splitting resistance of CLT. These reasons make CLT useful for long, wide floor slabs and long single-story walls [Karacabeyli and Douglas, 2013]. Any softwood lumber species or combination can be used to manufacture a CLT panel as long as the lumber has a minimum specific gravity of 0.35 and is published in the National Design Specification for Wood Construction [AWC, 2018] in the United States or the CSA O86 [CSA O86:19, 2019] in Canada. The lumber must be kiln dried to a moisture content of approximately 12%. The longitudinal planks of lumber must be 1200f-1.2E MSR or visual grade No. 2 minimum. The transverse planks of lumber must be visual grade No. 3 minimum [APA, 2020].

The current CLT product standard was developed by the American National Standards Institute and The Engineered Wood Association and published in 2020 [APA, 2020]. FPInnovations released the CLT Handbook for the United States and Canada in 2013. The CLT

Handbook aims to provide guidance for design and construction of CLT [Karacabeyli and Douglas, 2013].

2.2.2 Glue-Laminated Timber

Glued-laminated timber (GLT) is an engineered timber product stacked with layers of lumber (spanning in the same direction) laminated together. GLT is common in beams due to capability for long spans – up to approximately 50 meters [How et al., 2016]. Typically, there is a four-phase process to manufacture GLT: drying and grading lumber, end jointing lumber, face gluing the laminations, and finishing and fabrication. Compared to sawn lumber and other building materials, GLT offers aesthetic, economic, structural, and sustainability advantages [Smulski, 1997]. GLT can be used for beams, vertical columns, and structural panels. Figure 2.2 illustrates the configuration of a GLT beam.

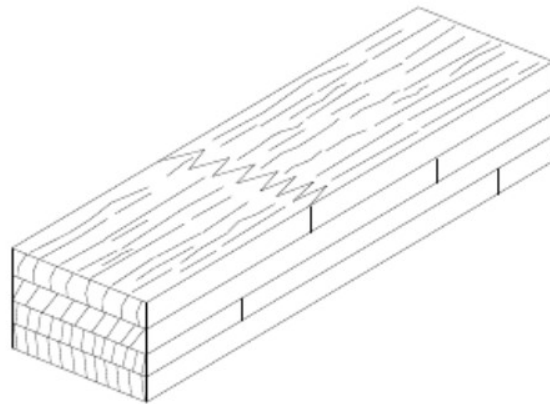


Figure 2.2: Straight Glulam Beam [How et al., 2016]

Originally patented in 1901, GLT became a mainstream building material during World War II. With the increasing popularity, the first manufacturing standard for GLT was created in 1963. The current manufacturing standard is *ANSI A190.1-2022 Product Standard for Structural Glued Laminated Timber* [Smulski, 1997]. This standard lays out the permitted

lumber, moisture content, tolerances, and laminations [APA, 2022].

When used as a floor system, GLT is comprised of nominal lumber that is glued-laminated together into panels. The floor systems typically have plywood spanning across the boards. Figure 2.3 illustrates the orientation of a GLT floor.



Figure 2.3: GLT Floor Panel

2.2.3 *Nail-Laminated and Dowel-Laminated Timber*

Nail-laminated timber (NLT) and dowel-laminated timber (DLT) are structural panels consisting of dimensional lumber planks placed on edge and connected together on the wide face using either nails or dowels. NLT panels typically consist of two rows of nails spaced less than 300 mm apart [Hong, 2014]. DLT consists of one row of hardwood dowels. Each panel can be prefabricated up to 12 ft wide and 60 ft long. The thickness of the floor is typically between 4 in and 12 in depending on the size of lumber used [Epp, 2018]. Figures 2.4 and 2.5 illustrate the configuration of NLT and DLT panels, respectively.

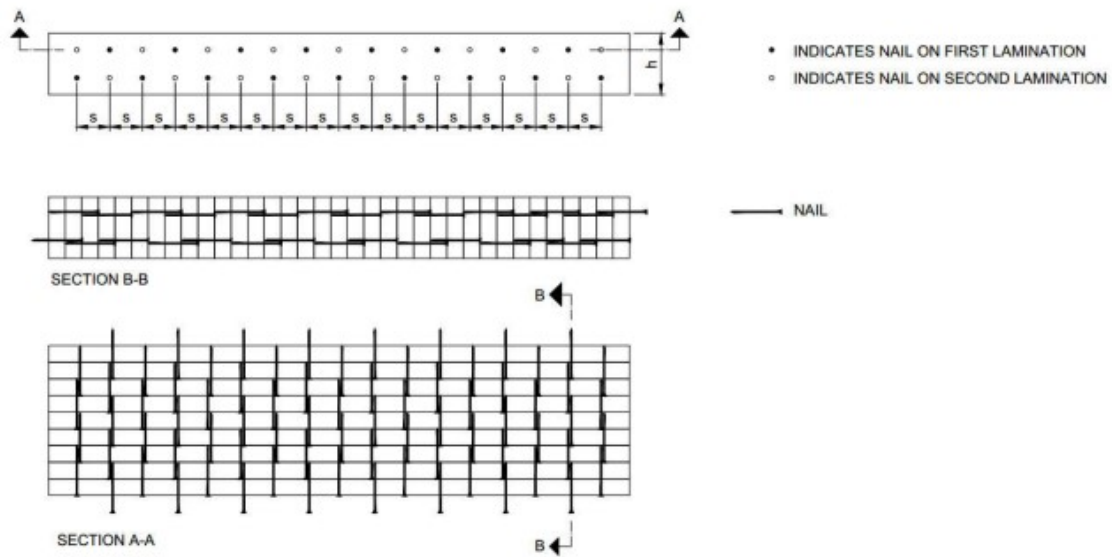


Figure 2.4: Nailing Pattern of NLT [Werner, 1997]

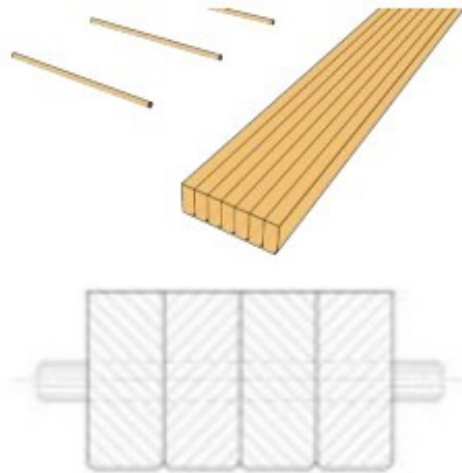


Figure 2.5: Configuration of DLT [StructureCraft, 2021]

NLT is the oldest mass timber product and dates back to the 19th century. NLT became less popular with the rise of steel and concrete, but was still commonly used in bridge decks until the 1960s. The concept was re-introduced in the building world by Julius Natterer is

the 1970s. DLT was developed in Switzerland in the late 1990s. The first DLT production plant in North America was installed in 2017 and has started to gain popularity in the area as a result. [Epp, 2018].

There currently is no standard specifically regulating the manufacturing NLT and DLT. The National Design Specification for Wood Construction (NDS) regulates the dimensional lumber used in NLT and DLT Panels [AWC, 2018]. Several manufacturers of these panels have released design guides to assist users with design of their products [StructureCraft, 2021].

2.2.4 Mass Plywood Panels

Mass Plywood Panels (MPP) are an engineered mass timber product manufactured by gluing layered veneers together to create a larger panel. The veneers are typically composed of nine layers (seven in the long-ply direction and two in the cross-ply direction). These veneers are then laminated together in the same direction. Figure 2.6 illustrates the configuration of the veneer and MPP. MPP can be manufactured in widths of up to 12 ft, lengths of up to 48 ft, and thicknesses of up to 2 ft [Soti et al., 2021].

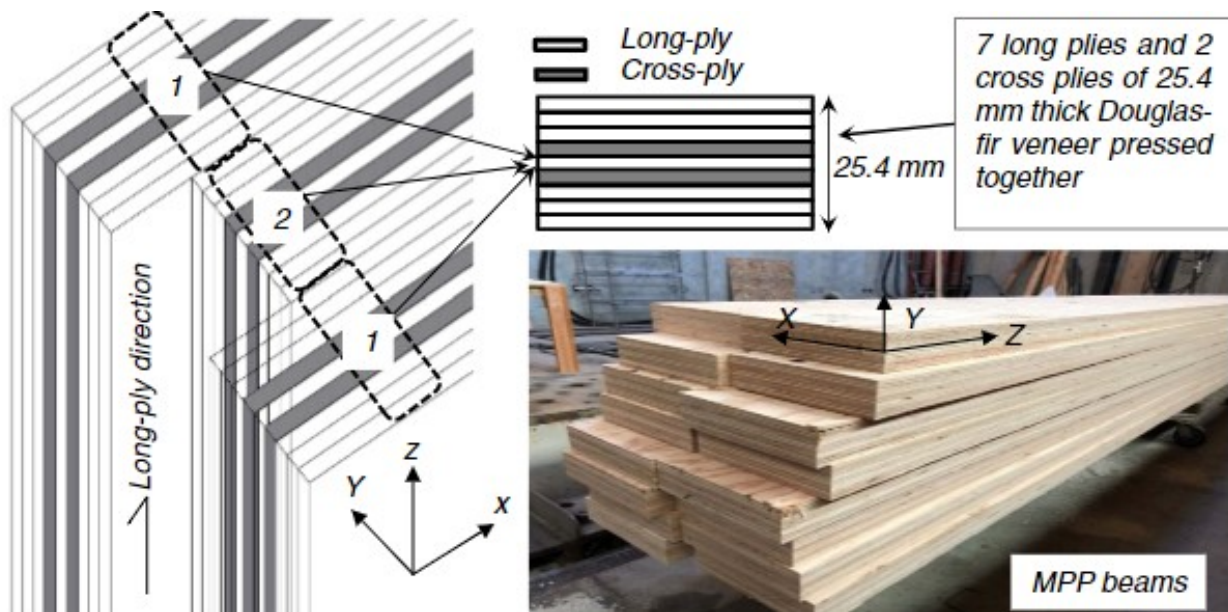


Figure 2.6: Details of MPP [Soti et al., 2021]. Each panel has 7 layers (5 layers in the long-ply and 2 in the cross-ply direction).

MPP is a new material and has only been used in a few mass timber construction projects up to this point [Soti et al., 2021]. Since the building material is new, there is no official standard governing the manufacturing of MPP. The APA, however, has certified MPP from different manufacturers as Cross-laminated Timber Panel [Boise Cascade, 2022].

2.3 Previous Research on Vertical Vibration of Mass Timber Floors

The following section summarizes the methods and results of the research that is most relevant to vibrations in mass timber floors.

2.3.1 Jarnerö et al. [2015]

Jarnerö et al. [2015] studied the vibration properties of prefabricated timber floor elements. Since timber floors are lightweight, they are more prone to vibration due to human activity than heavier floors – like concrete floors. The vibration performance of timber floors is

dictated by the floor mass, stiffness, and damping. For mass and stiffness there are existing methods of calculation for several floor types, but only rough estimates are available for damping. [Jarnerö et al. \[2015\]](#) performed laboratory tests of CLT specimens with different boundary conditions to monitor the damping in the presence of different boundary conditions.

The specimens [Jarnerö et al. \[2015\]](#) tested were three-layer CLT panels approximately 2400 mm wide. The CLT panels were glued and screwed to glulam beams with 460 mm spacing. The mass of the tested CLT panels was 511 kg yielding a static load of 41.7 kPa. Figure 2.7 below shows an image of the laboratory setup.



Figure 2.7: CLT Laboratory Setup [[Jarnerö et al., 2015](#)]

[Jarnerö et al. \[2015\]](#) performed *in situ* tests during different points of construction. There were seven stages of construction in which the *in situ* tests were run, including uncoupled, coupled, and tests in stages after adding stories above. The *in situ* tests were performed on the CLT floor of a bedroom 5.1 m long and 3.1 m wide. The floor was excited using an electromagnetic shaker. The shaker locations can be seen in Figure 2.8 and coincide with the excitation locations of the laboratory tests. The laboratory test performed by [Jarnerö et al. \[2015\]](#) analyzed the CLT panels under both free-free and simply-supported boundary

conditions.

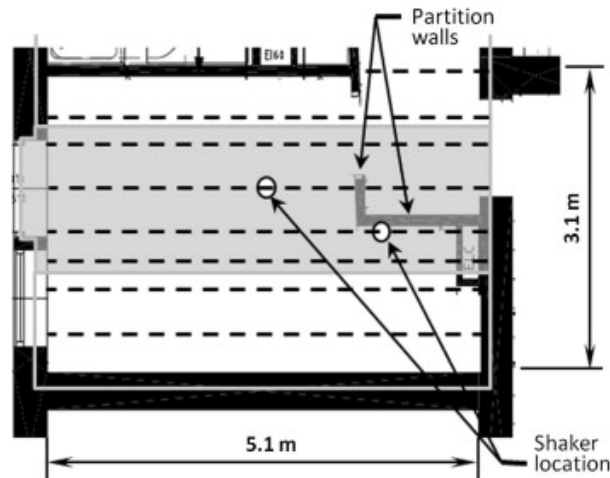


Figure 2.8: *In Situ* Floor Dimensions and Shaker Location [Jarnerö et al., 2015]

For the first five modes of the Jarnerö et al. [2015] free-free laboratory test, the damping ratios ranged from 1.2%–1.7%. The first six modes of the simply-supported laboratory test resulted in damping ratios ranging from 1.4%–2.6%. However, the lower damping ratios correlated to the higher frequency modes in the simply-supported test. The laboratory tests showed that changing the boundary conditions changes the damping in the vibration response of the CLT panels. Jarnerö et al. [2015] observed that there were only small changes in the fundamental mode frequency with different boundary conditions, but there were frequency changes in the higher modes. The damping ratio of the first five modes were significantly higher for the *in situ* tests [Figure 2.9]. The damping ratios ranged from 3.5%–8.0%. The damping ratios of the CLT panels implemented into a building are approximately 4 times larger than the laboratory tests. Jarnerö et al. [2015] concludes that the current design guideline value of 1%–2% damping for timber floors could be increased to recognize the increase of damping ratios of the panels in a building, but further research needs to be performed on the *in situ* damping ratios to provide a new design value.

	Frequency (Hz)					Damping (%)				
	Mode	Mode	Mode	Mode	Mode	Mode	Mode	Mode	Mode	Mode
	1	2	3	4	5	1	2	3	4	5
Coupled	21.4	23.4	31.1	34.9	39.6	5.7	5.5	4.3	4.6	3.5
3rd storey walls	22.1	25.9	31.4	34.7	39.0	5.5	4.3	5.5	4.8	4.2
3rd storey floor	23.2	25.7	32.3	38.0	44.1	5.8	4.8	3.9	4.2	4.0
4th storey	22.8	26.4	33.5	41.5	44.1	8.0	4.5	5.3	4.2	4.0
6–7th storey	20.7	22.1	27.0	33.8	39.3	7.0	5.0	5.0	5.6	5.6
7–8th storey	21.7	23.5	29.3	37.2	46.9	6.5	7.9	6.2	5.0	4.2

Figure 2.9: *In Situ* Modes, Frequencies, and Damping Ratios [Jarnerö et al., 2015]

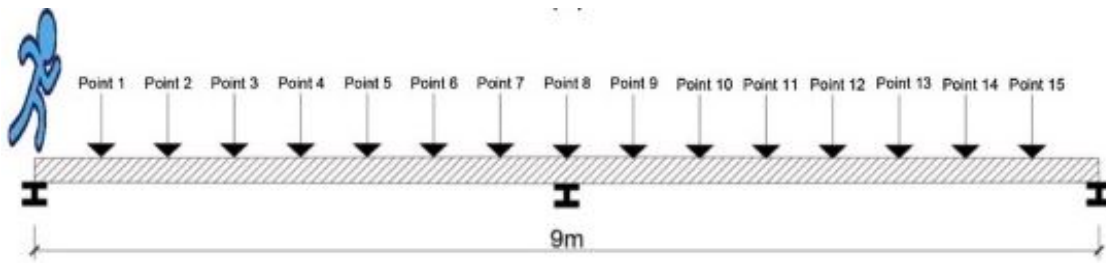
2.3.2 Huang et al. [2020]

Huang et al. [2020] performed a numerical study in OPENSEES with the intent of investigating whether boundary conditions affect the performance of a CLT floor. Previous research had indicated that boundary conditions influence the vibration response of timber floors. Eurocode 5 specifies an 8 Hz frequency minimum in installed floors, but alternative standards propose the consideration of human activity and the resulting vibration response as a method of designing for serviceability. The overall objective of Huang et al. [2020] was to investigate the effect of boundary conditions and reduce vibration of CLT floor systems.

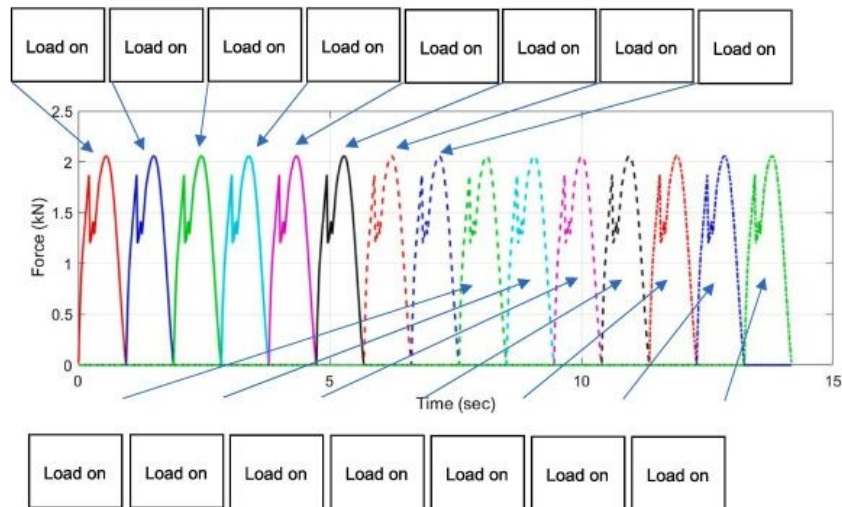
The numerical study modeled three-layer CLT panels (120 mm thick) that were 9.0 m long and 6.6 m wide. The CLT was modeled as three-layer orthogonal beams, and each layer was connected using springs with a large stiffness value. Springs with large stiffness values connected the CLT to steel beams for the boundary conditions.

Huang et al. [2020] considered running footfalls as the excitation. Each step was modelled

as a force-time history as with two peaks. The first peak corresponded to a heel strike and the second to the toe pushing off the ground. The second peak had a larger amplitude with a force of about 2.1 kN. The loading locations and profile are shown below in Figure 2.10.



(a) Running Footfall Load Positions



(b) Running Footfall Load Protocol

Figure 2.10: Running Footfall Loads [Huang et al., 2020]

At the University Centre Farnborough in the UK, a laboratory test was performed to validate the Huang et al. [2020] model. The laboratory test resulted in a fundamental natural frequency of 7.5 Hz in the CLT floor. The OPENSEES model analysis resulted in a fundamental natural frequency of 7.6 Hz. The acceleration over time was similar in the

testing and model [Figure 2.11], but the peak accelerations differed. Huang et al. [2020] theorized that the differences may have resulted from either high-frequency noise during laboratory tests or randomness in real human excitation.

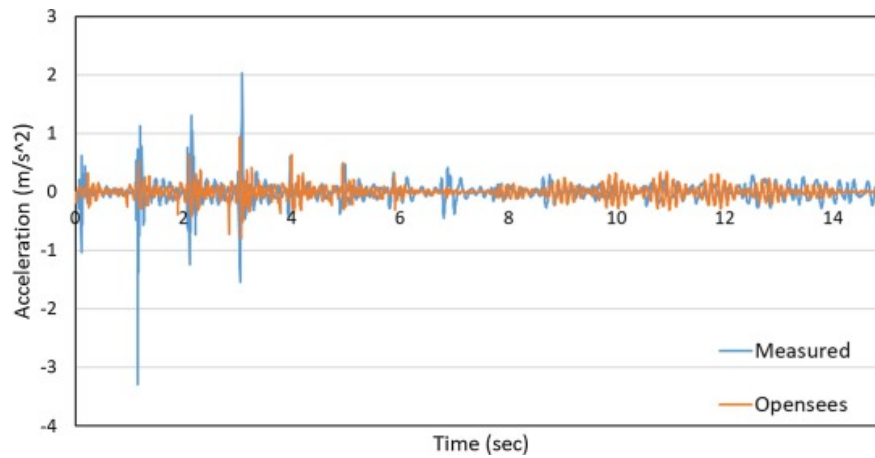
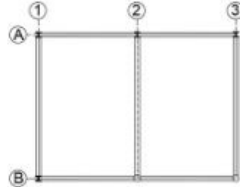
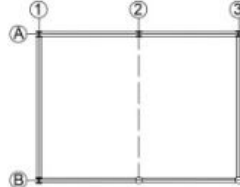
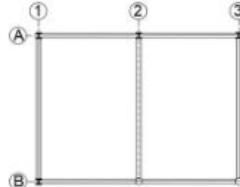

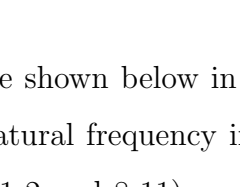
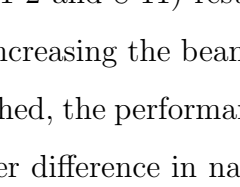
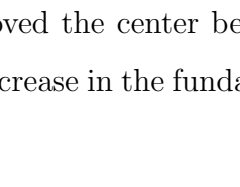



Figure 2.11: Comparison of Numerically Modelled and Measured Vertical Acceleration [Huang et al., 2020]

After validating the model, Huang et al. [2020] performed a parametric study to test the effects of different boundary conditions on the system. The setup of the first test matched the first model, and the rest of the setup is described below in Table 2.1.

Table 2.1: Testing Setup [Huang et al., 2020]

Test No.	Size of beam parallel to the longitudinal direction	Size of beam parallel to the transverse direction	Explanatory drawings of boundary conditions
1	UB203×133×30	UB 406×140×46	
2	UB406×140×46	UB 406×140×46	
3	UB203×133×30	UB 406×140×46	
4	UB305×165×54	UB533×165×85	
5	UB533×165×85	UB533×165×85	
6	UB254×146×43	UB457×152×82	
7	UB457×152×82	UB457×152×82	
8	UB178×102×19	UB305×127×48	
9	UB305×127×48	UB305×127×48	
10	UB127×76×13	UB254×102×28	
11	UB254×102×28	UB254×102×28	

The first three natural frequencies of each test case are shown below in Table 2.2. For the tests with large beams (Tests 4-7) the fundamental natural frequency increased to approximately 9.7 Hz. The tests with smaller beams (Tests 1-2 and 8-11) resulted in a lower fundamental natural frequency of approximately 7.2 Hz. Increasing the beam size improved the performance of the CLT floor; once a certain size is reached, the performance of the floors were not improved. With larger beams, there was a smaller difference in natural frequency between one-way and two-way floor systems. Test 3 removed the center beam of the test, doubling the span of the floor. This test resulted in large decrease in the fundamental natural frequency (2.0 Hz).

Table 2.2: First Three Natural Frequencies of the Floor System Under Different Testing Conditions, as Analysed Using OPENSEES Simulated Time-History Data [Huang et al., 2020]

Test No.	1	2	3	4	5	6	7	8	9	10	11
f_1 (Hz)	7.6	7.9	2.0	9.7	9.8	9.8	9.7	7.2	7.7	7.1	7.2
f_2 (Hz)	10.0	9.2	3.2	15.0	15.5	15.3	15.1	10.4	14.6	12.3	13.9
f_3 (Hz)	14.4	14.6	7.6	32.0	32.3	32.3	32.0	28.2	29.0	27.6	27.6

The study concluded that first fundamental modal frequency of the OPENSEES model matched well with the lab results. The study also concluded that beam spacing and boundary conditions significantly impact the frequency response of the mass timber floors.

2.3.3 Milojević et al. [2023]

Many CLT floors are constructed with a layer of concrete topping. The concrete spans across the joints of the CLT panels, providing stiffness across the entire floor. Milojević et al. [2023] modelled different of inter-panel connections of bare CLT panels to study how each joint affects the mode shapes and frequencies of the system. The types of connections studied were monolithic slabs, no connection, single surface spline, and half-lapped joint. The monolithic slabs were a slab with no joints. The no connection slabs were 2 slabs with no connection at the joint. The single surface spline was 2 slabs with a plywood spline at the joint. The half-lapped joint was 2 slabs with a half-lapped joint with a nail connecting the joint. An equivalent modulus of elasticity and shear modulus were calculated to accurately model the stiffness of the connections. Figure 2.12 below displays how to calculate the applicable moments of inertia of a single surface spline. Equation 2.1 shows how to calculate

the effective modulus of elasticity.

$$E_{eq} = E_{con} \frac{l_{eq} I_{con}}{l_{con} I_{eq}} \quad (2.1)$$

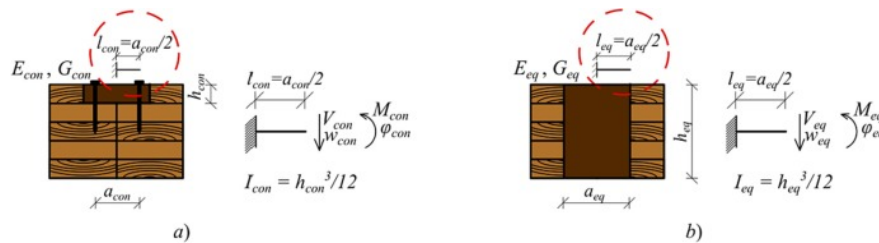


Figure 2.12: Single Surface Spline Connection: a) Actual, b) Equivalent Elastic Strip. [Huang et al., 2020]

Milojević et al. [2023] modeled a low-frequency floor (LFF) and a high-frequency floor (HFF). The LFF model contained two 5-layer CLT panels 6 m long by 3 m wide and totaled 20 cm thick. The CLT was C24 with a modulus of elasticity of 11,000 N/mm^2 and 370 N/mm^2 in the major and minor directions, respectively. The density of the CLT was 420 kg/mm^3 . The HFF model used the same 5-layer CLT, but the panels were 4 m long by 2 m wide. For both cases, the study included one-way and two-way boundary conditions.

The modes were analyzed using Abaqus CAE. For the one-way LFF condition, all four connection types were analyzed. The case with no connection between the two panels was the most different when compared to the other cases. The frequencies of the modes in the strong direction were identical for the monolith and no connection cases, but the weak direction modes differed by approximately 2 Hz – 26% in the first weak direction mode. The single surface spline and half-lapped joint connections were almost identical except for a 3.25% difference in the 6th mode. The two connection types and the monolithic slab were similar except for the mode where there is bending along the connection line. Figure 2.13 shows the result summary for the one-way LFF modal analysis. For the two-way boundary condition,

Milojević et al. [2023] only analyzed the monolithic slab, single surface spline connection, and half-lapped joint connection. The single surface spline and half-lapped joint connections were similar again. The monolith slab produced similar results to the connections except for the 1st and 5th modes since there was bending at or along the connection. Figure 2.14 shows the result summary for the two-way LFF modal analysis.

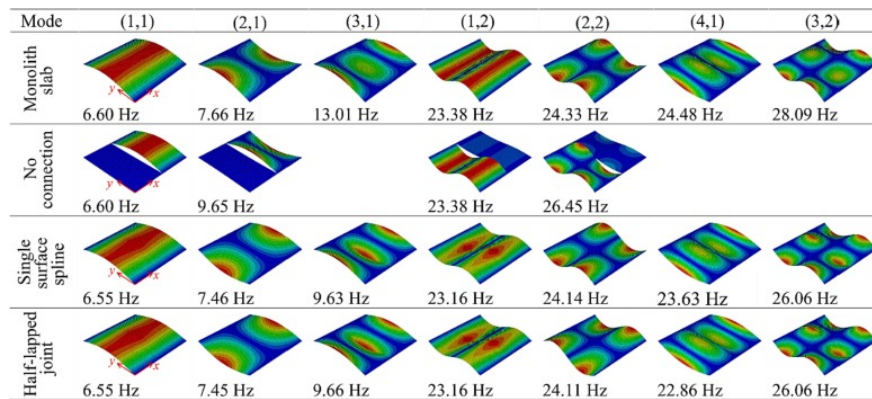


Figure 2.13: Mode Shapes and Associated Natural Frequencies of 6 m \times 6 m Square CLT Floor (One-Way Boundary), Considering Different Inter-Panel Connection Types [Milojević et al., 2023]

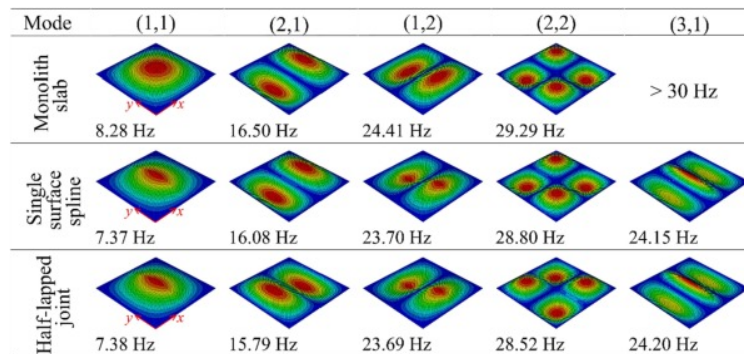


Figure 2.14: Mode Shapes and Associated Natural Frequencies of 6 m \times 6 m Square CLT Floor (Two-Way Boundary), Considering Different Inter-Panel Connection Types [Milojević et al., 2023]

For both the one-way and two-way HFF analyses only the monolithic, single surface spline, and half-lapped joint connections were considered. For the one way analysis, the first two modes were similar for all three cases. The monolithic slab frequency, however, differed from the inter-panel connections by about 26% in the 3rd mode. This difference again comes from bending along the connection. The two-way analysis produced similar results; the 2nd mode was similar for all three cases, but the frequency of the first mode differed by over 2Hz. The result summary of the one-way and two-way boundary conditions can be seen in Figure 2.15 and Figure 2.16 below.

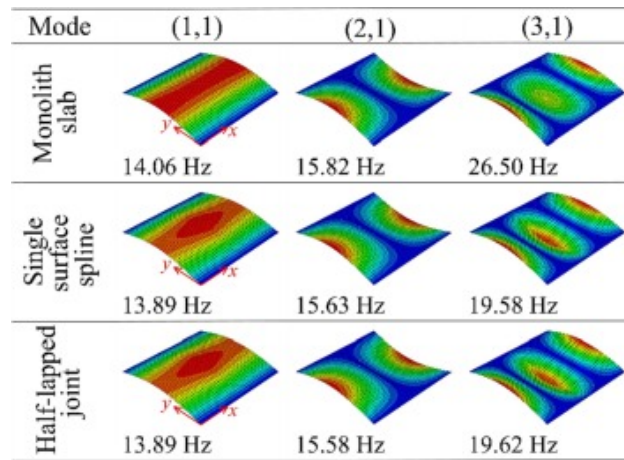


Figure 2.15: Mode Shapes and Associated Natural Frequencies of 6 m \times 6 m Square CLT Floor (One-Way Boundary), Considering Different Inter-Panel Connection Types [Milojević et al., 2023]

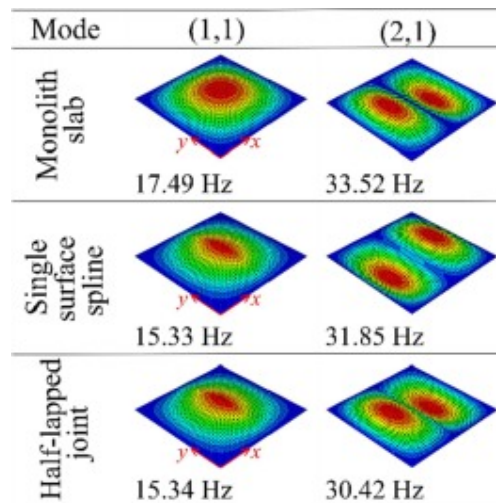


Figure 2.16: Mode Shapes and Associated Natural Frequencies of 6 m \times 6 m Square CLT Floor (Two-Way Boundary), Considering Different Inter-Panel Connection Types [Milojević et al., 2023]

Milojević et al. [2023] found that the connections made an impact on mode shape and

frequencies of CLT floors; the connections made higher impact on high-frequency floors than low-frequency floors. The biggest differences came in modes where there was bending at the connection line (ie shorter vs longer spans). Using this information, [Milojević et al. \[2023\]](#) concluded that connection lines should be kept away from critical walking paths. Also, [Milojević et al. \[2023\]](#) suggests that future studies should include experimental results, since this study was based solely on numerical simulation.

2.3.4 *Dolan et al. [1999]*

Architectural trends required longer floor spans to accommodate larger open spaces in both residential and commercial construction. The longer wood floor spans were more likely to produce perceptible vibration under footfall loading. [Dolan et al. \[1999\]](#) presented a design criterion for wood floors based on previous research.

[Dolan et al. \[1999\]](#) discussed previous research on wood floor design criterion. They concluded these design criteria were difficult to implement by designers due to various reasons: required knowledge of the in-situ floor system damping, no damping was considered, or ignoring composite action between joists and sheathing.

The proposed design criterion was that the fundamental frequency of the floor system exceed 15 Hz. This criteria also ignores damping but was investigated experimentally to ensure the assumption was alright. [Dolan et al. \[1999\]](#) looked at previous research on wood floor systems. The research showed that all wood floors over 15 Hz were considered acceptable when subjected to a heel-drop test, but not all floors under 15 Hz were acceptable. The results of each tested floor were based on whether an evaluator thought the floor vibrations induced by the heel drop tests were annoying or acceptable.

The study concluded that the proposed design criteria was acceptable. The criteria requires the fundamental frequency of a wood floor system be over 15 Hz. Effects of damping were assumed to be negligible since any damping effect would decrease the vibrations of the floor system [[Dolan et al., 1999](#)].

2.4 Vertical Vibration Design Guides

2.4.1 U.S. Mass Timber Floor Vibration Design Guide Overview

The U.S. Mass Timber Floor Vibration Design Guide was developed for the WoodWorks – Wood Product Council [Breneman et al., 2021]. The design guide aimed to guide designers to limit the human-induced vibration of mass timber floor systems. There is currently no vibration requirements in the United States, but vibration may control serviceability design.

Breneman et al. [2021] briefly discussed the dynamics of floor vibration, design considerations, and design methods before providing recommendations for modeling the mass timber floor systems for vibrations. The post-processing steps for human-induced vibrations were also discussed. The post-processing steps were followed by 3 examples exploring different software and boundary conditions.

Breneman et al. [2021] provided recommendations to designers modeling mass timber floor vibrations. The element recommendations were to use shell elements to model the floors instead of plates or membranes, frame elements to model the beam and column system, and joint elements to define connectivity between elements as well as provide restraints to the model. Solid elements were rarely used for models. It was recommended to model only one-story in each model, not the entire building. The entire floor should be modeled to accurately capture continuity between spans in the same story. The beam system of each story should be modeled accurately, but only half the length of each column should be used. The bottom of each column should be pin-restrained and the top should horizontally-restrained. The horizontal restraints prevent lateral and torsional modes.

Mass timber floors have anisotropic properties which could be modeled using isotropic material with section property modification factors, orthotropic materials, or layered shell elements. The recommended approach was to apply generic isotropic material properties to a shell section, since this was the most simple approach. The section properties of the model can be adjusted to the appropriate stiffness in accordance with Figure 2.3 where effective properties refer to the designed floor and the reference and gross properties refer to the generic

sections defined in the modeling software. Composite sections could be modeled using the same isotropic models if the composite section properties were calculated [Breneman et al., 2021].

Table 2.3: SAP Modifier Equations [Breneman et al., 2021]

Orientation	Property Modification Factor
Strong axis axial	$f_{11} = \frac{EA_{\text{eff},0}}{E_{\text{ref}} * A_{\text{gross}}}$
Weak axis axial	$f_{22} = \frac{EA_{\text{eff},90}}{E_{\text{ref}} * A_{\text{gross}}}$
In-plane shear	$f_{12} = \frac{GA_{\text{eff},e}}{G_{\text{ref}} * A_{\text{gross}}}$
Strong axis flexure	$m_{11} = \frac{EI_{\text{eff},f,0}}{E_{\text{ref}} * I_{\text{gross}}}$
Weak axis flexure	$m_{22} = \frac{EI_{\text{eff},f,90}}{E_{\text{ref}} * I_{\text{gross}}}$
Out-of-plane torsion*	$m_{12} = \min(v_{13}, v_{23})$
Strong axis out-of-plane shear	$v_{13} = \frac{GA_{\text{eff},f,0}}{G_{\text{ref}} * A_{\text{gross}}}$
Weak axis out-of-plane shear	$v_{23} = \frac{GA_{\text{eff},f,90}}{G_{\text{ref}} * A_{\text{gross}}}$

A modal analysis was recommended to be performed to provide the frequencies used in

post-processing. The number of modes varied depending on the size and geometry of the model. The mesh of the shell elements was recommended to be fine enough that adjacent joints were no more than 3 ft apart. Manual meshing was recommended to ensure a consistent mesh. Joints were recommended to be created along the beams so the software could mesh the floor elements to the beam elements.

Nonstructural walls were recommended to be modeled using spring elements. The recommended stiffness of each spring was 1 kip/ft of wall length. Variable damping coefficients were recommended to vary based on the floor type, but bare mass timber floors were recommended to be damped between 1% and 2% [Breneman et al. \[2021\]](#).

2.4.2 Design Guide for Timber-Concrete Composite Floors in Canada

The Design Guide for Timber-Concrete Composite Floors in Canada focused on the design of timber-concrete composite (TCC) floors in building construction emphasising floor systems [\[Cuerrier-Auclair, 2020\]](#). The design guide provided background on TC systems, discussed bending equations for composite action, shear connection mechanical properties, deflection, vibration performance, ultimate limit state design, fire resistance, and finally provided design examples. Following the scope of this thesis, the chapter on vibration performance will be discussed.

[Cuerrier-Auclair \[2020\]](#) noted that the vibrational behavior of a floor system due to human walking-induced vibration could be the most critical aspect of vertical floor design. Vibration could be correlated to the frequency and deflection of the floor system. Typically, the fundamental natural frequency of the floor was not significantly influenced by orthotropic behavior of floor systems and could be approximated using the Euler-Bernoulli beam equation.

By evaluating the vibration response of an NLT-concrete composite floor, a CLT-concrete composite floor, and a concrete slab - glulam beam composite floor [Cuerrier-Auclair \[2020\]](#) developed a design criterion equation to limit the length of a floor slab based on its stiffness and mass [Equation 2.2]. In the equation, $(EI)_{eff}^{1m}$ refers to the effective bending stiffness

of a 1 m wide strip in $\text{N}\cdot\text{m}^2$ and m_L refers to the mass per unit length of the same strip in kg/m .

$$L \leq 0.329 \frac{((EI)_{eff}^{1m})^{0.264}}{m_L^{0.207}} \quad (2.2)$$

Cuerrier-Auclair [2020] provided a few limitations and recommendations: the floor span length should be reduced by 20% if the supplementary dead load is lower higher than the structural dead load, the effective stiffness of a TCC floor cannot be increased to account for additional stiffness provided by partitions, do not increase the span for a multi-span floor, and the design criteria might not address all occupant performance expectations.

2.5 Conclusions and Research Needs

The research discussed in this chapter indicates that:

- Mass timber is a strong building material that is currently used in floors, beams, and other structural components.
- Boundary conditions largely influence the vibration response of mass timber floors.
- Using software to model mass timber floors can accurately predict the mode shapes and frequencies of the in situ floor.

The research in this section shows that CLT can adequately resist live loads and footfall excitation, and that CLT can be accurately modeled using software. The same tests have not been run on other types of mass timber floors. There has also been a lack of research on mass timber floor response to vertical seismic ground motions. The modeling techniques discussed in Section 2.4.1 will be adapted to model mass timber floors under seismic vertical vibration. The research presented in this thesis aims to validate that different types of mass timber floors can adequately perform under footfall and seismic vertical excitation.

Chapter 3

SPECIMEN DESIGN AND CONSTRUCTION

3.1 Introduction

The work in this thesis involves the modeling of mass timber floor systems used in the NHERI TallWood Project 10-story test and comparing the results of the model and dynamic testing. The NHERI Tallwood Project 10-story building is a full scale 10-story mass timber building that was tested at the NHERI@UCSD shake table in San Diego, California. This chapter focuses on describing the design and construction of the gravity system and floor diaphragms as that is most pertinent to the current scope. Then, the design of the other building elements, including the lateral force resisting system and the nonstructural building elements, are briefly discussed.

3.2 Beam and Gravity Column Design

The beam and gravity column layout was influenced by the footprint of the building and by limiting the maximum span lengths. The footprint was construed to fit on the platform of the shake table. The beams system generally spanned in the east-west direction. The columns were typically spaced at 10.5 ft on center. There were a few beams that span in the north-south direction which created both one-way and two-way floor sections. Figure 3.1 below illustrates the typical beam and column plan view. The plan contains the shake table coordinate axes, a north arrow, and grid lines which correspond to the grid lines in the full detailed drawing set in Appendix A.

The gravity members were designed using ASD to satisfy a 2-hour fire rating. The dead and live load combinations from ASCE 7-16 were used for design as well [ASCE, 2016]. The live load and dead loads used were 65 and 64.4 psf, respectively, and reflected the apartment

apartment occupancy from ASCE [2016]. The gravity members were 1.8E 2650 Grade LVL members. The beams and gravity columns were 12.25 in by 11.875 in. The buckling demand vs capacity ratio for the gravity columns was 0.34, and the bending demand vs capacity ratio for the beams was 0.44 considering factored gravity loads. Busch [2023] provides more details on the design of the gravity system.

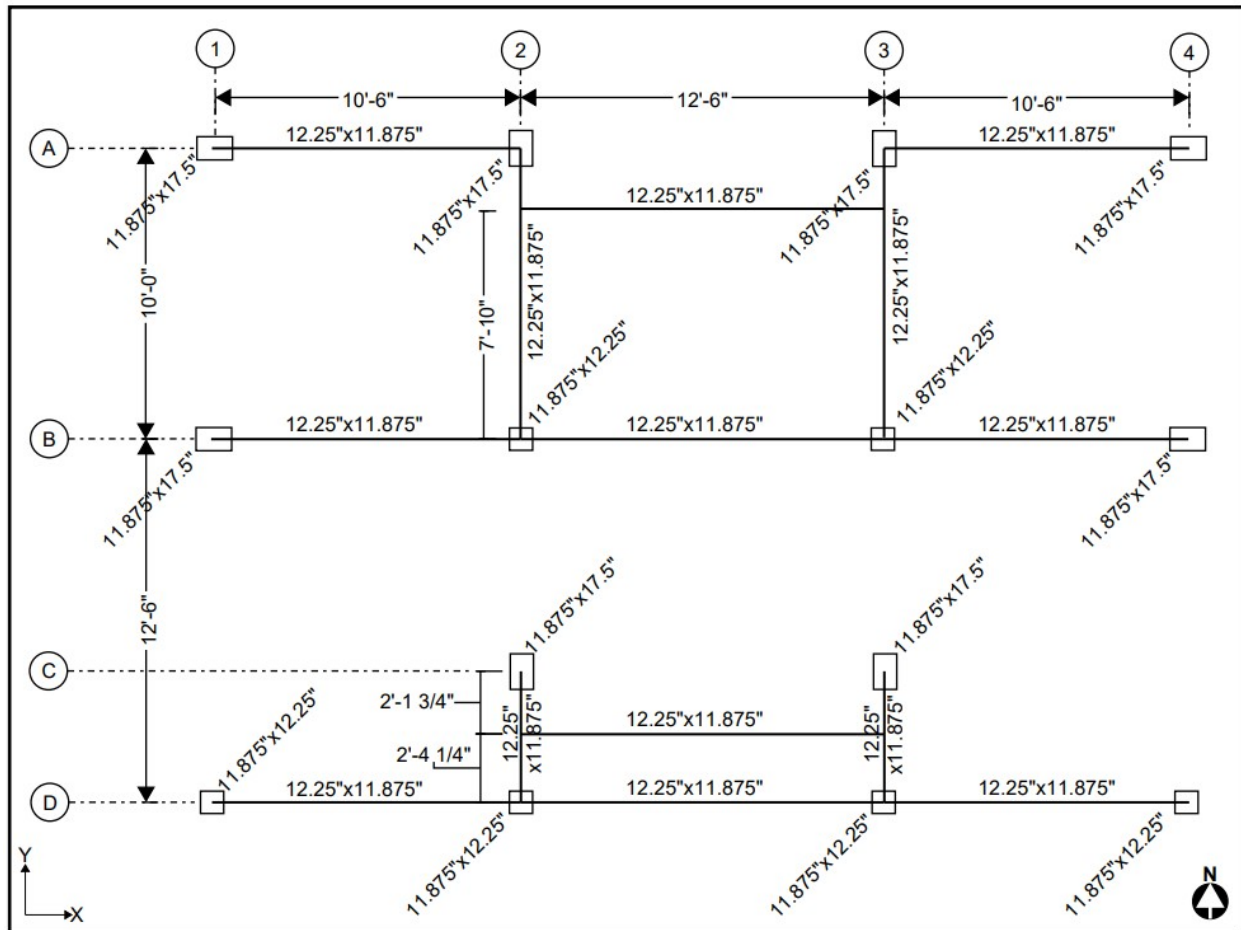


Figure 3.1: Typical Beam and Column Plan View

3.3 Floor Design

There were five different types of floors used in the 10-story building. Table 3.1 summarizes the floor type for each level. This section describes the typical floor layout, then discusses the material properties and section properties of the different floor types.

Table 3.1: Floor Type at Each Level

Floor Type	Levels
CLT	2-3
GLT	4-5
NLT	6
DLT	7
VLT	8-11

3.3.1 Floor Layout

The floors were approximately 34 ft by 34 ft in plan view. The strong axis of the diaphragm spanned in the north–south direction, while the weak axis spanned in the east-west. The center of the diaphragm contained a 14.5 ft by 7.5 ft rectangular cut out for the stairs as well as a landing platform on the east side of the stairwell. There were a few key spans which were used for data analysis throughout the paper: northeast cantilever, central span, west span, and the northeast cantilever. Figure 3.2 labels the key spans.

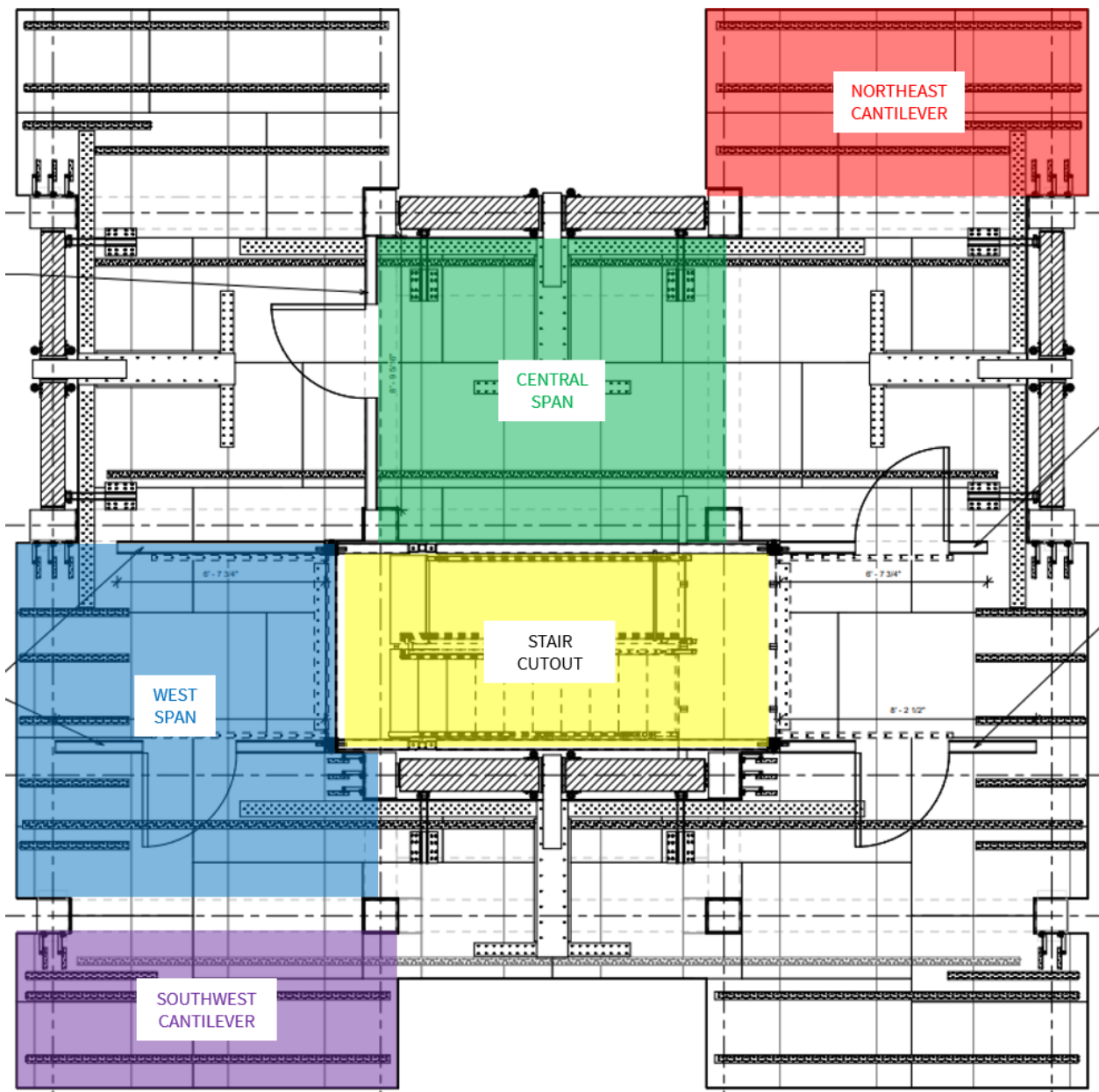


Figure 3.2: Labeled Floor Spans

The weak axis direction had small cantilevers approximately 1.5 ft long in each span without a rocking wall. Floors 4–11 contained Simpson Strong Tie angles supporting the weak axis cantilevers at the columns. Figure 3.3 shows the one of the angles installed.

There were several straps (manufactured by Simpson Strong Tie) spanning in the east–west direction on each floor which assisted in transmitting the lateral loads through the diaphragm. The angle and strap location varied from floor to floor. Appendix A illustrates the floor dimensions and locations of the straps and angles.



Figure 3.3: Weak Axis Support Angle

3.3.2 Cross Laminated Timber

The CLT panels were supplied by Mass Timber Services. Each panel measured up to 7.5 ft in width and spanned up to the full 34 ft. The panels were 5-ply and measured approximately 7 in thick. The lumber used in the CLT was visually graded European Spruce. CLT panels comprised the floor diaphragm for Floors 2 and 3. The panels were connected together by a Simpson Strong Tie diaphragm spline strap which was screwed to each panel. Figure 3.4 illustrates the typical CLT layout. Appendix A contains the full detailed drawings.

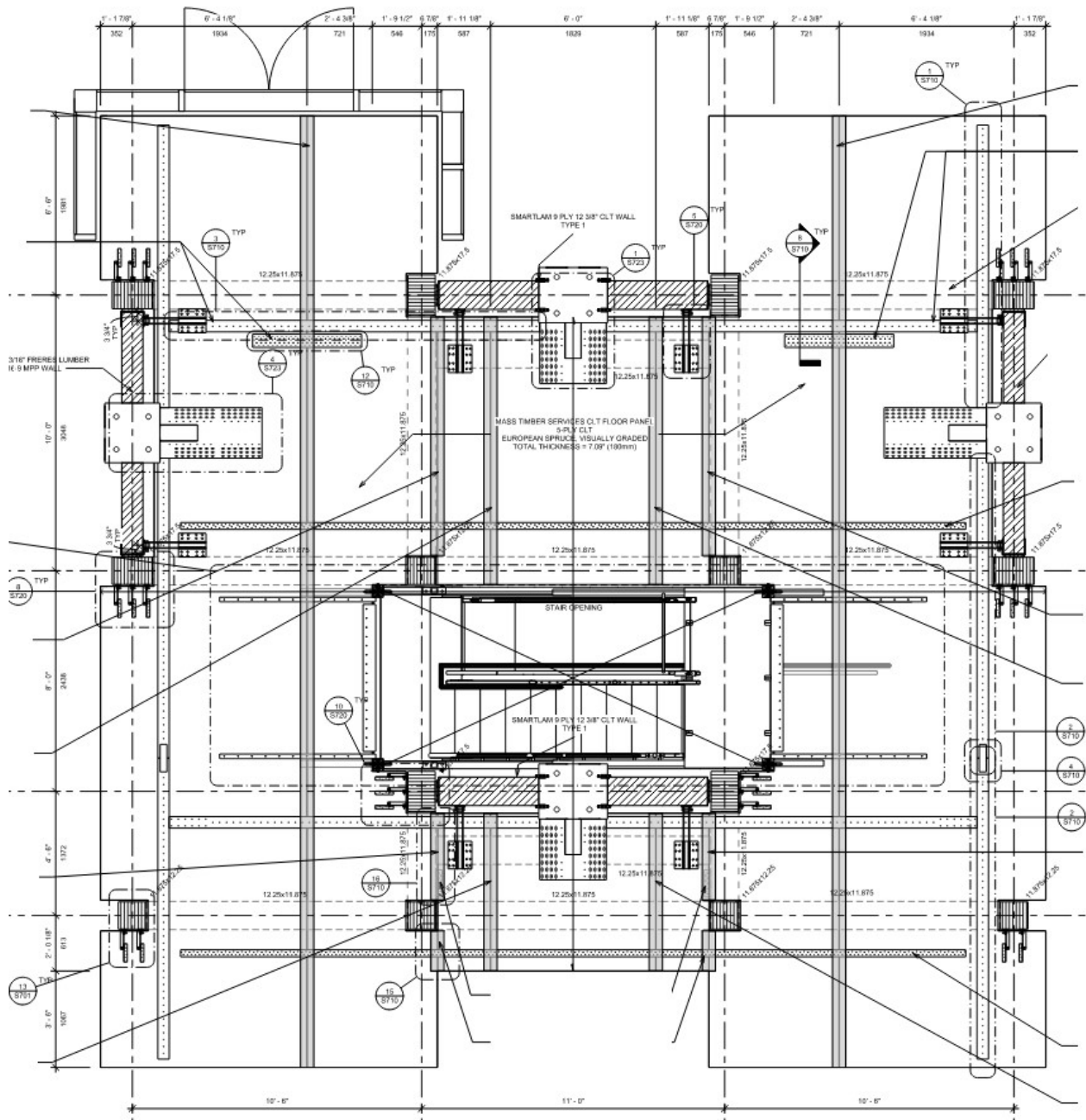


Figure 3.4: Typical CLT Layout

The CLT was Grade C24 [OIB, 2020]. The following material properties of lumber are summarized below in Table 3.2: strong axis modulus of elasticity (E_0), weak axis modulus

of elasticity (E_{90}), strong axis shear modulus (G_0), and weak axis shear modulus (G_{90}).

Table 3.2: CLT Material Properties

Material Property	Value
E_0 (ksi)	1,682.44
E_{90} (ksi)	53.66
G_0 (ksi)	94.27
G_{90} (ksi)	7.25

Using the material properties from above, the sections properties of the CLT were determined. The key section properties for the CLT were the effective axial stiffness (EA_{eff}), bending stiffness (EI_{eff}), and shear stiffness (GA_{eff}) for both the strong and weak axes. The equations used to calculate each section property come from the CLT Handbook [Karacabeyli and Douglas, 2013] and were applied to the 5-ply CLT floor system; Equations 3.1–3.3 were for the strong axis, and Equations 3.4–3.6 were for the weak axis. The parameters t (lumber thickness) and b (width) were 1-3/8 in and 12 in, respectively. Table 3.3 below summarizes the section properties per ft of CLT.

$$EA_{eff} = (3E_0 + 2E_{90})bt \quad (3.1)$$

$$EI_{eff} = (3E_0(\frac{1}{12}bt^3)) + (2E_{90}(\frac{1}{12}bt^3)) + (2E_0(bt)(2t)^2) + (2E_{90}(bt)(t)^2) \quad (3.2)$$

$$GA_{eff} = \frac{(4t)^2}{[2(\frac{t}{G_0b}) + 2(\frac{t}{G_{90}b})]} \quad (3.3)$$

$$EA_{eff} = (2E_0 + 3E_{90})bt \quad (3.4)$$

$$EI_{eff} = (2E_0(\frac{1}{12}bt^3)) + (3E_{90}(\frac{1}{12}bt^3)) + (2E_0(bt)(t)^2) + (2E_{90}(bt)(2t)^2) \quad (3.5)$$

$$GA_{eff} = \frac{(4t)^2}{[2(\frac{t}{G_0b}) + 2(\frac{t}{G_{90}b})]} \quad (3.6)$$

Table 3.3: CLT Section Properties

Section Property	Strong Axis	Weak Axis
EA_{eff} ($10^6 lbf/ft$)	85.94	58.18
EI_{eff} ($10^6 lbf - in^2/ft$)	436.62	127.53
GA_{eff} ($10^6 lbf/ft$)	0.89	0.89

3.3.3 Glued Laminated Timber

The GLT panels were supplied by Mass Timber Services. Each panel measured up to approximately 3 ft in width and spanned up to the full 34 ft. The panels were approximately 6 in thick including the European Spruce lumber and used OSB Plywood topping. GLT panels comprised the floor diaphragm for Floors 3 and 4. The panels were connected together by a 5/8 in sheet of OSB plywood. Figure 3.5 below illustrates the typical GLT layout.

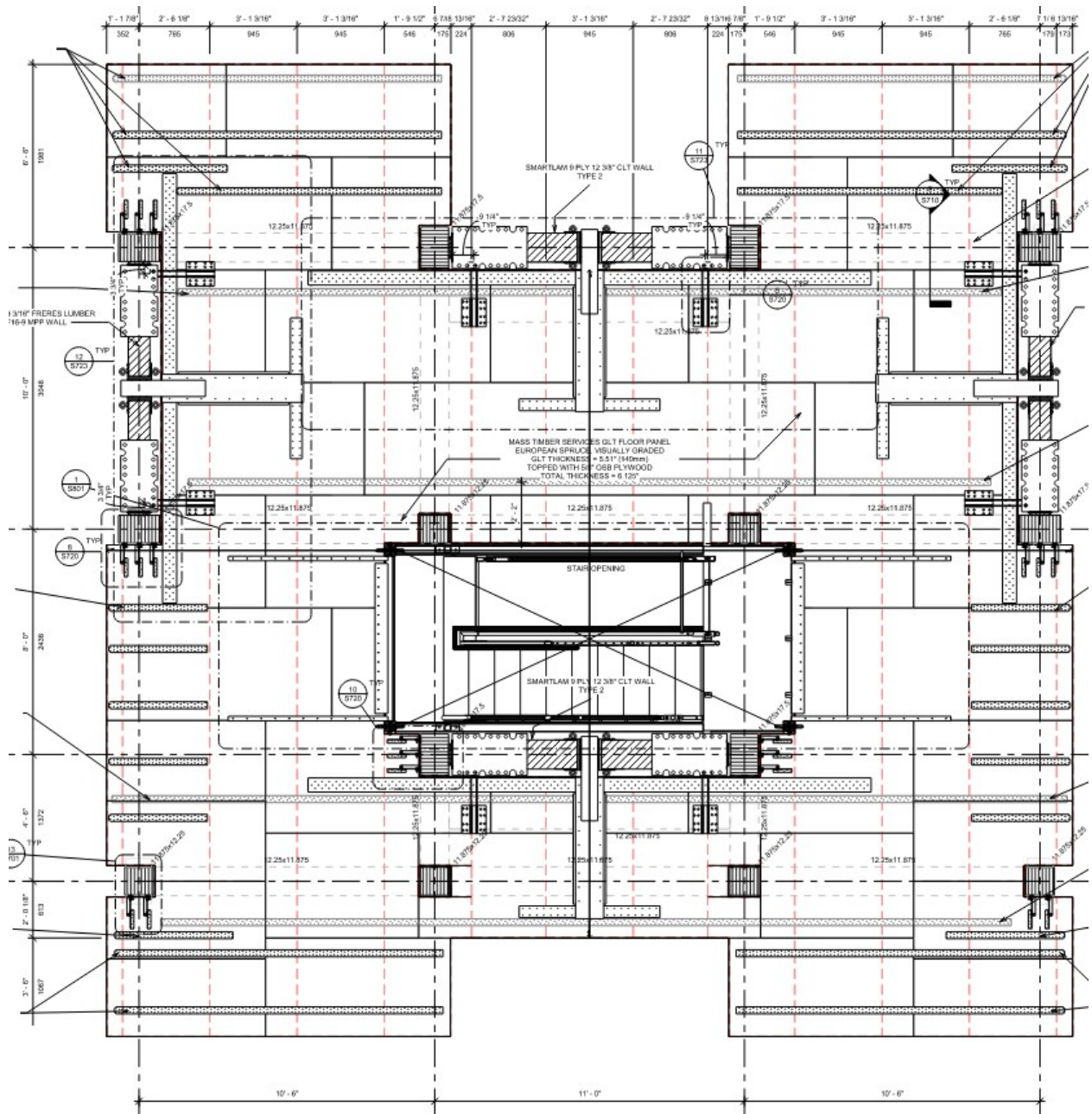


Figure 3.5: Typical GLT Layout

The GLT was Grade GL24h [OIB, 2020]. The following material properties of lumber are summarized below in Table 3.4: strong axis modulus of elasticity (E_0), weak axis modulus

of elasticity (E_{90}), strong axis shear modulus (G_0), and weak axis shear modulus (G_{90}). The weak axis properties were assumed to be 0 since GLT was considered a one-way diaphragm. The shear modulus was calculated using a G/E ratio of 0.078 pulled from Table 5-1 of the FPL Handbook [Forest Products Laboratory, 2010].

Table 3.4: GLT Material Properties

Material Property	Value
E_0 (ksi)	1,667.93
E_{90} (ksi)	0
G_0 (ksi)	130.1
G_{90} (ksi)	0

Using the material properties from above, the sections properties of the GLT were determined. The key section properties for the GLT were the effective axial stiffness (EA_{eff}), bending stiffness (EI_{eff}), and shear stiffness (GA_{eff}) for both the strong and weak axes. Basic stiffness equations were used to determine the section properties of the GLT (Equations 3.7–3.9). The section properties in the weak axis were assumed to be 0 since GLT was considered a one-way diaphragm. Table 3.5 below summarizes the section properties per ft of GLT.

$$EA_{eff} = E_0(bt) \quad (3.7)$$

$$EI_{eff} = E_0\left(\frac{1}{12}bt^3\right) \quad (3.8)$$

$$GA_{eff} = G_0(bt) \quad (3.9)$$

Table 3.5: GLT Section Properties

Section Property	Strong Axis	Weak Axis
EA_{eff} ($10^6 \text{ lbf}/\text{ft}$)	110.28	0
EI_{eff} ($10^6 \text{ lbf} - \text{in}^2/\text{ft}$)	279.02	0
GA_{eff} ($10^6 \text{ lbf}/\text{ft}$)	8.6	0

3.3.4 Nail and Dowel Laminated Timber

The NLT and DLT panels were supplied by StructureCraft. Each panel measured up to approximately 6 ft wide and spanned up to the full 34 ft. The panels were approximately 6 in thick including the plywood topping. NLT panels comprised the floor diaphragm for Floor 6, and DLT panels comprised the floor for Floor 7. The panels were connected by an 8 in wide and 5/8 in thick OSB plywood splice strap. Figure 3.6 illustrates the typical NLT or DLT layout.

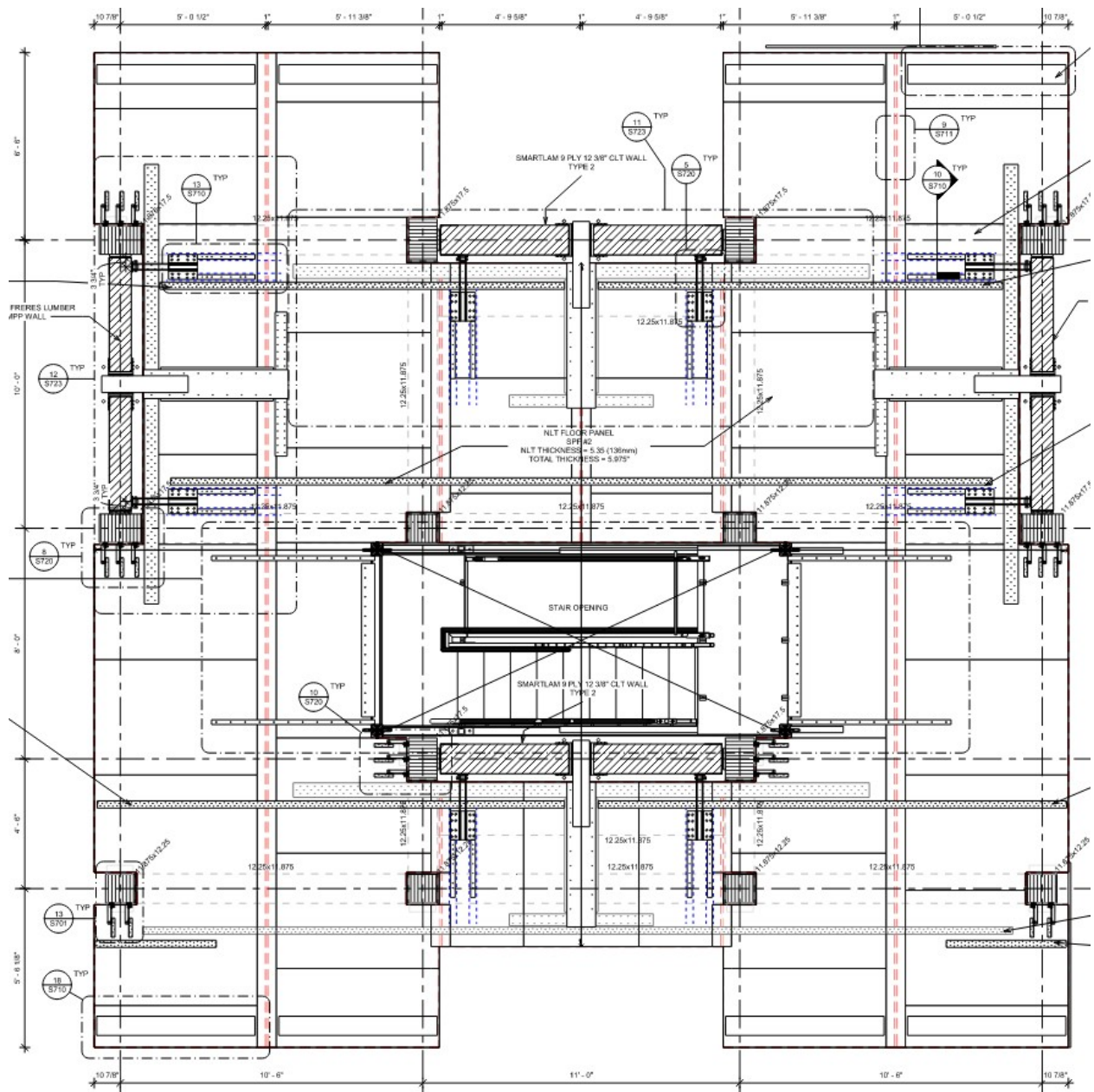


Figure 3.6: Typical NLT/DLT Layout

StructureCraft [2021] provided the material properties for the NLT and DLT panels. The material properties of the SPF #2&btr are summarized below in Table 3.6: strong axis modulus of elasticity (E_0), weak axis modulus of elasticity (E_{90}), strong axis shear modulus

(G_0), and weak axis shear modulus (G_{90}). The weak axis properties were assumed to be 0 since NLT and DLT were considered one-way diaphragms. The shear modulus was calculated using a G/E ratio of 0.078 pulled from Table 5-1 of the FPL Handbook [Forest Products Laboratory, 2010].

Table 3.6: NLT and DLT Material Properties

Material Property	Value
E_0 (ksi)	1,400
E_{90} (ksi)	0
G_0 (ksi)	109.2
G_{90} (ksi)	0

Using the material properties from above, the sections properties of the NLT and DLT were determined. The key section properties for the NLT and DLT were the effective axial stiffness (EA_{eff}), bending stiffness (EI_{eff}), and shear stiffness (GA_{eff}) for both the strong and weak axes. The same basic stiffness equations used for the GLT (Equations 3.7–3.9) were used to determine the section properties of the NLT and DLT. Table 3.7 below summarizes the section properties per ft of NLT and DLT.

Table 3.7: NLT and DLT Section Properties

Section Property	Strong Axis	Weak Axis
EA_{eff} ($10^6 lbf/ft$)	89.88	0
EI_{eff} ($10^6 lbf - in^2/ft$)	214.38	0
GA_{eff} ($10^6 lbf/ft$)	7.01	0

3.3.5 *Veneer Laminated Timber*

The VLT panels were supplied by Boise Cascade and are a type of mass plywood panel. Each panel measured up to 4 ft wide and spanned up to the full 34 ft. The panels were 6-ply VLT and measured approximately 6.375 in thick. Each ply is a LVL lamination. VLT floors comprised the floor diaphragm for Floors 8–11. The panels were connected together by a Simpson Strong Tie diaphragm spline strap which was screwed to each panel. Figure 3.7 illustrates the typical VLT layout.

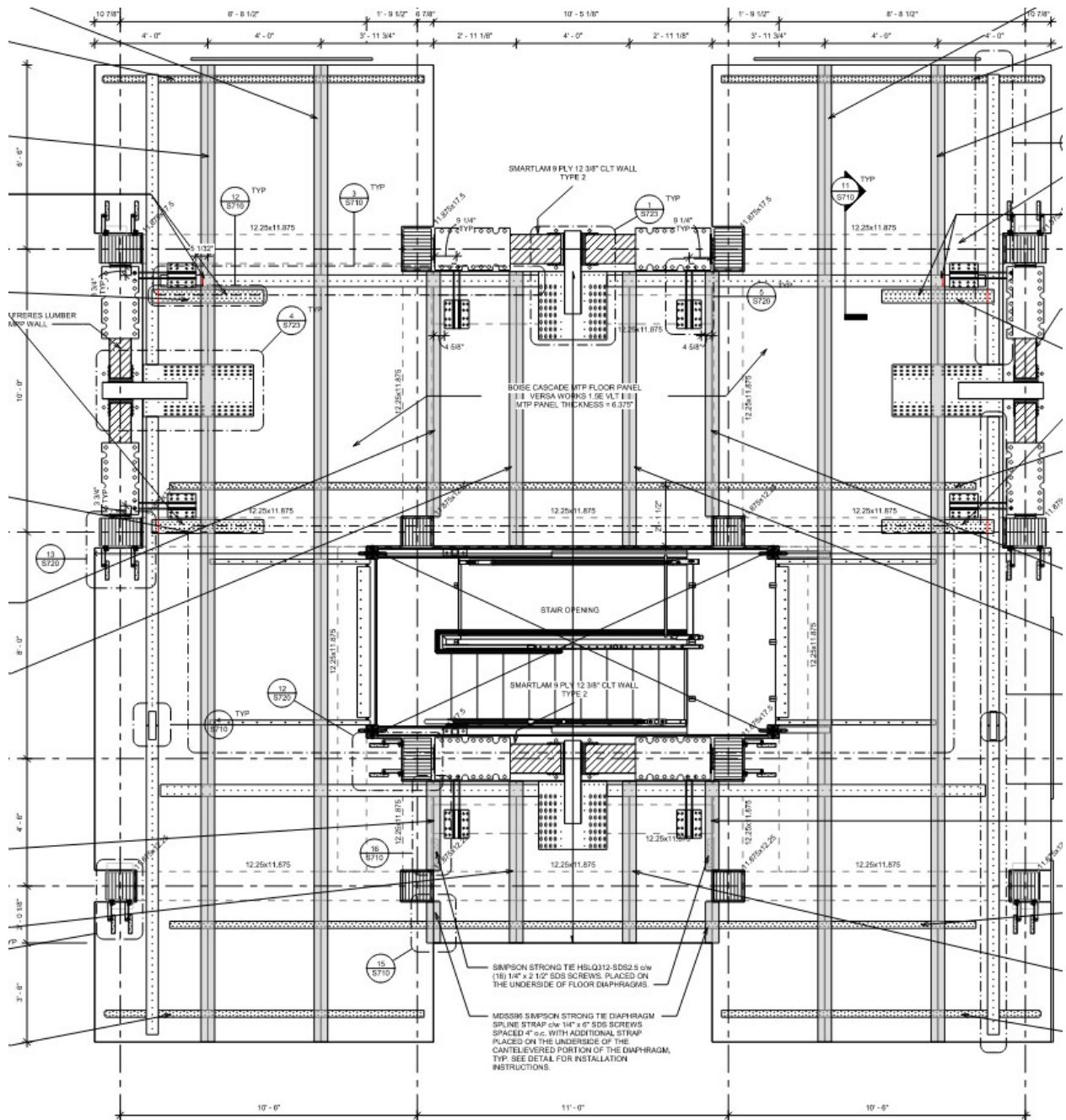


Figure 3.7: Typical VLT Layout

Boise Cascade [2022] provided the section properties for the VLT. No material properties were needed for the VLT since the section properties were provided. The key section

properties for the VLT were the effective axial stiffness (EA_{eff}), bending stiffness (EI_{eff}), and shear stiffness (GA_{eff}) for both the strong and weak axes. Boise Cascade [2022] did not test the weak axis for 6-ply VLT panels. The effective stiffness of the 1, 2, and 3-ply panels divided by the moment of inertia of each section size to calculate the modulus of elasticity for test. These values were averaged to find the effective modulus of elasticity for the weak axis: 63.53 ksi. Using the effective modulus of elasticity, the weak axis section properties were determined using the basic stiffness equations. Table 3.8 below summarizes the section properties per ft of VLT.

Table 3.8: VLT Section Properties

Section Property	Strong Axis	Weak Axis
EA_{eff} ($10^6 lbf/ft$)	114.75	4.83
EI_{eff} ($10^6 lbf - in^2/ft$)	380	16.36
GA_{eff} ($10^6 lbf/ft$)	2.6	0.42

3.4 Diaphragm Construction

Each floor panel was constructed by the manufacturer before being transported to site for installation. The floor diaphragms were installed one panel at a time for each floor. The panels were lifted into place using a crane. The panels were then connected by the spline straps or plywood onsite after installation. Figures 3.8 and 3.9 below show the installation of the floor panels.



Figure 3.8: Crane Lifting Panel



Figure 3.9: Workers Guiding Panel Into Place

3.5 Design of Other Building Elements

The NHERI TallWood 10-Story Test focuses on more than floor diaphragms. The design of the other building elements (structural rocking walls, nonstructural walls, and stairs) are briefly described in the following sections.

3.5.1 Structural Rocking Walls

The rocking walls materials were CLT in the East and West directions and MPP in the North and South directions. The walls were post-tensioned the full height with threaded rod. Columns bound both sides of the rocking walls. UFPs were designed at each floor connecting the rocking walls to the boundary columns, allowing the walls to dissipate energy. The rocking walls were designed using performance based seismic design methodologies with nonlinear numerical modeling completed in OpenSees [[Wichman, 2023](#)].

3.5.2 Nonstructural Walls

Three types of nonstructural walls were used in the 10-story building: a curtain wall, steel exterior walls, and steel interior walls. The walls were designed for wind, seismic, and gravity loads using LRFD load cases found in ASCE 7-16 [[ASCE, 2016](#)]. Although the load case design was performed, drift compatibility design was the main focus. The nonstructural walls were detailed with a slip compatible connections to prevent drift in the walls during lateral drift of the structural system. The curtain wall was glass with steel framing and was connected to the northwest section of the building from the ground up to Floor 3 [[Wynn et al., 2022](#)]. The other exterior walls were cold-formed steel framed and were connected to the rest of the exterior from the ground up to Floor 4 [[Roser et al., 2022](#)]. Each section of exterior wall contained different details. The interior walls were cold-formed steel framed and were located at various location on the floor diaphragm on Floors 4-6 [[Ji et al., 2022](#)].

3.5.3 Stairs

The stairs used in the 10-story test were prefabricated steel stairs. The stairs were located in the center of the floor diaphragm to provide access to each floor. The stairs were self-supporting for eight stories, but the top two stories transferred gravity loads to the floor columns [Sorosh et al., 2022a]. The stairs were analyzed using a finite element numerical model and were designed for drift compatibility under the ground motions [Sorosh et al., 2022b].

Chapter 4

INSTRUMENTATION AND EXPERIMENT PROTOCOL

4.1 Introduction

This chapter discusses the instrumentation used during the testing of the 10-story building. The discussion of instrumentation is limited to the sensors used to measure the vertical response of the floors. For a complete description of the instrumentation measuring the lateral response see [Wichman \[2023\]](#) and [Busch \[2023\]](#). Then, the two types of vertical excitation experiments were performed on the floors of the NHERI TallWood Project's 10-Story building are discussed. The first test was a heel drop test to identify the floor frequencies and the second test was a series of vertical seismic ground motions. This chapter outlines the methods used for each test.

4.2 Instrumentation

To record accelerations in the vertical directions, accelerometers were used during the tests. The accelerometers were placed at various locations on the floors that correspond to high movement locations in the mode shapes of the floors which are discussed in [Chapter 5](#). The northeast cantilever (NEC) and southwest cantilever (SWC) were placed at the end of each cantilever. The central span (CS) and west span (WS) accelerometers were placed at the middle of each span. These locations correspond to heel drop testing locations discussed in [Section 4.3](#). Accelerometers were also placed at the end of a beam near the center of mass (COM) to capture the input vertical floor at each level. There was also an accelerometer located at the center of the shake table which was used to capture the input ground motion. The possible locations for the accelerometers on each floor are illustrated below in [Figure 4.1](#), and [Table 4.1](#) summarizes which accelerometer locations were used at each level. The

acceleration data collected by the vertical accelerometers were used for the data analysis discussed in Chapter 7.

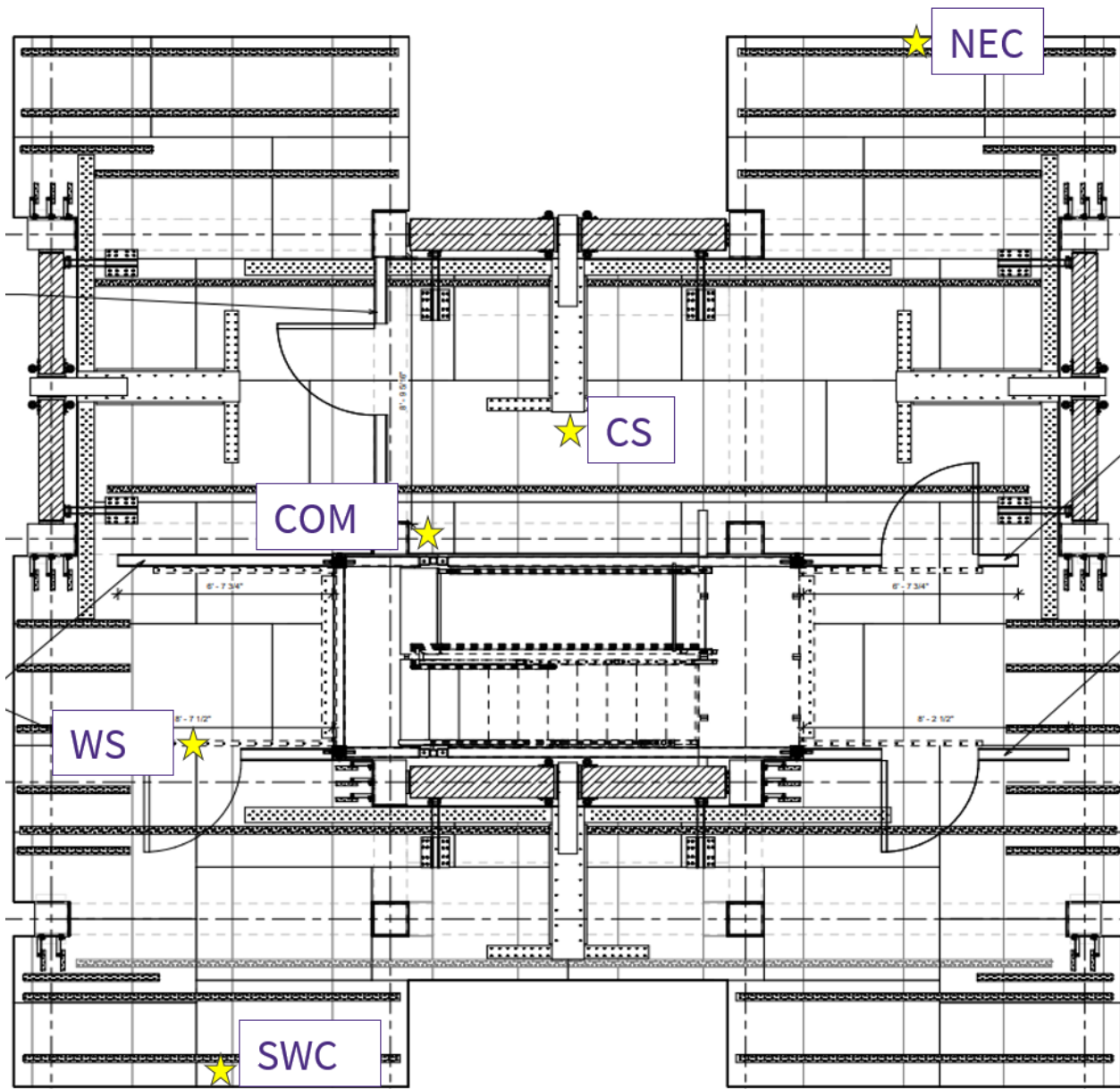


Figure 4.1: Possible Vertical Accelerometer Locations

Table 4.1: Accelerometer Locations by Level

Level	COM	NEC	SWC	WS	CS
2	X	X	X	X	
3	X	X	X	X	
4	X	X	X		X
5	X	X	X	X	
6	X	X	X	X	
7	X	X			
8	X	X	X	X	
9	X	X			X
10	X		X	X	
11	X	X	X	X	

4.3 Heel Drop Testing

To identify the frequencies of the different floor types and spans, heel drop tests were performed at each level at the NEC, CS, WS, and SWC locations in Figure 4.1. The heel drop tests were performed by KPFF using methods and instrumentation that they commonly employ to investigate the vertical vibration response of existing floor systems to human induced vibrations. To record data, KPFF provided a single accelerometer which was wired into a portable data acquisition system. The acceleration data was processed on proprietary software by KPFF identifying the natural frequencies present at each location which are presumed to be the natural frequencies for the span sections. The natural frequencies are summarized below in Table 4.2.

The floor frequencies are not consistent within each span or floor type. The identified frequencies were used to calibrate the SAP models which will be discussed later in Chapter 6.

Table 4.2: Heel Drop Test Floor Frequencies (Hz)

Level	NE Cantilever	West Span	SW Cantilever	Central Bay
2	14.1	32.8	18.7	35.2
3	14.1	32.3	18.7	35.0
4	14.1	32.7	18.9	38.3
5	16.9	25.4	18.0	35.2
6	14.5	24.5	14.2	30.3
7	17.6	26.0	16.8	39.4
8	13.1	31.1	18.3	30.3
9	12.4	31.6	17.8	28.6
10	11.2	16.7	17.5	32.5
11	11.4	26.9	17.7	32.1

4.4 Ground Motions for Seismic Testing

A design suite of ground motions was developed for use at the NHERI TallWood Project Shake Table site. The ground motions were designed for a site in the Capital Hill neighborhood in Seattle, Washington. The design suite included 11 ground motions scaled to multiple hazard levels (43, 275, 475, 975, and MCE) in accordance with ASCE 7-16 [ASCE, 2016]. The ground motions used for testing were selected from the design suite [Wichman, 2023].

The MCE hazard level vertical ground motions were scaled to match the target response spectra which was calculated for the MCE hazard level following methods from ASCE [2016]. The vertical ground motions of the remaining hazard levels were scaled down proportionately to the horizontal ground motions. Wichman [2023] provides more details on the methods used for scaling the ground motions. The target response spectra and the response spectra of the input ground motions are illustrated below in Figure 4.2. Table 4.3 summarizes the scale

factor used for vertical ground motion as well as the record ID's from the ground motion databases, the ground motion hazard level, and the earthquake name.

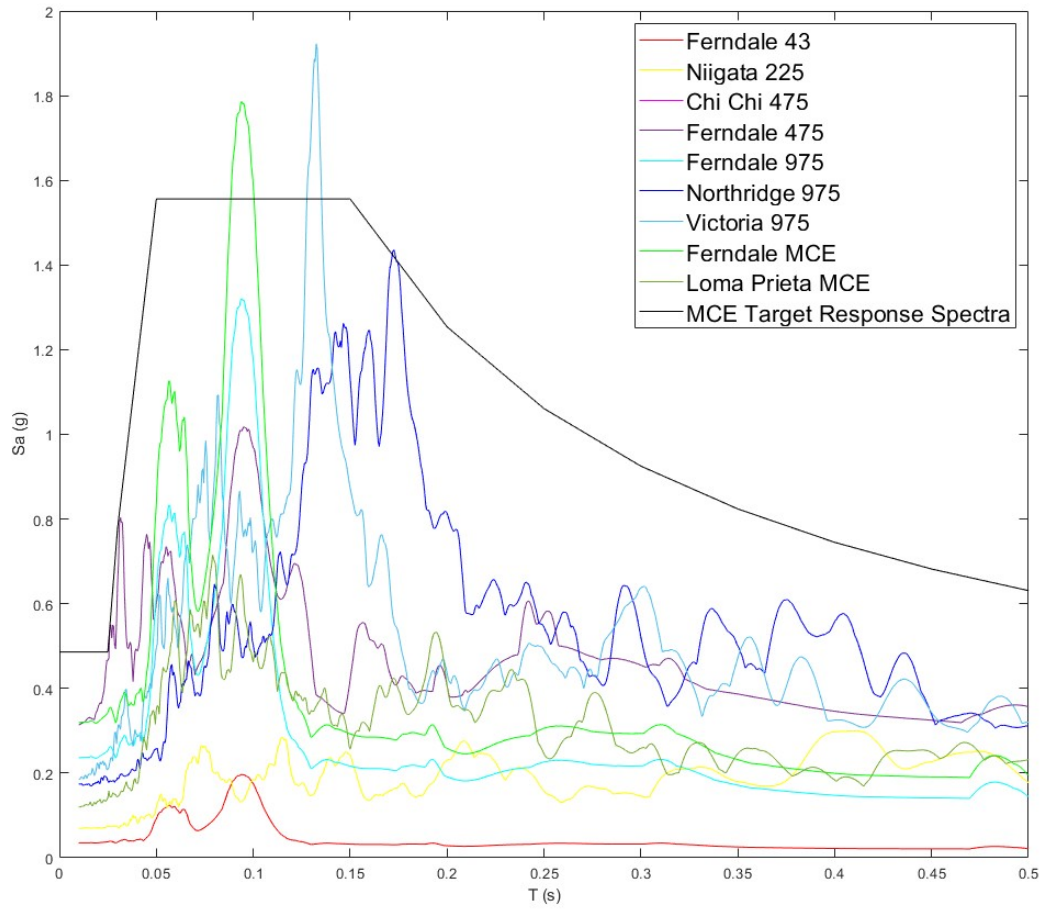


Figure 4.2: Vertical Ground Motion Response Spectra

Table 4.3: Vertical Ground Motion Scale Factors

Hazard Level	Record ID	Earthquake Name	Scale Factor
43	subRSN2000905	Ferndale	0.213
225	4213	Niigata	1
475	3471	Chi Chi	1
475	subRSN2000905	Ferndale	1
975	subRSN2000890	Ferndale	0.277
975	964	Northridge	0.716
975	268	Victoria	1
MCE	subRSN2000890	Ferndale	0.496
MCE	761	Loma Prieta	1

Chapter 5

NUMERICAL MODEL DEVELOPMENT

5.1 Introduction

The numerical models were developed using SAP2000 structural analysis software. Each floor was initially modeled as a single-story model starting with the CLT floor. Recommendations from [Breneman et al. \[2021\]](#) were used for model development. Isotropic shell elements were used to model the CLT and VLT; layered shell elements were used to model the DLT, NLT, and GLT. The isotropic shells were used since this is most-commonly used for floor models in industry. Layered shells were used for floor types that could not be accurately represented by isotropic shells [Section 5.4.3]. The single-story models were then combined into a full-building gravity-system model. This chapter discusses the development of the different models then summarizes the preliminary results of the different models.

5.2 U.S. Mass Timber Floor Vibration Design Guide Recommendations

The U.S. Mass Timber Floor Vibration Design Guide was summarized in Chapter 2. The following recommendations were in the development of the floor numerical models:

- Modeling each level individually.
- Modeling the beams and columns as frame elements and the floors as shell elements (either isotropic or layered shell elements).
- Meshing with spacing of no larger than 36 in.
- Using a damping ratio of 2% for the bare mass timber floors.

Breneman et al. [2021] also recommends using springs to model exterior nonstructural walls. Initially, springs were not incorporated in the models, but were added and will be discussed in Chapter 6.

5.3 Isotropic Shell Element Model Development

Starting with the recommendations from Breneman et al. [2021], the models of the floor systems were developed using SAP2000. This section discusses the development of the simplified, isotropic material approach for each material type.

5.3.1 Beam and Column Development and Boundary Conditions

The beams and columns were modeled using line elements. The locations of each beam align with Figure 3.1. The columns span 10' and were connected to the beams at the center. The beam and column connection does not restrain rotation, so a moment release was added to each beam end. An elastic glulam beam material was created for the beams and columns. The beams and columns were each assigned a line element section that contained the appropriate dimensions and material properties from Chapter 3. The columns were pinned at the top and bottom for the model restraints.

5.3.2 Mass Distribution

For the floor models, the mass of the floor and the wing plates were the only masses considered. The mass of the straps, stair landing, and other steel connections were ignored. The mass of the floor and wing plates were summed at each level and distributed across each floor area. The simplification of mass assumptions may have impacted the model results since mass directly affects the frequencies of the floor spans.

The mass of each floor type and the wing plate were provided by the the manufacturers of each product. The total weight of each floor (including the floor and wing plates) is summarized in Table 5.1 below.

Table 5.1: Floor Weights

	CLT	GLT	NLT/DLT	VLT
Weight (kips)	20.2	17.7	17.5	20.6

The mass of the interior nonstructural walls were considered on the applicable levels, but will be discussed in more detail later in this chapter.

5.3.3 Isotropic Floor Properties

The floor was modeled using isotropic shell elements. A generic isotropic floor material was defined for the shells with material properties close to the CLT. The material properties of the Generic Floor material are displayed below in Table 5.2. Although the rocking walls were not modeled, a lateral restraint was placed at the center joint of each wall location. These restraints removed the torsion and lateral modes from the models.

Table 5.2: Generic Floor Material Properties

Property	Value
Weight (k/in ³)	1.505 10 ⁻⁵
E (ksi)	1400
G (ksi)	700

The section properties were modified by dividing the properties in Tables 3.3 and 3.8 by the section properties of the generic floor in SAP2000. The mass of each floor was divided the mass of the generic floor to obtain the mass modifier. Table 5.3 below summarizes the section property modifiers that were calculated for each floor type. Figure 5.1 illustrates the direction of the stiffness property modifier.

Table 5.3: Isotropic Shell Element Stiffness Modifiers

Stiffness Modifier	CLT	VLT
Membrane f11 Modifier	0.488	0.045
Membrane f22 Modifier	0.721	1.0714
Membrane f12 Modifier	0.015	0.042
Bending m11 Modifier	0.256	0.045
Bending m22 Modifier	0.875	1.048
Bending m12 Modifier	0.015	0.069
Shear v13 Modifier	0.015	0.069
Shear v23 Modifier	0.015	0.422
Weight Modifier	1.198	1.643

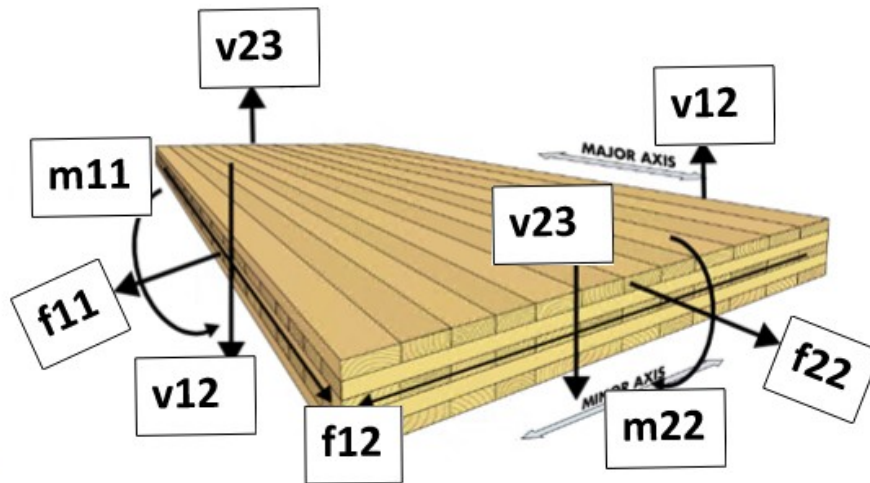


Figure 5.1: Stiffness Modifier Directions

5.3.4 Model Validation

The isotropic models were validated by comparing the deflection and fundamental modal frequency of the CLT northeast cantilever to a simple cantilever.

For the deflection validation, the cantilever beam had the same length of the north cantilever at 6.5 ft. The stiffness coefficient from Chapter 3 was adjusted for the 110 in width of the north CLT cantilever. The mass of the north CLT cantilever was applied as a distributed dead load on the cantilever beam. Equation 5.1 is the equation for cantilever deflection due to a distributed load.

$$\Delta = \frac{wl^4}{8EI} \quad (5.1)$$

The deflections due to the dead load are summarized in Table 5.4. The deflections were the same magnitude which validated that the model was working. Many variables could have contributed to the minor difference in values such as shell behavior, shear deformation, or the approximate variables in the deflection equation. However, the main reason for the difference likely stemmed from the fact that the CLT model was not really a fixed cantilever but a continuous shell element; a fixed cantilever would be expected to be stiffer than a continuous system which is reflected by the lower deflection in the representative cantilever beam.

Table 5.4: Model Validation Deflections (in)

Isotropic CLT North Cantilever	Representative Cantilever Beam
0.05	0.028

The modal properties of the isotropic CLT model were validated by comparing the first modal frequency of the north CLT cantilever to the first modal frequency of a representative

uniform cantilever beam. Equation 5.2 is the equation for the first modal frequency of a uniform cantilever beam from Chopra [2014].

$$\omega = \frac{3.516}{L^2} \sqrt{\frac{EI}{m}} \quad (5.2)$$

The modal frequencies are summarized below in Table 5.5. The frequencies were the same magnitude which validated that the model was working. The minor difference in value could have been attributed to same variables discussed with the deflection validation.

Table 5.5: Modal Frequency Validation

Isotropic CLT North Cantilever (Hz)	Representative Cantilever Beam (Hz)
15.257	19.299

5.3.5 Ground Motion Implementation

The ground motions discussed in Chapter 4 were implemented in SAP2000 using time history functions. Each ground motion was uploaded as a .csv file and assigned the corresponding dt in seconds. Figure 5.2 below shows an implemented ground motion.

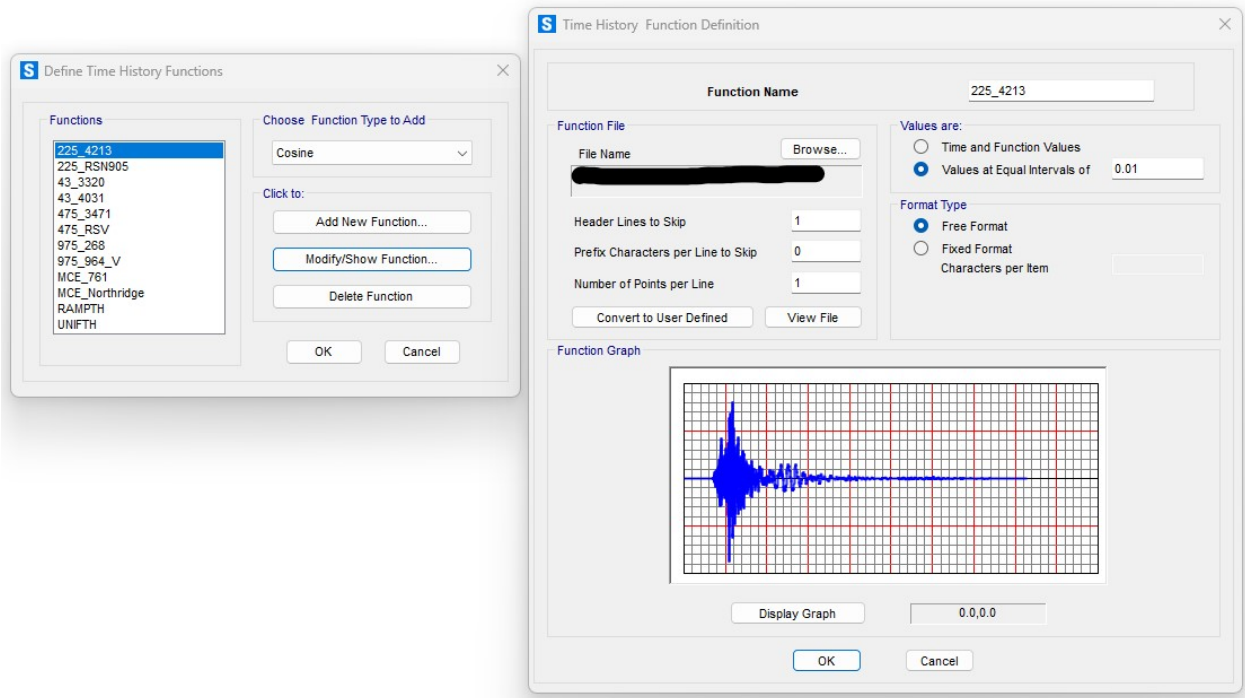


Figure 5.2: Time History Function in SAP2000

Each function was assigned a load case, so that SAP could run the analysis. The scale factor converted the ground motion from units of g to whichever desired acceleration units. In this case, 386.4 was used to achieve units of kip/s^2 . The load case is also where the modal damping ratio is set. Equivalent viscous damping of 0.02 was selected based on [Breneman et al. \[2021\]](#).

5.3.6 Area Meshing

Early in the model development, automatic area meshing was used to mesh the large area sections of the isotropic CLT model. Automatic meshing produced accurate results if the areas were drawn along beam lines; if the areas were not drawn along beam lines, then the shell could not mesh to the beam for support. Figures 5.3 and 5.4 illustrate the CLT model before and after automatic meshing.

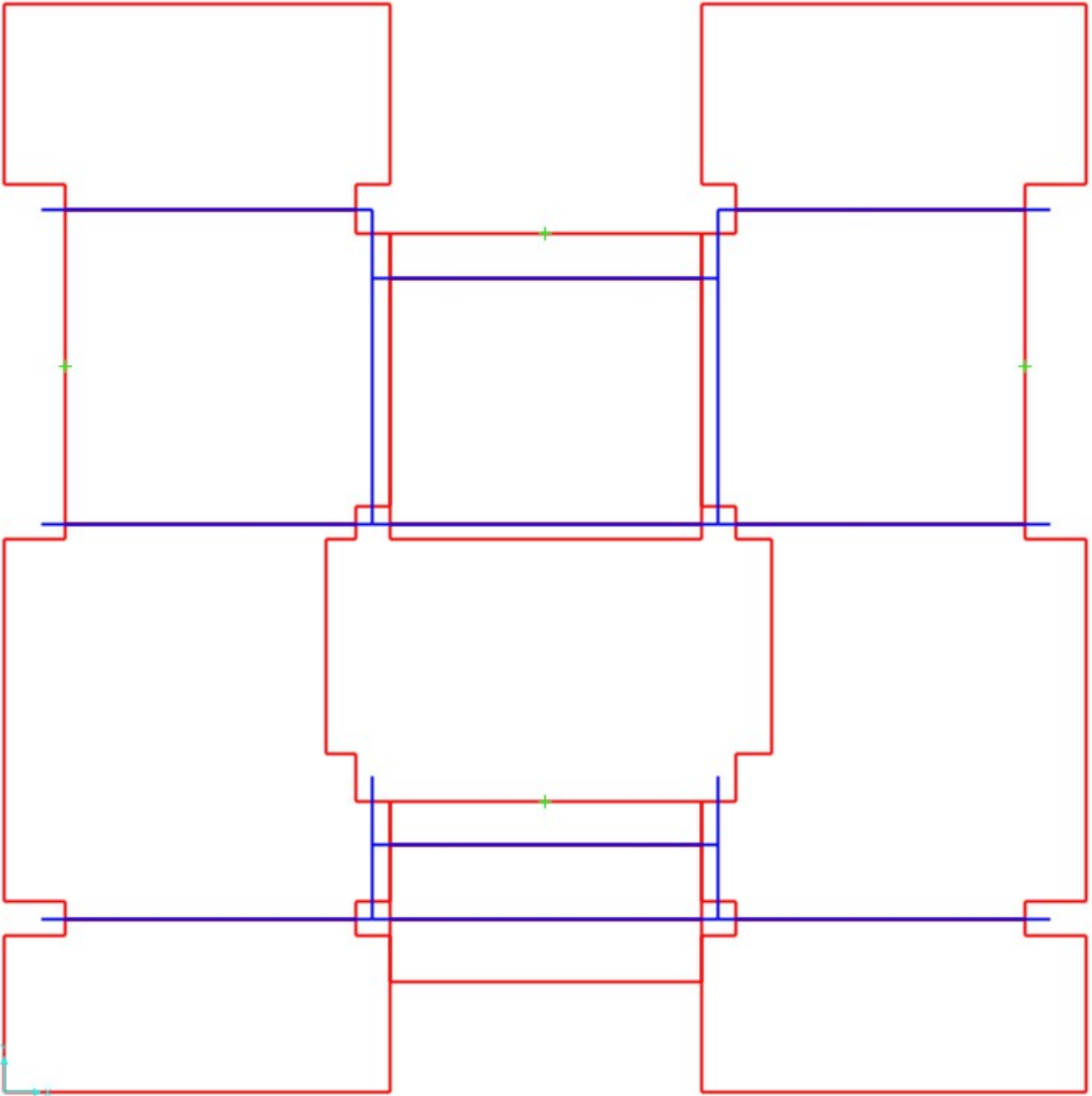


Figure 5.3: CLT Model Before Meshing

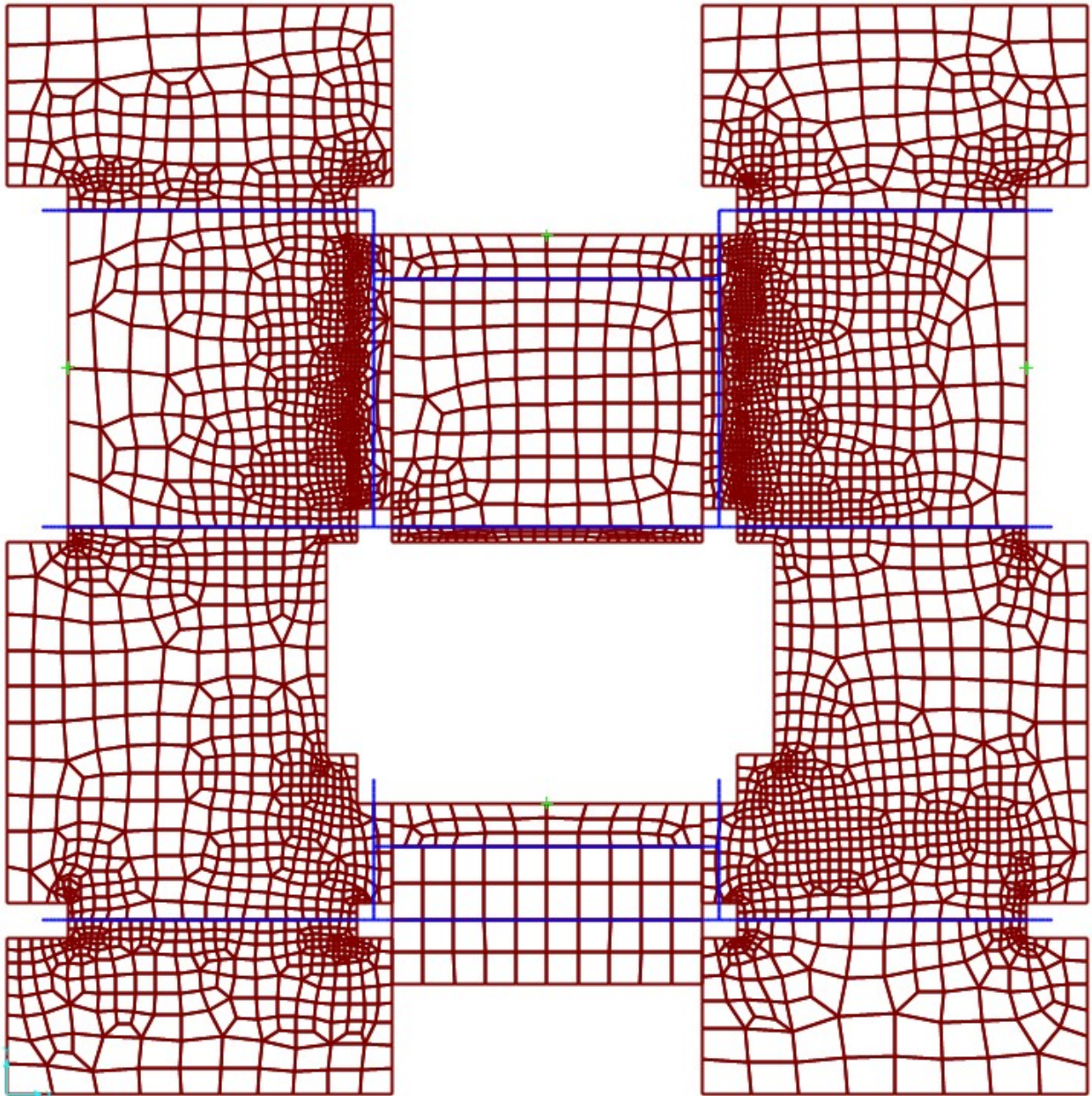


Figure 5.4: CLT Model After Automatic Meshing

After the model was validated, the CLT model was manually meshed to provide consistent results and ensure that each node was properly connected to the surrounding nodes. [Breneman et al. \[2021\]](#) recommended meshing with nodal spacing of 24 in or less. For the CLT model, the target nodal spacing was approximately 12 in for the manual mesh. SAP2000 had several tools for manually dividing the areas. The "Divide Area Into Objects of This Maximum Size" tool was convenient for rectangular areas, but could not divide non-quadrilateral areas. This tool also did not ensure that the nodes of multiple areas would align. The most convenient tools were the "Divide Area Based on Points on Area Edges" tools. The "Intersections of Visible Straight Grid Lines" was mostly used for the CLT model since the grid visually represented the mesh before dividing the areas. [Figure 5.5](#) displays the manual mesh used in the CLT model.

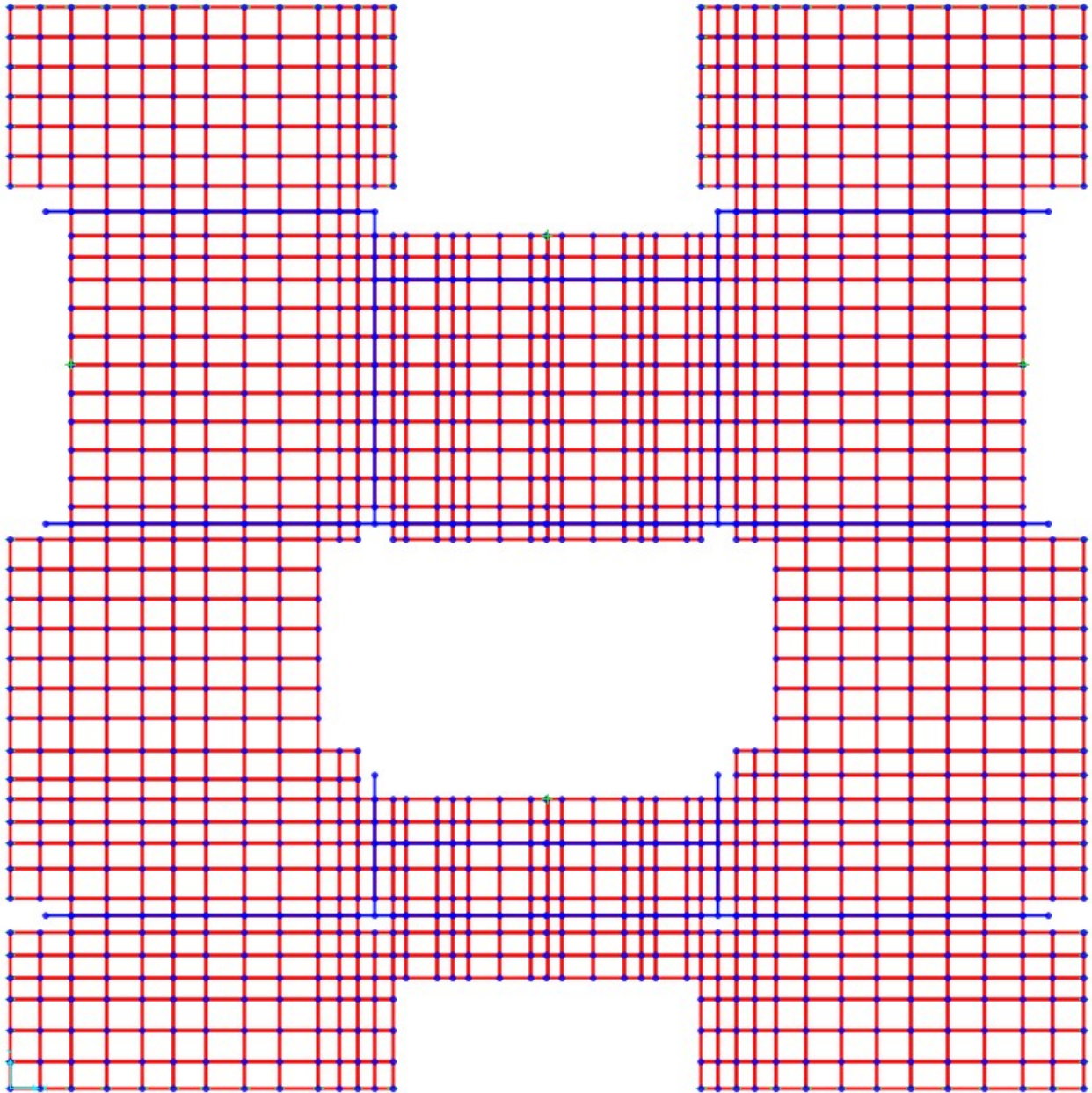


Figure 5.5: CLT Model After Manual Meshing

5.3.7 Beam to Floor Connection

When SAP2000 meshed the shell areas to the beam element, the 6 degrees of freedom were constrained (deflections and rotations). The detailed connection between each floor and the beams – see Figure 5.6 – calls for one row of screws. The single row of screws may not have fully constrained the rotation between the floor and beams.

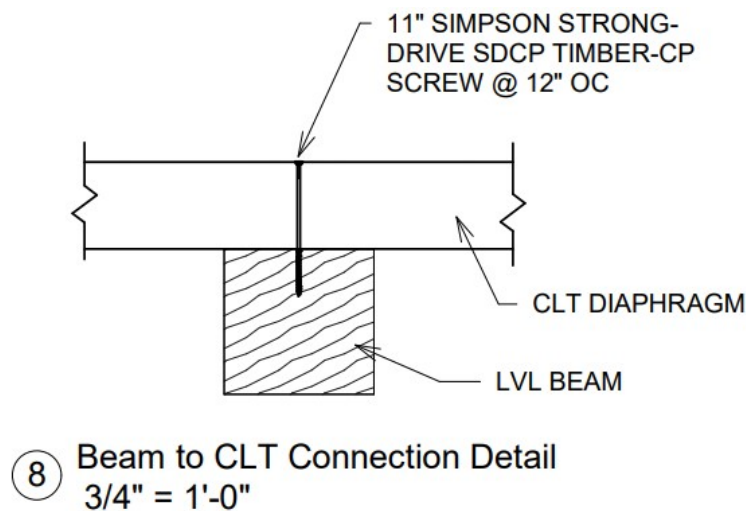


Figure 5.6: Beam to CLT Connection Detail

A second model was developed in SAP2000 to release the rotations between the floor and beams, so both could be used in model calibration. First, the beams were offset below the shell areas by 0.19 in – larger than the SAP2000 meshing tolerance – to prevent the shell and from being constrained together. Joints were added to the beam in line with the nodes of the meshed floor. A weld joint constraint was then defined to constrain the displacements of nodes. A weld constraint is a specific joint constraint that constrains the selected degrees of freedom of each node within a specified tolerance. The chosen tolerance was 0.2 in which allowed for displacement constraints between the floor and beams, but not between two floor nodes.

5.3.8 *Weak Axis Angle Support*

The VLT floors has the weak axis angles discussed in Chapter 3 to support the weak axis cantilevers. The angle was modeled using a stiff, massless line element. The line elements were inserted 0.19 in below the shell, similar to the beams, so that the rotations could be released using the previously defined weld constraint. The angles were inserted in all the locations with an angle present in the drawings [Appendix A].

5.3.9 *One-way Floor System Isotropic Shells*

The one-way floor systems (GLT, NLT, and DLT) were initially modeled using the same isotropic shell element method. The zero stiffness in the weak axis was modeled using small stiffness values in that direction. Due to the small weak axis modifiers, the weak axis cantilevers had a large deflection from the dead load. The max dead load deflection was 1.22 in. Visual inspection of the in situ floor system determined that the deflection was not that large. The isotropic method would not work for the one-way systems due to the weak axis cantilevers, so layered shell models were developed, as described in the next section.

5.4 *Layered Shell Element Model Development*

The goal of using layered shell elements was to develop a model that would reflect the weak axis bending behavior of the NLT, DLT, and GLT floors. These floor types have more resistance to negative bending than positive bending in the weak axis direction. Figure 5.7 illustrates the one-way mass timber when bending is applied in the weak axis. The weak axis cross-section contains a mass timber layer and a strap layer. When a bending moment is applied, the compression and tension forces form a couple which keeps the cross section in equilibrium. For the one-way mass timber, when the cross-section is in positive bending, the strap layer would be in compression and the mass timber layer would be in tension causing the timber to separate – resulting in no tension resistance in the moment couple. When the cross-section is in negative bending, the mass timber layer would be in compression (pushing

the timber together) and the strap layer would be in tension resolving the moment couple.

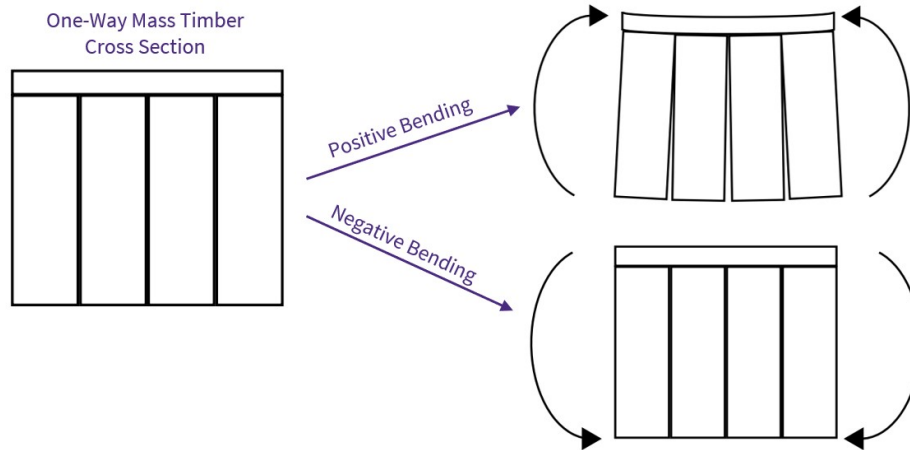


Figure 5.7: Weak Axis Cross Section in Bending

5.4.1 Square Floor Model Development

To check if a layered shell element would work for representing this behavior, a simple 10 ft by 10 ft square model was developed, pin-supported on two sides. Nonlinear properties were needed to model the compression only behavior of the NLT in the weak axis. The NLT material was assigned the given modulus of elasticity of 1400 ksi, and the nonlinear stress-strain curve was adjusted to be a compression only elastic material. Figure 5.8 below illustrates the stress-strain curve used for the simple model.

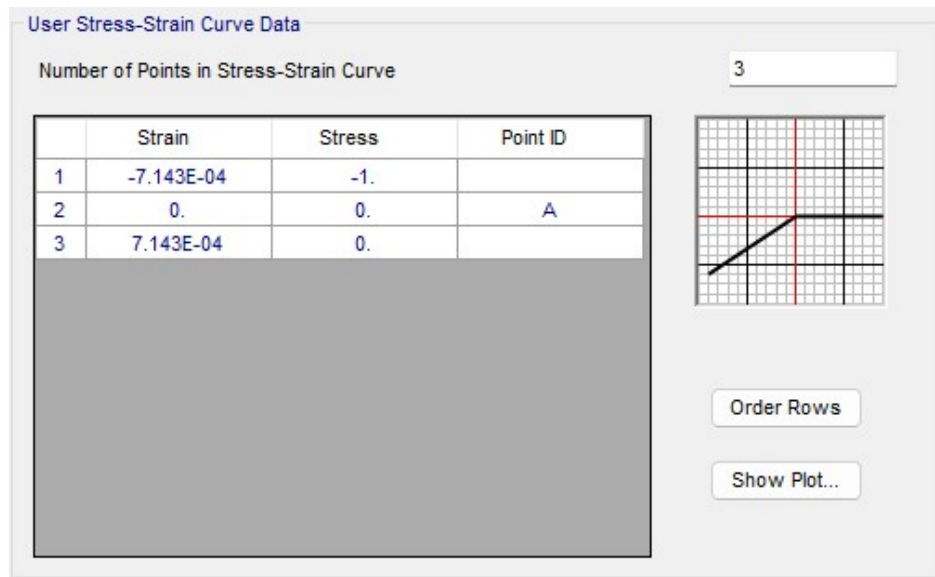


Figure 5.8: NLT Stress-Strain Curve

Figure 5.9 illustrates the cross section used for the simple model. The strap layer was a steel layer representing the diaphragm straps on the different floors. The steel had a modulus of elasticity of 29,000 ksi. The mass timber layer was assigned the NLT material from Figure 5.8. The thickness of both layers are labeled on the figure. Layered shell elements allowed for the individual layers to be linear, nonlinear, or inactive in each stress component direction. Table 5.6 summarizes the behavior of each layer in the different component axes.

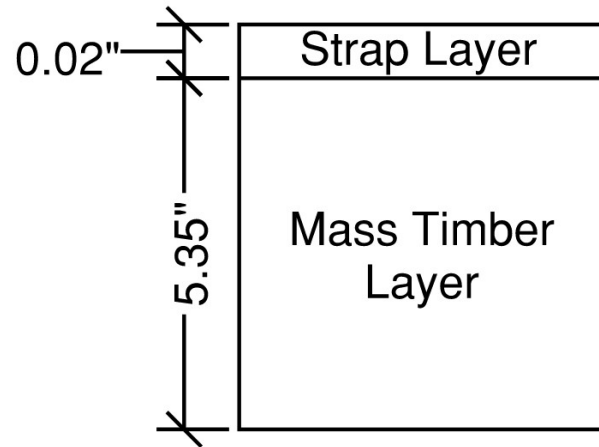


Figure 5.9: Simple Model Shell Element Layers

Table 5.6: Simple Model Shell Element Layer Behaviors

Layer	Strong Axis Direction	Weak Axis Direction
Strap	Inactive	Linear
Mass Timber	Linear	Nonlinear

A dead load was applied to the simple model in the positive vertical direction, to test the negative bending resistance of the cross section. The resultant peak deflection was 1.978 in. To validate the results, a second deflection was calculated using Equation 5.3, the deflection equation for a simply supported beam. The effective stiffness of the cross section (EI) was calculated using a cross section analysis similar to a reinforced concrete beam – the method is described below.

$$\Delta = \frac{5wl^4}{384EI} \quad (5.3)$$

The cross section analysis started by defining parameters of the cross section and materials: the thickness of the wood (t_w) was 5.35 in, the thickness of the steel (t_s) was 0.183

in, the width (b) was 120 in, the modulus of elasticity of the wood (E_w) was 1,400 ksi, and the modulus of elasticity of the steel (E_s) was 29,000 ksi. A generic neutral axis (x) and curvature (Φ) were assumed. The strain was calculated at the bottom fiber of the wood and at the center of the steel using Equations 5.4 and 5.5. The stresses were calculated by multiplying the strains by the respective modulus of elasticity [Equation 5.6]. The wood above the neutral axis was in tension, and the tensile stress was considered to be zero. The compression (C) and tension (T) forces in the wood and steel were calculated using Equations 5.7 and 5.8, respectively. The tension and compression forces were not initially equal which meant the cross section was not in equilibrium. A new neutral axis was selected until the compression and tension were equal. The moment (M) in the cross section was calculated by multiplying the forces by the distance to the neutral axis [Equation 5.9]. Finally, the effective stiffness was calculated using Equation 5.10, and could be used to calculate the beam deflection. Figure 5.10 illustrates the above process of cross section analysis.

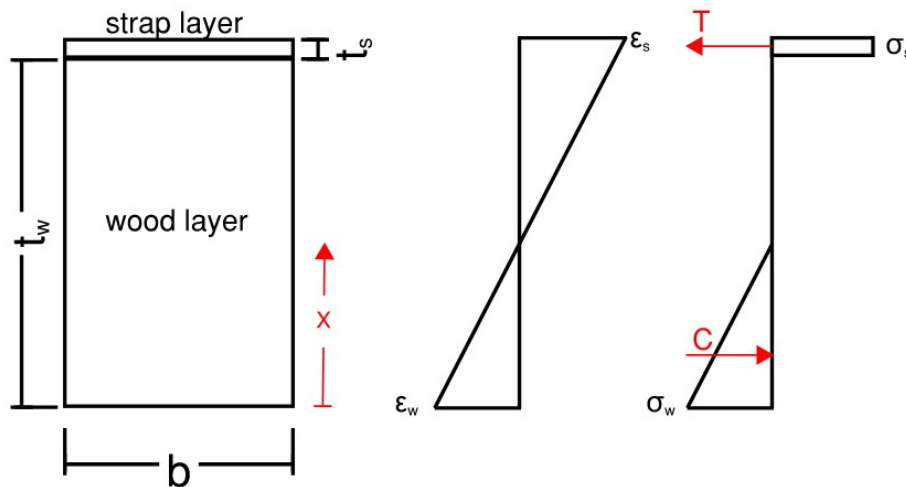


Figure 5.10: Cross Section Analysis Illustration

$$\epsilon_w = x * \Phi \quad (5.4)$$

$$\epsilon_s = (tw + \frac{ts}{2} - x) * \Phi \quad (5.5)$$

$$\sigma = \epsilon * E \quad (5.6)$$

$$C = \sigma_w * b * \frac{x}{2} \quad (5.7)$$

$$T = \sigma_s * b * tw \quad (5.8)$$

$$M = (C * \frac{2x}{3}) + (T * (tw + \frac{ts}{2} - x)) \quad (5.9)$$

$$EI = \frac{M}{\Phi} \quad (5.10)$$

The deflection of the simple-support beam was 1.996 in. Table 5.7 summarizes the results. The results validated the layered shell worked in negative bending. A dead load was applied in the negative direction to check if the simple model worked for positive bending. An error occurred while analyzing the model since the deflection was too large. This result was expected since the only resistance to positive bending was the thin steel strap.

Table 5.7: Simple Layered Shell Model Deflection Validation (in)

Simple Model	Simply Supported Beam
1.978	1.996

5.4.2 Square Model Development with an Orthotropic Material

The simple floor model in Section 5.4.1 worked in one direction in bending, but needed to be updated to reflect the modulus of elasticity in the strong and weak axes. The simple model was updated to include an orthotropic NLT material in place of the isotropic material used before. The NLT had a modulus of elasticity of 1400 ksi in the strong axis direction but a modulus of elasticity of 95.2 ksi in the weak axis direction to reflect the perpendicular to

grain compression strength. Using the dead load applied in the positive vertical direction, the peak deflection was found for the strong and weak axis by alternating which sides the pin-supports were on. These deflections were compared to simply supported beam deflections calculated using the cross section analysis as before. Table 5.8 compares the results from the two methods.

Table 5.8: Orthotropic Material Model Deflection Validation

Model	Strong Axis Deflection (in)	Weak Axis Deflection (in)
SAP	1.037	2.297
Representative Beam	1.049	16.624

The values for the strong axis were close, but the values for the weak axis were significantly different. Investigation into the SAP Manual revealed that layered shells only use the strong axis modulus of elasticity of the orthotropic material when computing the section properties in both the strong and weak axes. Therefore, the 95.2 ksi modulus of elasticity in the weak axis was ignored when computing section properties.

5.4.3 Strong and Weak Axis Layered Shell Development

To solve the issue with the orthotropic material, the simple model was updated to include two NLT layers – one layer for the strong axis and one for the weak axis. The strong axis layer used the NLT material with a modulus of elasticity 1400 ksi. The weak axis layer used a new NLT weak axis material with a modulus of elasticity of 95.7 ksi and zero mass. The compression-only stress-strain diagram was applied to the weak axis material. Figure 5.11 illustrates the layers of the cross-section in each direction.

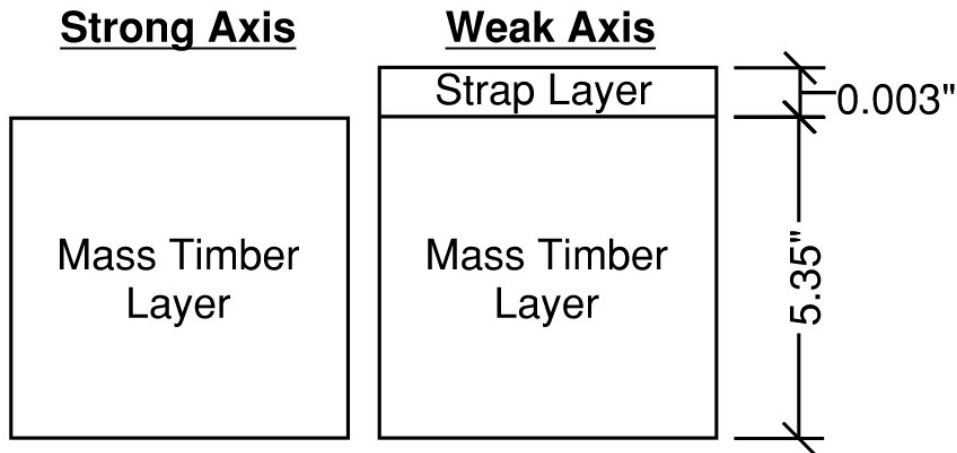


Figure 5.11: Multiple Layer Model Cross Section

Table 5.9 compares the deflection results of the multiple layered SAP model with the simple-support beam deflections. The difference in values for both the strong and weak axis were minor. Therefore, the multiple layer approach was validated as working.

Table 5.9: Multiple Layer Model Deflection Validation

Model	Strong Axis Deflection (in)	Weak Axis Deflection (in)
SAP	1.037	16.405
Representative Beam	1.049	16.624

5.4.4 Layered Shell Development Application to 10-Story Building Floor Systems

The layered shell method described in Section 5.4.3 was validated and needed to be applied to the one-way floor systems of the NHERI TallWood Project 10-story building. Three layers were used for the cross-section of the mass timber floors, similar to Figure 5.11. Since the manufacturer provided the same material properties for the NLT and DLT floor systems, they were combined into the same model. A separate model was developed for the GLT.

The floors were divided into four sections, so that the diaphragm straps could be distributed into appropriate sections. The four sections were divided by the beams: north cantilever, north span, south span, and south cantilever. Figure 5.12 overlays the section names onto the floor drawing. Instead of a diaphragm strap, the cantilevers had a strongback which was two 3x pieces of lumber nailed across the cantilever to support the weak axis. The strongbacks and straps were distributed across the cross section by distributing the areas across the width. Table 5.10 summarizes the properties of each layer for the different floor sections.

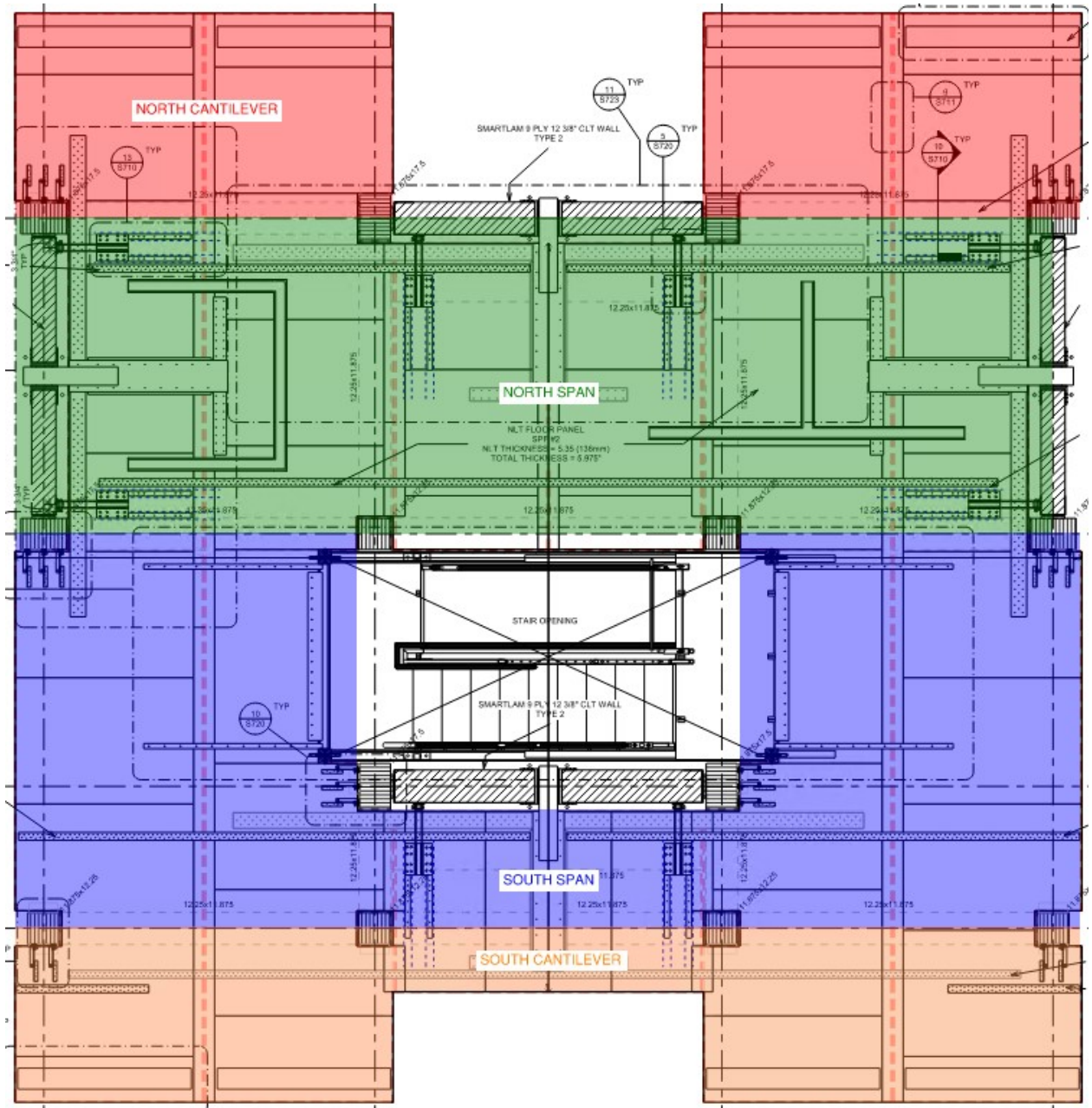


Figure 5.12: Strap Distribution Floor Section Labels

Table 5.10: One-Way Mass Timber Layer Definitions

Section	Layer	t (in)	E (ksi)
	Strap	0.005	29,000
NLT/DLT North Cantilever	SA Mass Timber	5.35	1,400
	WA Mass Timber	5.35	95.7
	Strap	0.002	29,000
NLT/DLT North Span	SA Mass Timber	5.35	1,400
	WA Mass Timber	5.35	95.7
	Strap	0.005	29,000
NLT/DLT South Span	SA Mass Timber	5.35	1,400
	WA Mass Timber	5.35	95.7
	Strongback	0.465	1,400
NLT/DLT South Cantilever	SA Mass Timber	5.35	1,400
	WA Mass Timber	5.35	95.7
	Strap	0.022	29,000
GLT North Cantilever	SA Mass Timber	5.51	1,668
	WA Mass Timber	5.51	114
	Strap	0.005	29,000
NLT/DLT North Span	SA Mass Timber	5.51	1,668
	WA Mass Timber	5.51	114
	Strap	0.019	29,000
NLT/DLT South Span	SA Mass Timber	5.51	1,668
	WA Mass Timber	5.51	114
	Strap	0.017	29,000
NLT/DLT South Cantilever	SA Mass Timber	5.51	1,668
	WA Mass Timber	5.51	114

5.4.5 Nonstructural Walls

As noted in Chapter 3, there were interior nonstructural walls on Levels 4-6. The interior walls weighed approximately 0.09 kip per ft of wall length. Due to the drift compatible connections, the nonstructural walls were assumed to add no additional stiffness to the floors. To incorporate the walls, a frame element was modeled along the center-line locations of the walls. Appendix B contains drawings of the nonstructural wall locations. The frame elements were assigned no mass or weight and small stiffness values. A line mass of $1.91\text{E-}05 \text{ kip} - \text{s}^2/\text{in}^2$ was added to each nonstructural wall element.

5.5 10-Story Model Development

The floors were combined into a full 10-story model to compare to the single-floor models and the 10-story test. The floor floor to floor heights were 11 ft typical, but was 13 ft between the ground and second floor. The base of each column was pinned, but the top of the columns were free to rotate. Each floor was modeled with the same properties and restraints as the corresponding single-story floor. Figure 5.13 displays the 10-story model in SAP.

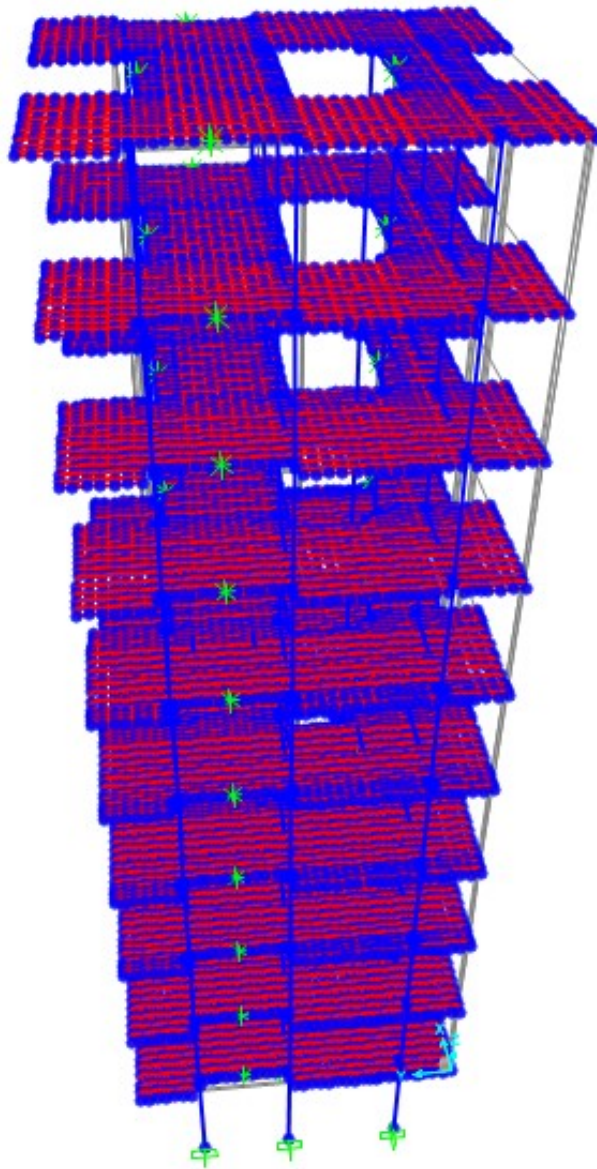


Figure 5.13: 10-Story Model

5.6 Preliminary Analysis Results

The preliminary frequency results of the single-story models are summarized in Tables 5.11 and 5.12 below. The table includes the frequency of the north cantilever, longer mid span,

short central span, and the south cantilever, as well as an image of each mode shape. The preliminary results for the 10-story model are summarized in Table 5.13. There is overlap in the 10-story model results since many of the modes lie between the fundamental mode of each span. The frequencies from the 10-story model were also lower than the single-floor models which means that modeling the full building introduces more flexibility into system.

Table 5.11: Preliminary Cantilever Results

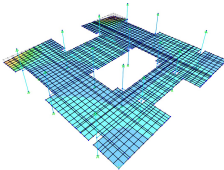
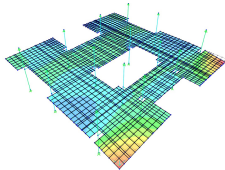
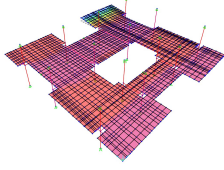
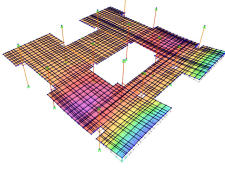
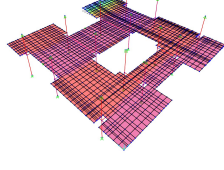
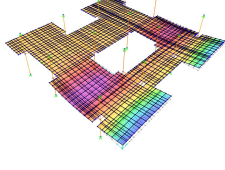
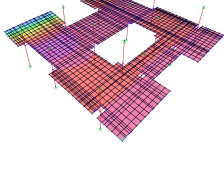
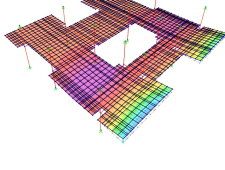
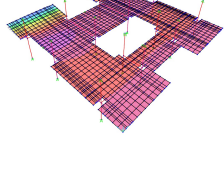
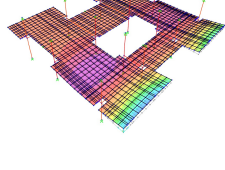
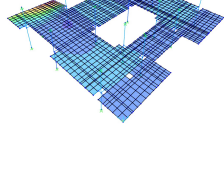
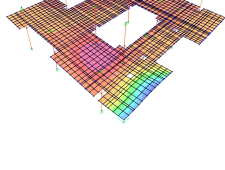
Material	Stories	North Cantilever		South Cantilever	
		Frequency (Hz)	Mode Shape	Frequency (Hz)	Mode Shape
CLT	2-3	10.076		12.66	
GLT	4	14.065		18.826	
GLT	5	13.981		17.665	
NLT	6	12.264		16.902	
DLT	7	12.409		16.908	
VLT	8-11	13.224		16.495	

Table 5.12: Preliminary Span Results

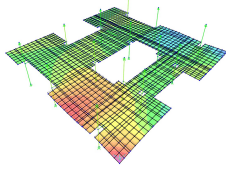
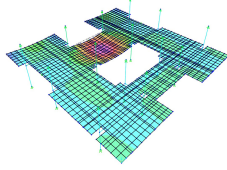
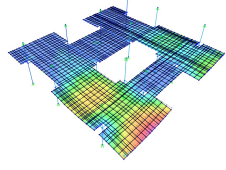
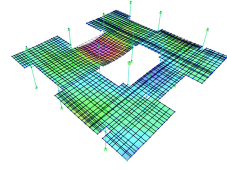
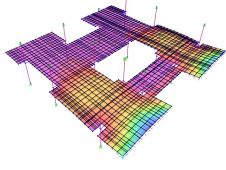
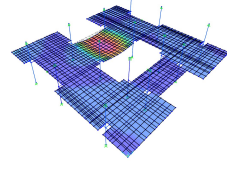
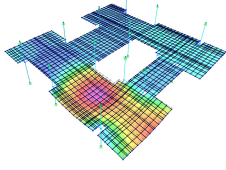
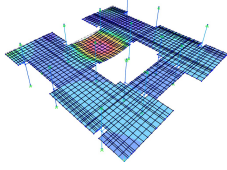
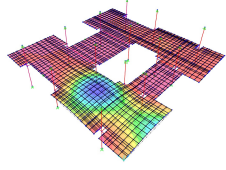
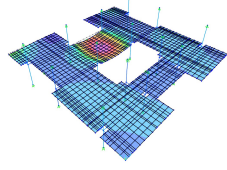
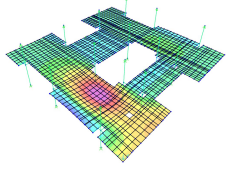
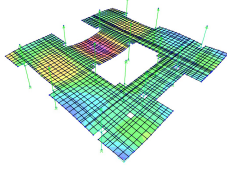
Material	Stories	Long Span		Central Span	
		Frequency (Hz)	Mode Shape	Frequency (Hz)	Mode Shape
CLT	2-3	18.971		27.232	
GLT	4	23.804		31.293	
GLT	5	22.47		29.497	
NLT	6	22.956		27.955	
DLT	7	23.025		28.702	
VLT	8-11	23.029		26.509	

Table 5.13: 10-Story Model Preliminary Results

Material	Level	NE Cantilever	SW Cantilever	West Span	Central Span
CLT	2	9.78	12.51	17.67	24.1
CLT	3	9.78	12.51	17.67	24.1
GLT	4	11.17	16.96	21.37	27.27
GLT	5	11.17	16.96	21.37	27.27
NLT	6	11.03	12.66	21.37	27.27
DLT	7	11.03	12.66	21.37	27.27
VLT	8	9.12	10.88	12.66	24.1
VLT	9	9.12	10.88	12.66	24.1
VLT	10	9.12	10.88	12.66	24.1
VLT	11	9.12	10.88	12.66	24.1

The a plot of the cumulative mass participation ratio vs the frequency for the 10-story model is shown in Figure 5.14. The largest jump in the mass participation ratio occurred at 12.66 Hz. The mode shape at this frequency is displayed in Figure 5.15. All of the north cantilevers, some of the south cantilevers, and the weak axis of some of the west spans are displacing in the mode shape.

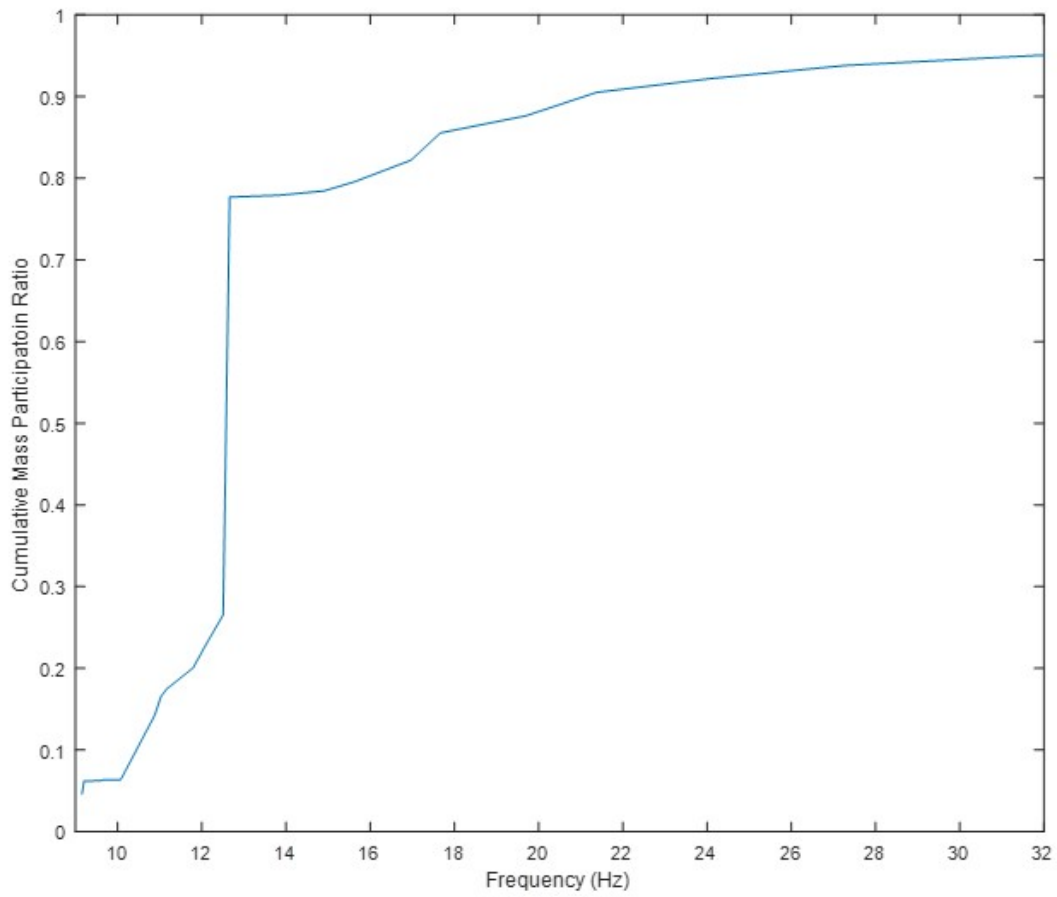


Figure 5.14: Cumulative Mass Participation Ratio

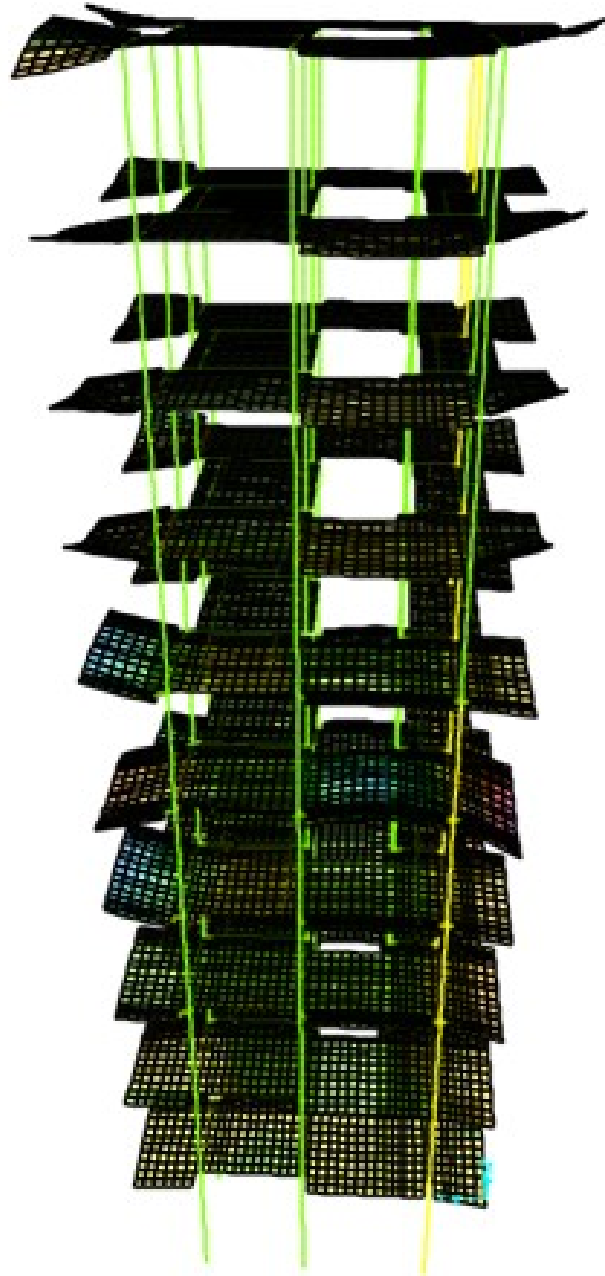


Figure 5.15: Mode Shape at 12.66 Hz

Chapter 6

NUMERICAL MODEL FREQUENCY CALIBRATION

6.1 Introduction

The single-floor SAP models were adjusted to approximately match the natural frequencies from footfall loading as shown in Table 4.2. The recorded natural frequencies were compared to the preliminary results from the single-floor models [Tables 5.11 and 5.12]. A few methods were used to adjust SAP model frequencies: redistributing the wing plate masses, accounting for length variation, stiffness adjustments, and including exterior wall springs. The methods are discussed in more detail throughout this chapter, then the adjusted SAP frequencies are compared to the heel drop test frequencies.

6.2 Comparison of Footfall and Numerical Model Natural Frequencies

Table 6.1 compares the numerical model frequencies from Tables 5.11 and 5.12 to the recorded footfall frequencies from Table 4.2. The percent difference ranged from 1% to 46%.

The central span (CS) and the west span (WS) tended to differ the most, and the numerical model natural frequencies were always lower than the footfall natural frequencies. This led to the frequency adjustment for length discussed in Section 6.4. The numerical model natural frequencies were consistently lower than footfall natural frequencies due to neglecting the exterior walls. Section 6.6 discusses the implementation of the exterior wall springs. Throughout the other floor types and spans, the results were inconsistent. This led to the stiffness adjustments discussed in Section 6.5.

Table 6.1: Numerical Model Natural Frequency Comparison to Footfall Natural Frequencies

Material		NEC	WS	SWC	CS
CLT	Original SAP Frequency (Hz)	10.08	18.97	12.66	27.32
	Measured Frequency (Hz)	14.1	35.52	18.7	35.1
	Percent Difference	29%	46%	32%	22%
GLT	Original SAP Frequency (Hz)	13.98	22.47	17.67	29.5
	Measured Frequency (Hz)	15.5	31.7	18.45	36.75
	Percent Difference	10%	29%	4%	20%
NLT/DLT	Original SAP Frequency (Hz)	12.41	23.03	16.91	28.7
	Measured Frequency (Hz)	14.5	28.37	16.8	34.85
	Percent Difference	14%	19%	1%	18%
VLT	Original SAP Frequency (Hz)	13.22	23.03	16.5	26.51
	Measured Frequency (Hz)	12.03	34.21	17.83	30.88
	Percent Difference	10%	33%	8%	14%

6.3 Redistributing Wing Plate Mass

There are four wing plates at each level which help the shear key transfer lateral forces to the diaphragm. There were two types of wing plates on the project, and each wing plate weighed several hundred pounds. In the SAP model, the weights of the four wing plates were summed and distributed across the entire floor area. The first adjustment made to the SAP models was to redistribute the mass of each wing plate by distributing each wing plate over the area of the span in which it is located. Figure 6.1 illustrates the areas each wing plate were redistributed.

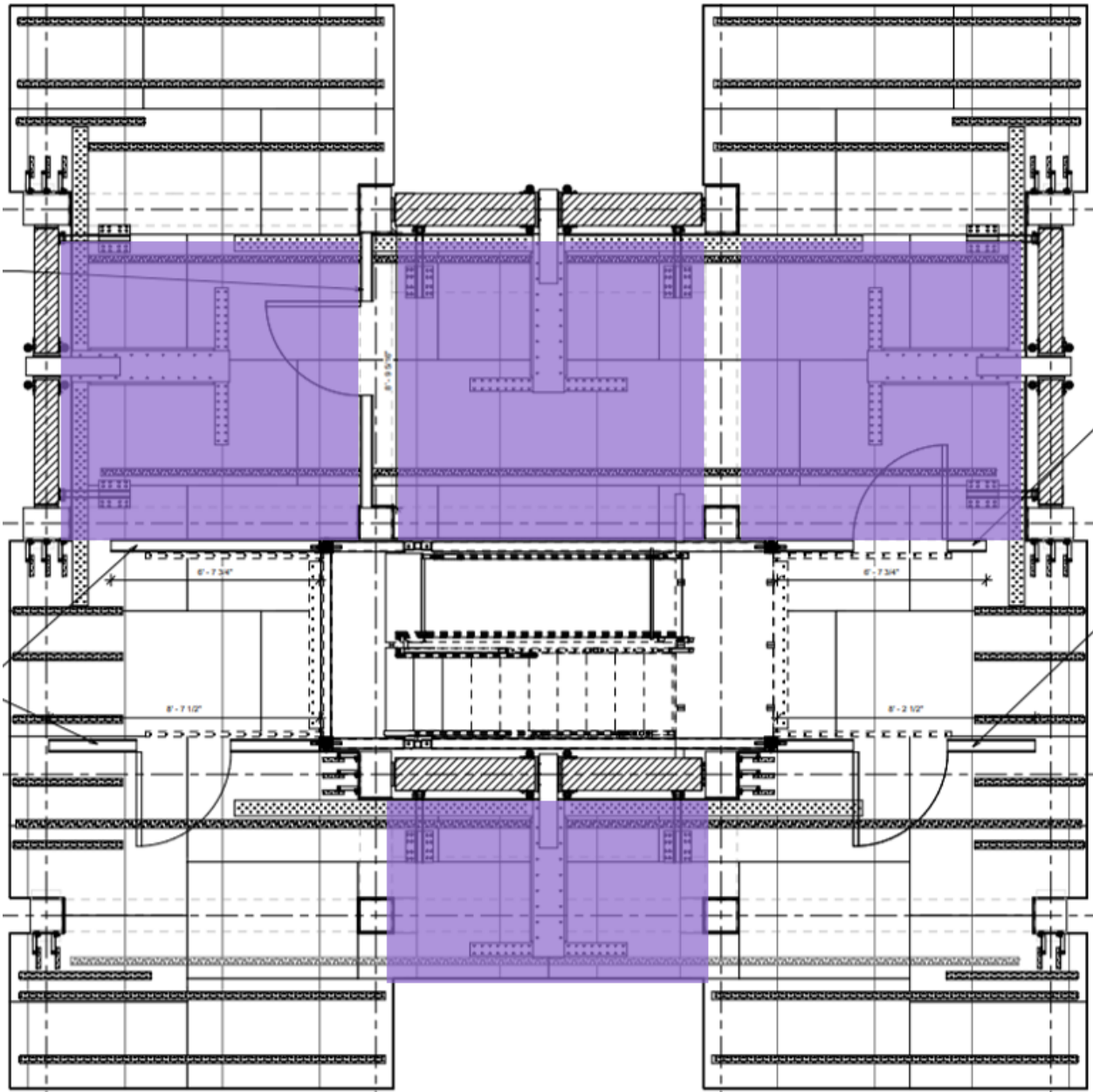


Figure 6.1: Area Distribution of Wing Plate Masses

6.4 Length Variation Adjustment

The SAP models used frame elements to model the beams which creates a center-line model. In the 10-story building, the floor spans are likely supported at the edge of the beams and not the center. The difference in length between the center-line spans and the edge support spans is large enough to cause the SAP models to underestimate the span frequency. Equations 6.1 and 6.2 [Irvine, 2010] below can be used to approximate the floor frequency of a one-way and two-way rectangular plate, respectively. For the equation, ω is the frequency, D is the stiffness coefficient, ρ is the density, h is the thickness, a is the span length, and b is the span width.

$$\omega = \sqrt{\frac{D}{\rho}} \left(\frac{3.55}{a^2} \right) \quad (6.1)$$

$$\omega = \sqrt{\frac{D}{\rho h}} \left(\left(\frac{\pi^2}{a} \right) + \left(\frac{\pi^2}{b} \right) \right) \quad (6.2)$$

Since the density, thickness, and stiffness coefficients are constant for the same floor cross-section, only the length and width change when accounting for beam edge versus center-line dimensions. Using a ratio of the edge support and center-line spans, factors were determined to increase the frequencies of the west and central spans. Equations 6.3 and 6.4 were used to calculate the factor for the west and central spans, respectively, which are summarized in Table 6.2.

$$\frac{\omega_1}{\omega_2} = \frac{a_2^2}{a_1^2} \quad (6.3)$$

$$\frac{\omega_1}{\omega_2} = \frac{\frac{\pi^2}{a_1^2} + \frac{\pi^2}{b_1^2}}{\frac{\pi^2}{a_2^2} + \frac{\pi^2}{b_2^2}} \quad (6.4)$$

Table 6.2: Frequency Increases Factors

Span	Frequency Increase Factor
West Span	1.19
Central Span	1.25

6.5 Stiffness Adjustments

The next adjustment was to change the stiffness of each floor type to match the heel drop frequencies more closely. For the isotropic shell elements, the property modifiers were adjusted; for the layered shell elements the moduli of elasticity were adjusted in each direction using trial and error. The strong axis stiffness properties heavily influenced the cantilevers while the weak axis properties were used to fine tune the west span and central span. Using the new stiffness property modifier, updated moduli of elasticity for the isotropic shell elements were back-calculated. Table 6.3 summarizes the original and adjusted moduli of elasticity for each floor type.

Table 6.3: Material Stiffness Adjustments

Material	E_{eff0} (ksi)	E_{eff0}' (ksi)	E_{eff90} (ksi)	E_{eff90}' (ksi)
CLT	1648.4	2200.3	53.7	71.7
GLT	1668	1200	114	86.5
NLT/DLT	1400	1200	95.7	95.7
VLT	1466.7	1025.4	63.1	63.1

6.6 Exterior Wall Springs

For levels two through four, spring links were added to the nodes along the outside of the floor geometry to represent the exterior walls. The WoodWorks Design Guide recommends a spring stiffness of 1.0 kip per foot of wall length [Breneman et al., 2021]. The recommended value was too stiff for these floor systems, possibly due to the slide tracks discussed in Chapter 3. The exterior wall spring stiffnesses were split into two sections: north cantilevers and south of the central span. The stiffness values for each section are summarized in Table 6.4 below. These values were reached through trial and error by starting at the recommended 1.0 kip/ft then decreasing until the numerical model natural frequency of the cantilevers matched the footfall natural frequency.

Table 6.4: Exterior Wall Spring Stiffness

Location	Spring Stiffness (kip/ft)
North Cantilever	0.137
South Section	0.327

6.7 Updated Frequencies

The updated frequencies for the single-floor models are compared to the initial frequencies and heel drop frequencies in Table 6.5. The frequencies were closer to the measured frequencies after the adjustments, but still varied between 0%-19%. These inaccuracies could have been caused by several uncertainties. First, the mass could have better discretized. The stiffness also could have been variable by span. Finally, there were other elements in the 10-story building that may have affected the floors; for example, the stairs may have influenced the stiffness in the central and west spans.

Table 6.5: Adjusted Numerical Model Natural Frequencies Comparison to Footfall Natural Frequencies

Material		NEC	WS	SWC	CS
CLT	SAP Adjusted Frequency (Hz)	14.1	28.8	18.7	35.49
	Measured Frequency (Hz)	14.1	35.52	18.7	35.1
	Percent Difference	0%	19%	0%	1%
GLT	SAP Adjusted Frequency (Hz)	13.57	28.71	18.19	34.02
	Measured Frequency (Hz)	15.5	31.7	18.45	36.75
	Percent Difference	12%	9%	1%	7%
NLT/DLT	SAP Adjusted Frequency (Hz)	12.86	32.22	18.23	33.79
	Measured Frequency (Hz)	14.5	28.37	16.8	34.85
	Percent Difference	11%	14%	9%	3%
VLT	SAP Adjusted Frequency (Hz)	12.75	30.83	17.09	29.95
	Measured Frequency (Hz)	12.03	34.21	17.83	30.88
	Percent Difference	6%	10%	4%	4%

Chapter 7

DATA ANALYSIS

7.1 Introduction

The data collected in the NHERI TallWood Project 10-Story Test was processed and used for comparison to the numerical models and to investigate overall floor performance. The accelerations were then used to calculate vertical floor response spectra for various locations and ground motions. Finally, the data was used to develop fragility curves which relate the vertical floor response to the input ground motions. This chapter presents the data and comparisons broken up into sections.

7.2 Data Processing

The accelerometer data from the 10-story test was processed in MATLAB. The data was filtered before the analysis using Butterworth filters. The frequency range for the filter was 0.1 Hz to 50 Hz and the order of filters was high frequency then low frequency.

7.3 SAP Model and Data Comparisons

The measured data and the predicted response from various SAP models were compared at the different instrumentation locations. The single-story and 10-story SAP models were analyzed using 2% and 7% damping. The peak accelerations were compared at every location, and the vertical response spectra were compared at levels four, eight, and eleven.

7.3.1 Peak Acceleration Comparison

The peak accelerations of the Ferndale MCE ground motion in the XYZ directions between the SAP models and measured data were compared using a 45° plot. The time history of

the vertical acceleration recorded on the table was used as the input time history in the SAP models. Any point above the line represents when the measured data was larger than the SAP model. Figures 7.1 and 7.2 display the 45° plot for measured data compared to the 10-story SAP model and single-floor SAP models, respectively. Appendix C contains additional 45° plots for other ground motions.

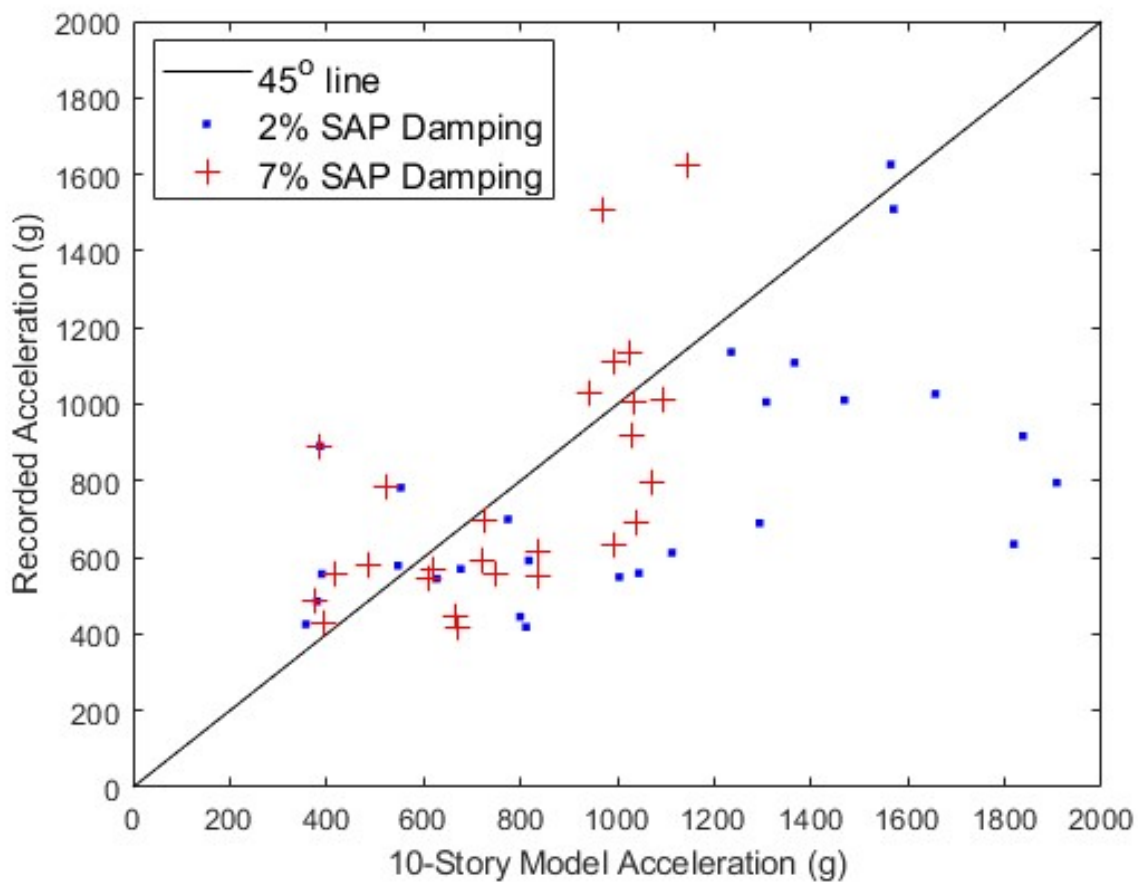


Figure 7.1: Peak Acceleration Comparison for Ferndale MCE: 10-Story SAP Model vs Measured Data

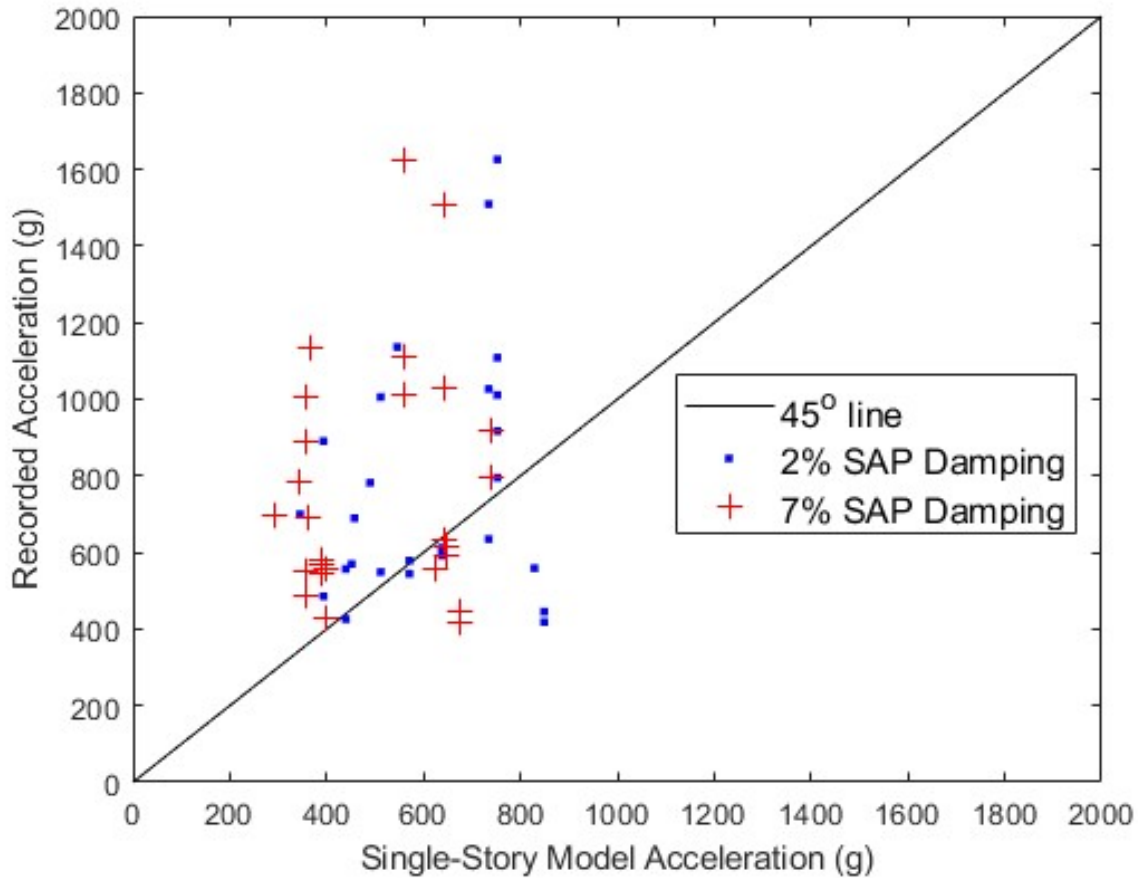


Figure 7.2: Peak Acceleration Comparison for Ferndale MCE: Single-Story SAP Model vs Measured Data

Based on the plots, modeling the full building provided a better prediction of peak vertical acceleration at the instrument locations than the single-story floor models. For the majority of the data points, using 7% damping in the 10-story SAP model was more consistently accurate than 2% damping. The single-story models were much more likely to underestimate the accelerations at the various accelerometer locations.

7.3.2 Response Spectra Comparison

For the response spectra, the measured data and SAP results were from the Loma Prieta MCE ground motion in the XYZ directions. The response spectra were again analyzed using 2% 7% damping in the SAP models. Figures 7.3-7.8 compare the response spectra at the different span locations on the fourth, eighth, and eleventh levels. The black vertical line on each plot represents the period (0.079 s) at the jump in modal mass participation ratio discussed in Chapter 5. The brown vertical line on each plot represents the average heel drop period for each span location: northeast cantilever, southwest cantilever, west span, and central span. The periods are 0.072, 0.057, 0.034, and 0.030 seconds, respectively.

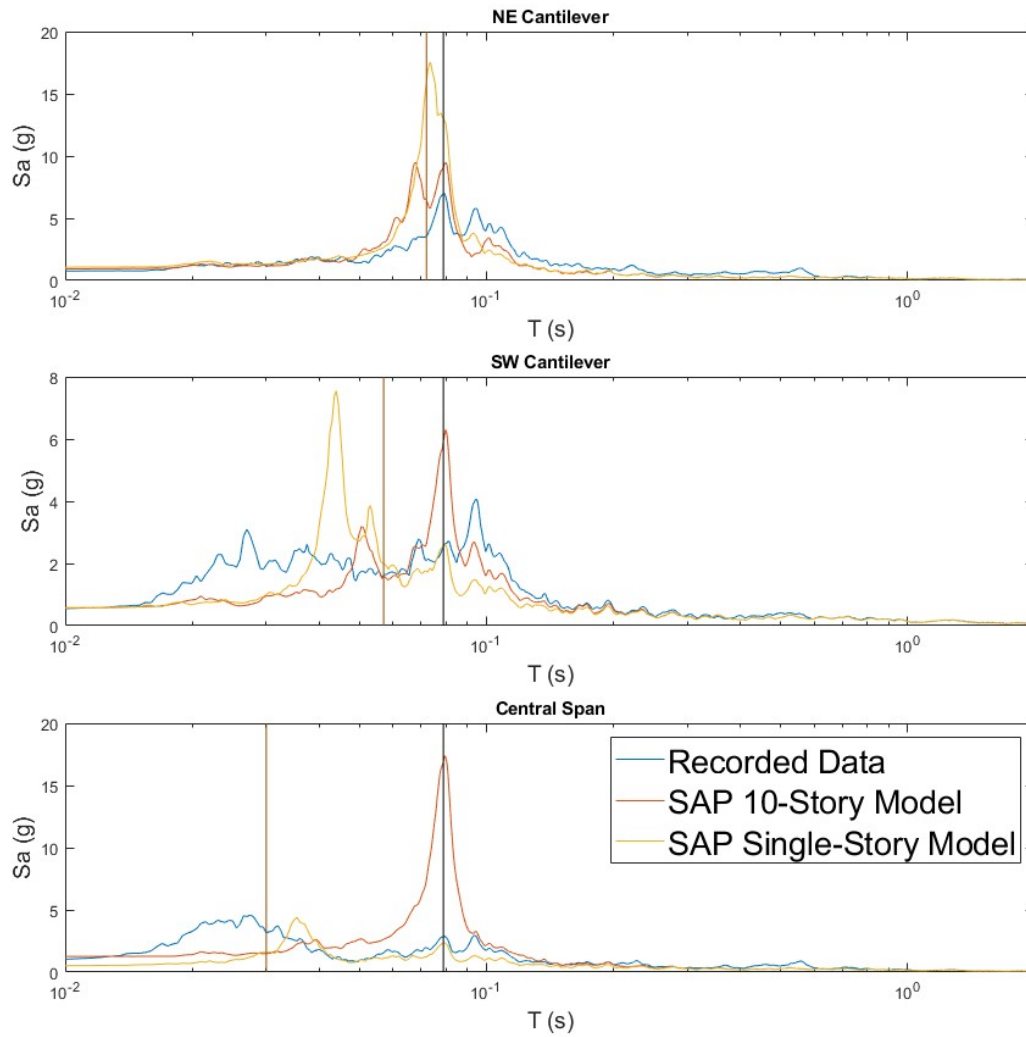


Figure 7.3: Level 4 Measured Data vs 2% Damped SAP Models Response Spectra

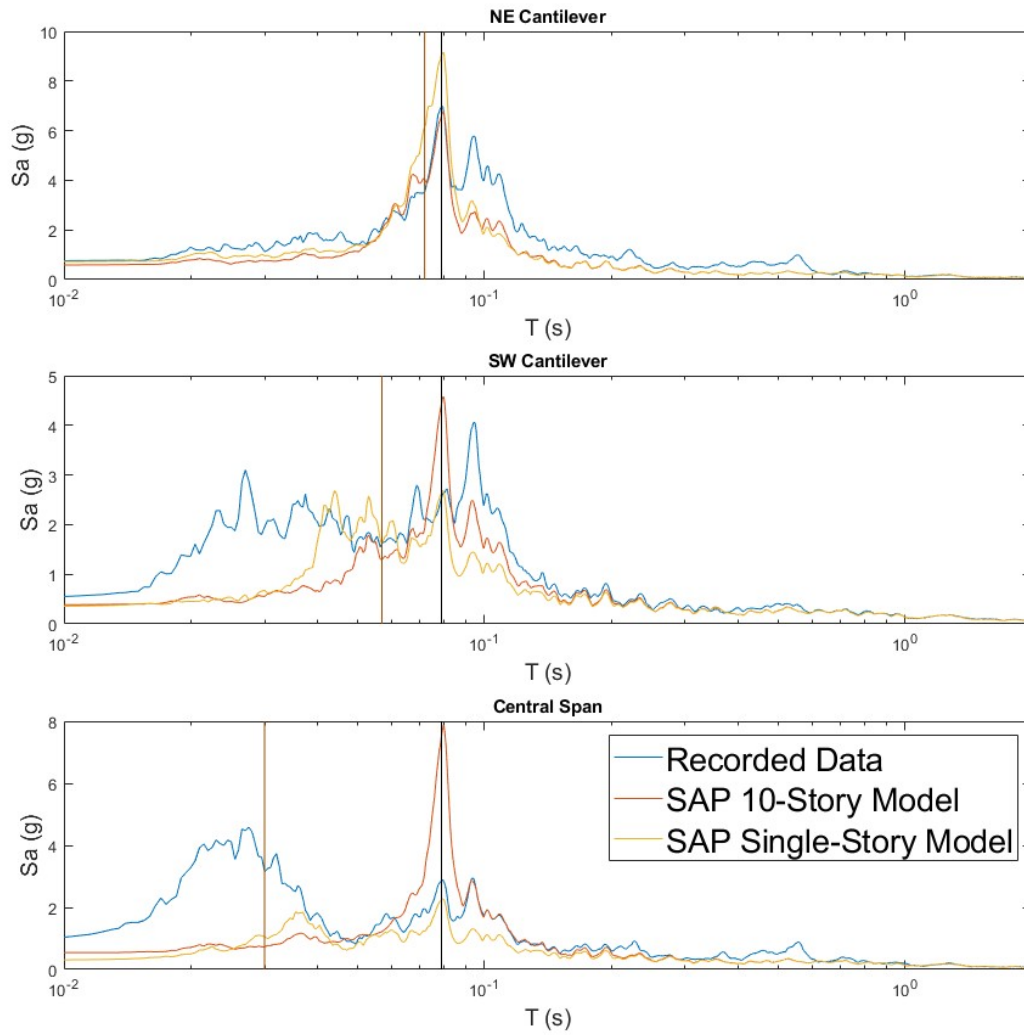


Figure 7.4: Level 4 Measured Data vs 7% Damped SAP Models Response Spectra

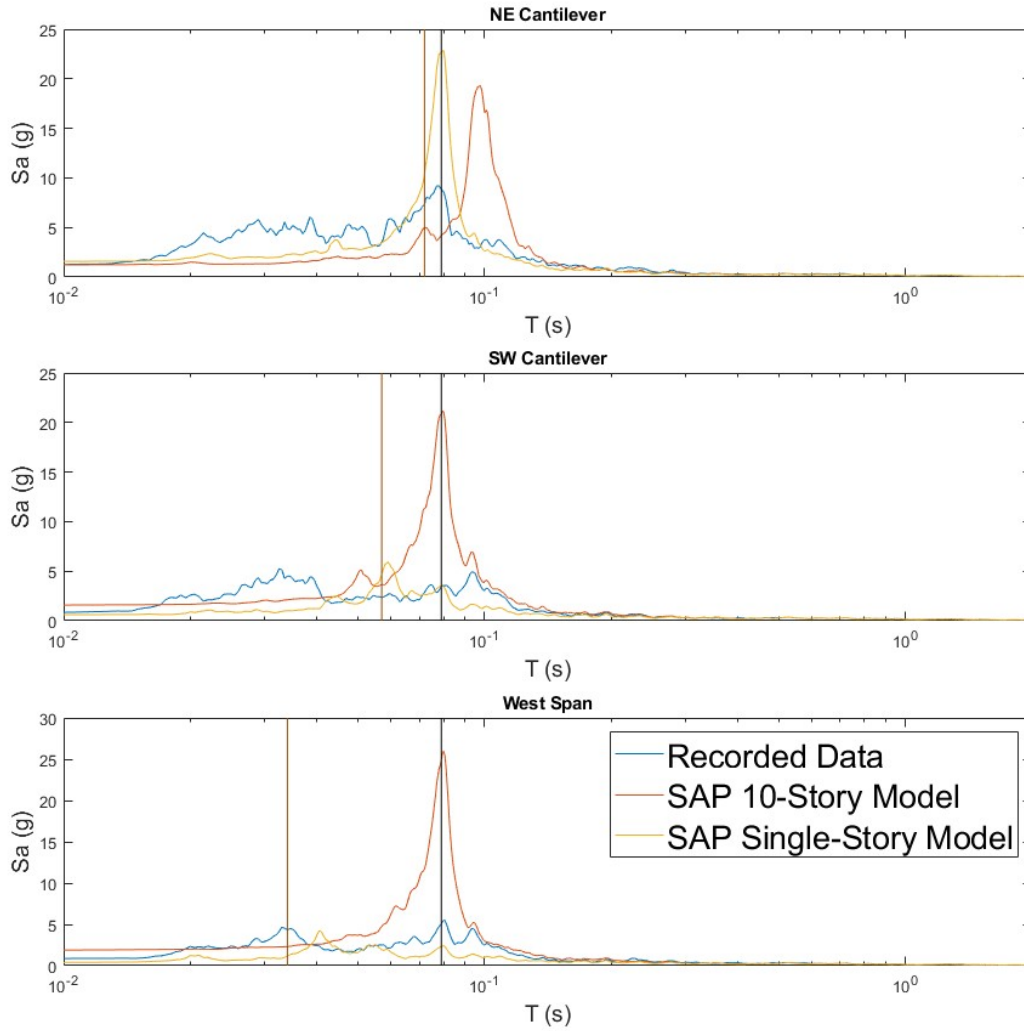


Figure 7.5: Level 8 Measured Data vs 2% Damped SAP Models Response Spectra

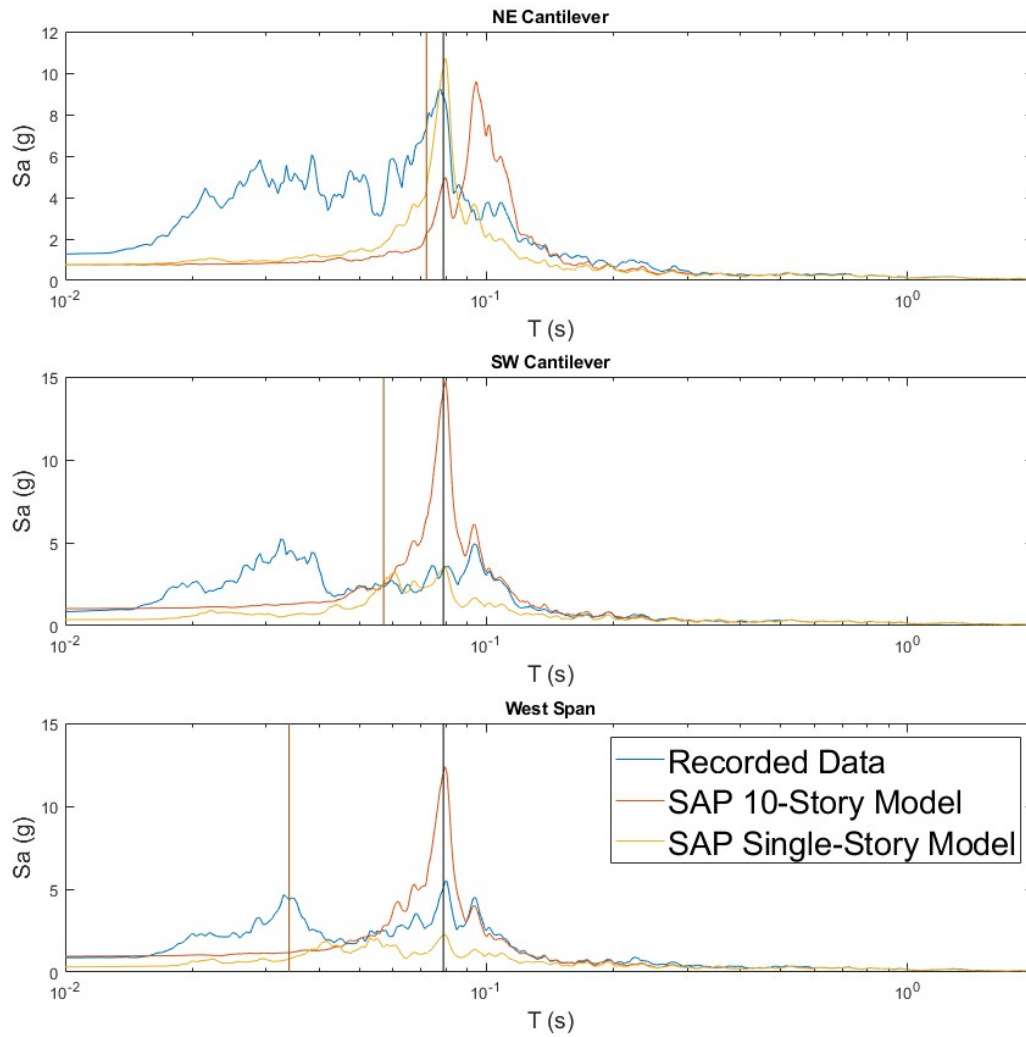


Figure 7.6: Level 8 Measured Data vs 7% Damped SAP Models Response Spectra

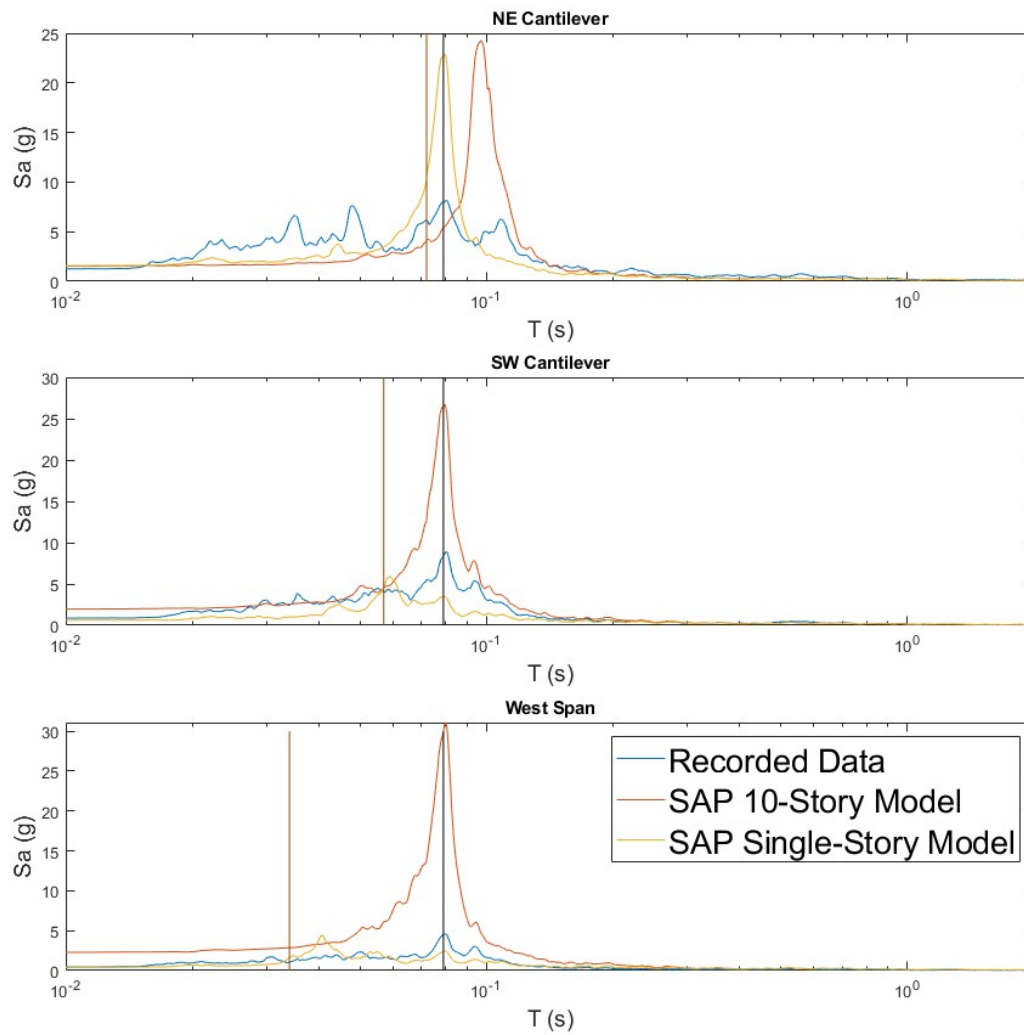


Figure 7.7: Level 11 Measured Data vs 2% Damped SAP Models Response Spectra

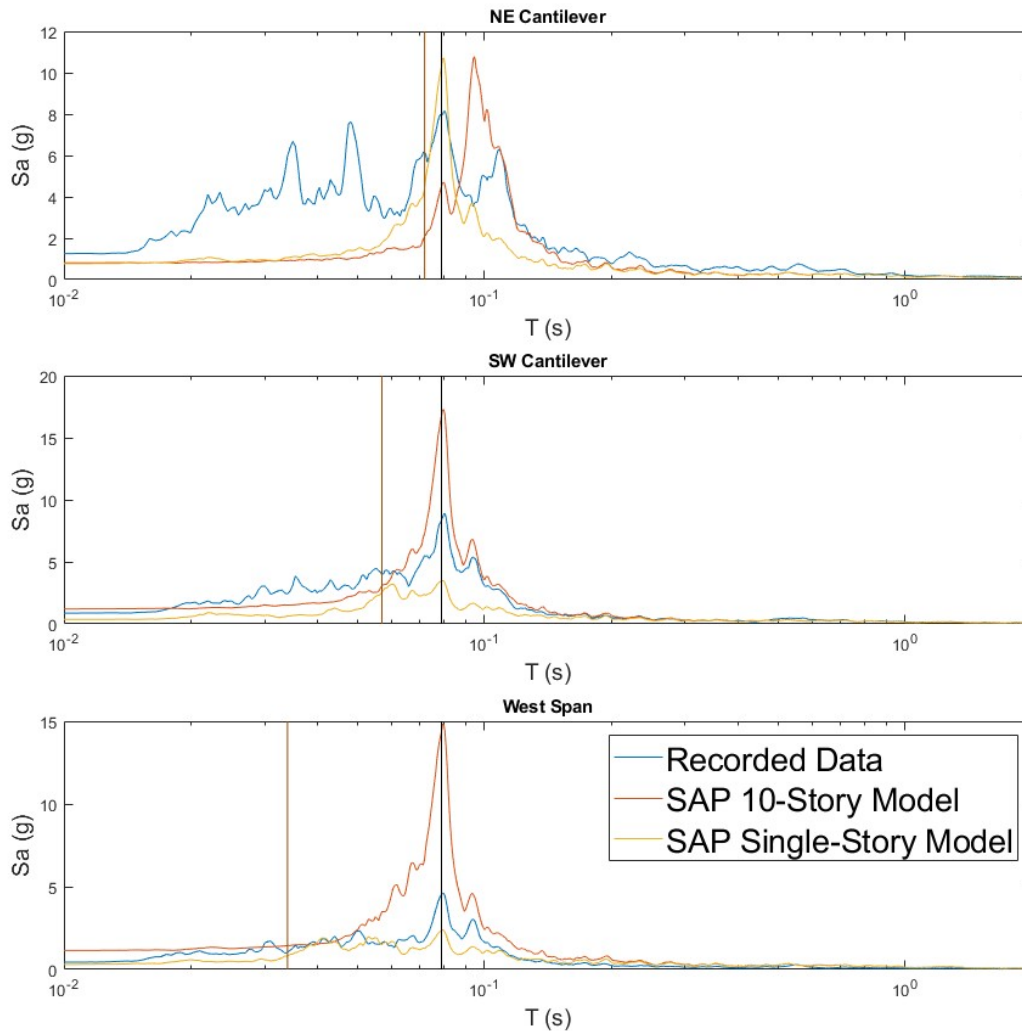


Figure 7.8: Level 11 Measured Data vs 7% Damped SAP Models Response Spectra

As with the peak accelerations, the 7% damped models were more consistently accurate than the 2% damped models. For the 7% damped models, the northeast cantilever matched more consistently than the other models. Due to this, it is possible that there was variable damping at the different span locations. The measured data response spectra have vertical response in the high frequency, low period range that the SAP models did not reflect.

7.3.3 Modeling Uncertainties

Based on the results discussed throughout this discussion, the SAP model results did not prove to consistently predict the accelerations that were measured in the 10-story test. There were a number of uncertainties that could have contributed to the discrepancy between the model results and the recorded data. The first uncertainty was the high frequency content that SAP was unable to predict. The damping also may have been variable for the different span locations. Finally, the floors and shake table had a vertical response to the horizontal ground motions which was not reflected in the SAP models since this was vertical time history was input to the SAP model. The following section discusses the horizontal ground motion results further.

7.4 Vertical Response Spectra for Horizontal Ground Motions

There was a quantifiable vertical response to the horizontal (X and Y) only motions. The following subsections discuss vertical response spectra for a few scenarios: X and Y motions compared to a Z motion, comparisons of horizontal motions at different hazard levels, and the comparison of an XYZ motion to the X and Y motion of the same hazard level. The viscous damping used to calculate all the response spectra in this section was 2%.

7.4.1 Vertical Response Spectra for Horizontal Motions and Low Amplitude Vertical Motion

Figures 7.9-7.12 compare the vertical response spectra of various horizontal-only ground motions with a vertical-only white-noise (WN) motion. The white-noise was a random, low-amplitude excitation run through the shake table between ground motions to calibrate the shake table. Figure 7.9 illustrates the vertical response spectra of the table and shows vertical response due to horizontal-only motion; however, the amplitude for the white-noise vertical motion is larger than the horizontal motions. The vertical response spectra at the various floor levels showed an increase in the vertical response due to horizontal-only motions relative to the vertical-only motion. The horizontal-only motions had more vertical response

in the high-frequency range than the low-frequency range.

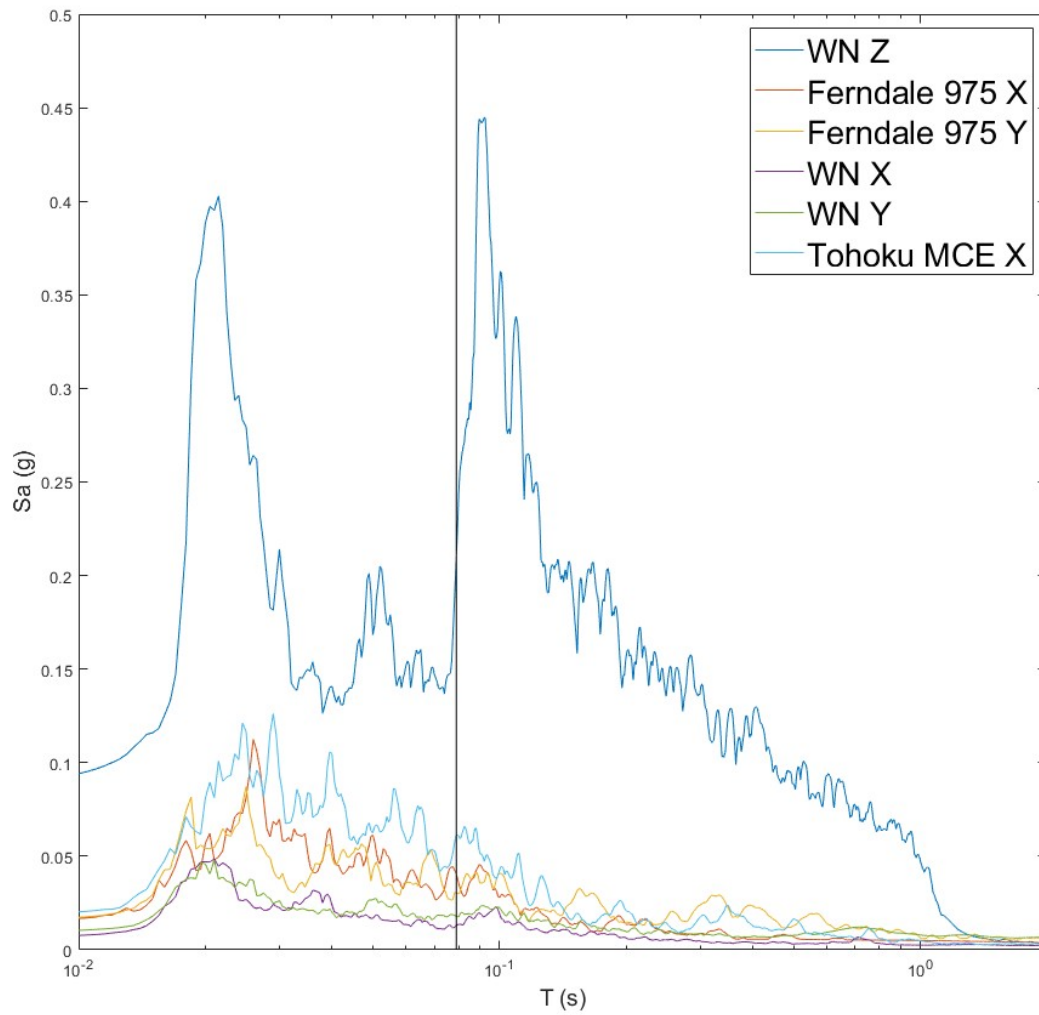


Figure 7.9: Shake Table Vertical Response Spectra for Horizontal-Only and Low-Amplitude Vertical-Only Motions

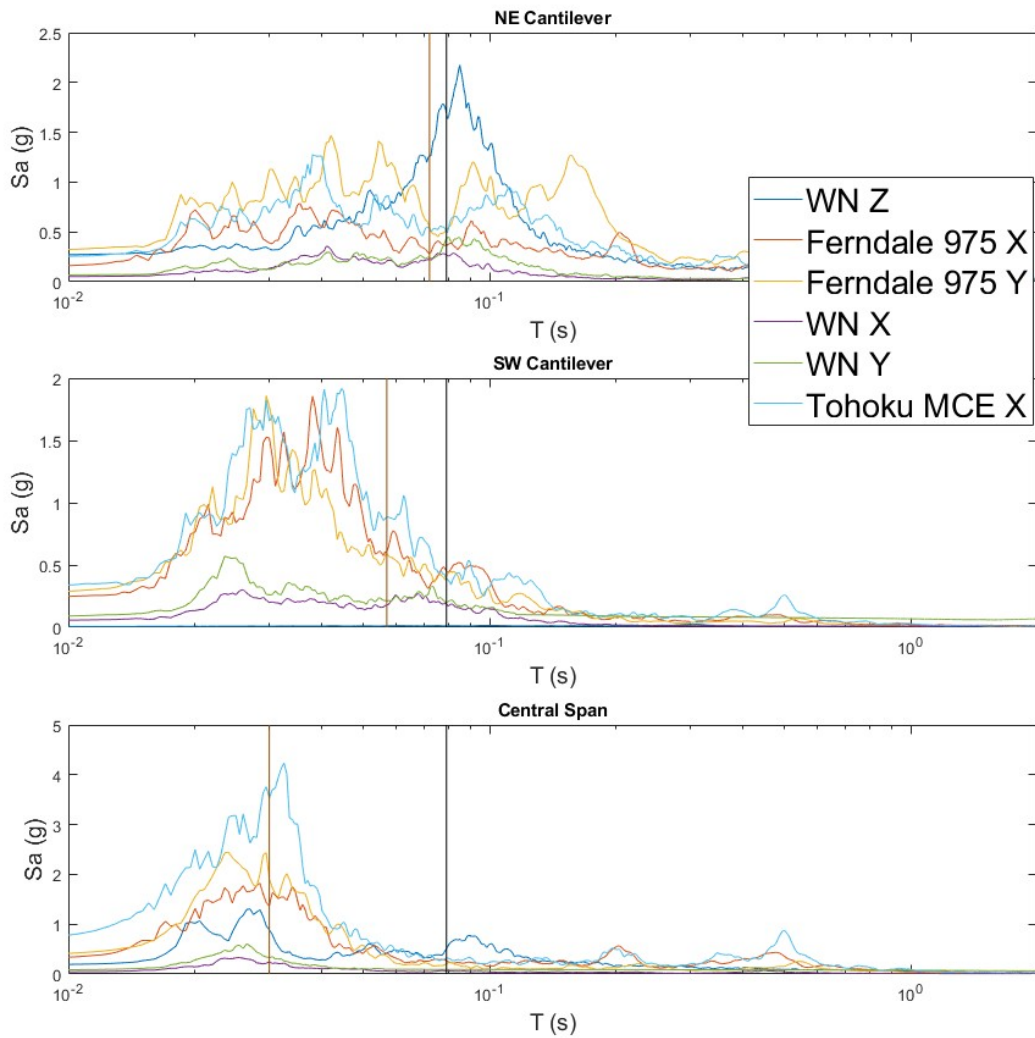


Figure 7.10: Level 4 Vertical Response Spectra for Horizontal-Only and Low-Amplitude Vertical-Only Motions

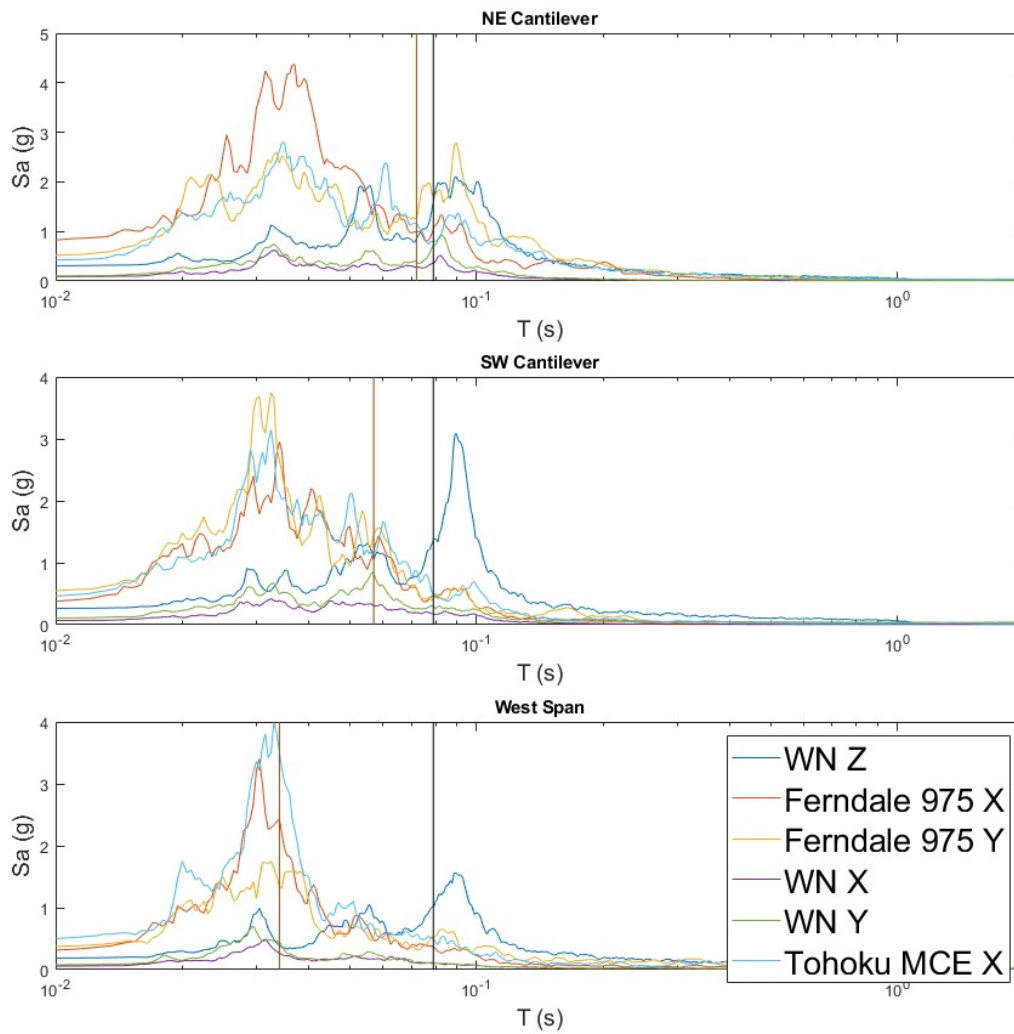


Figure 7.11: Level 8 Vertical Response Spectra for Horizontal-Only and Low-Amplitude Vertical-Only Motions

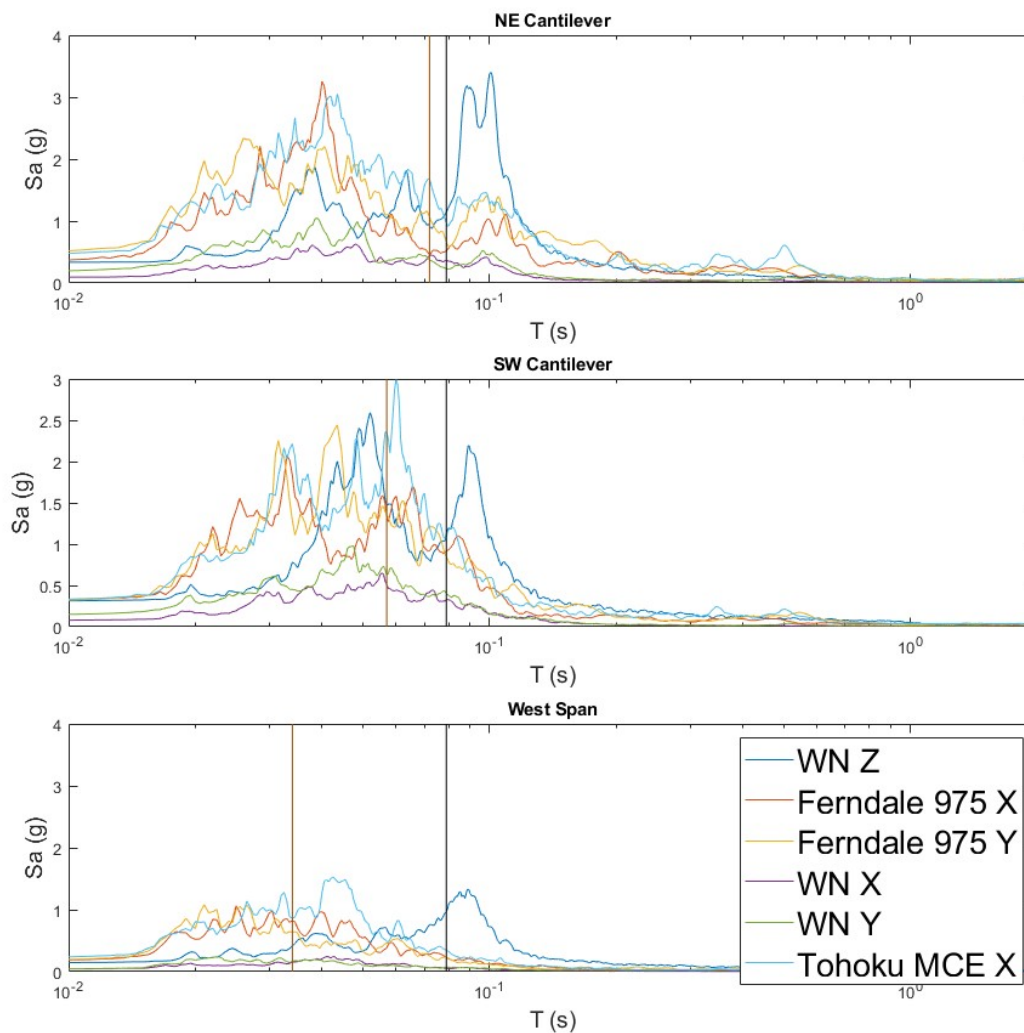


Figure 7.12: Level 11 Vertical Response Spectra for Horizontal-Only and Low-Amplitude Vertical-Only Motions

7.4.2 Vertical Response Spectra from Horizontal-Only Motions of Various Hazard Levels

To confirm that there was vertical response to horizontal-only input motions with varying amplitudes, response spectra were plotted together for varying hazard levels [Figures 7.13-

7.16]. For the smaller hazard levels, the vertical response had a lower amplitude than the larger hazard levels. The vertical response, however, was still significant at the table and floor locations for the smaller hazard levels.

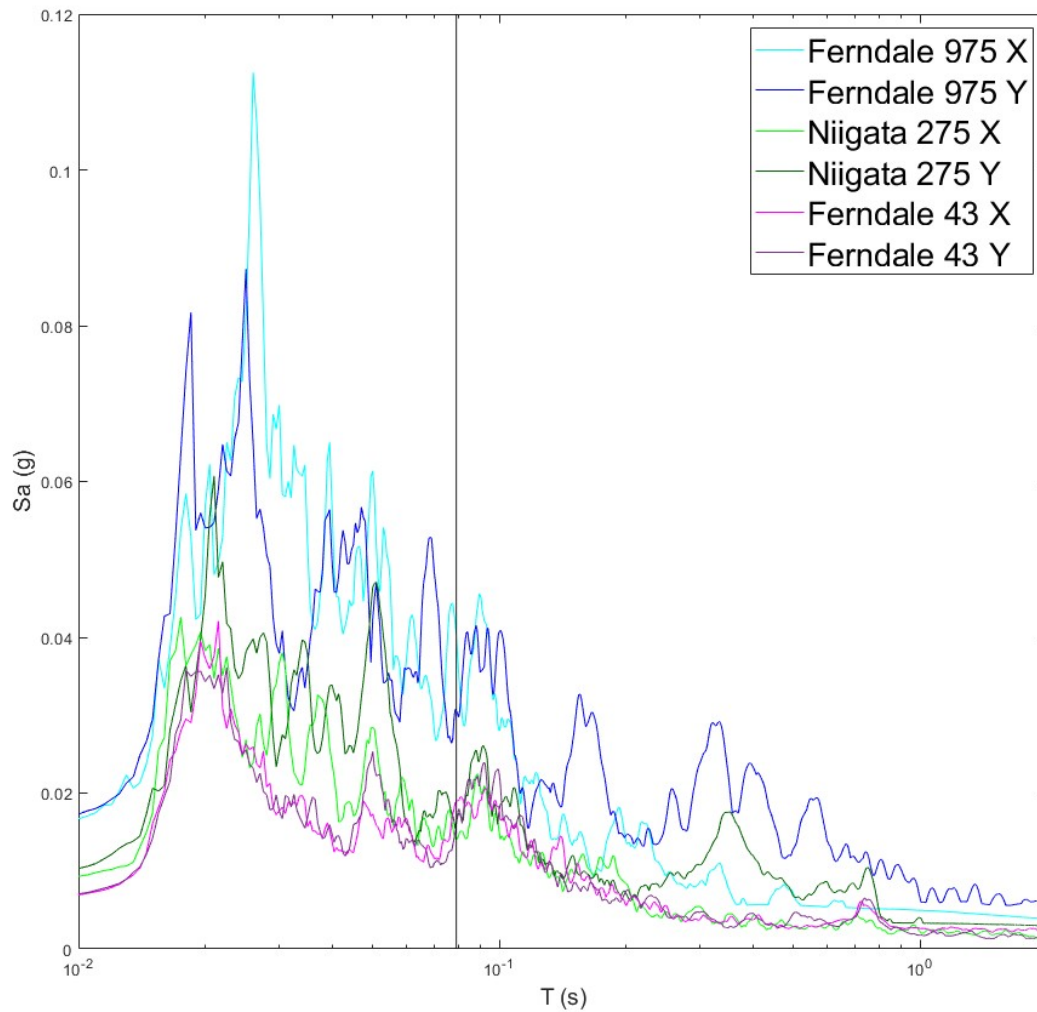


Figure 7.13: Shake Table Vertical Response Spectra for Horizontal-Only Motions of Varying Hazard Levels

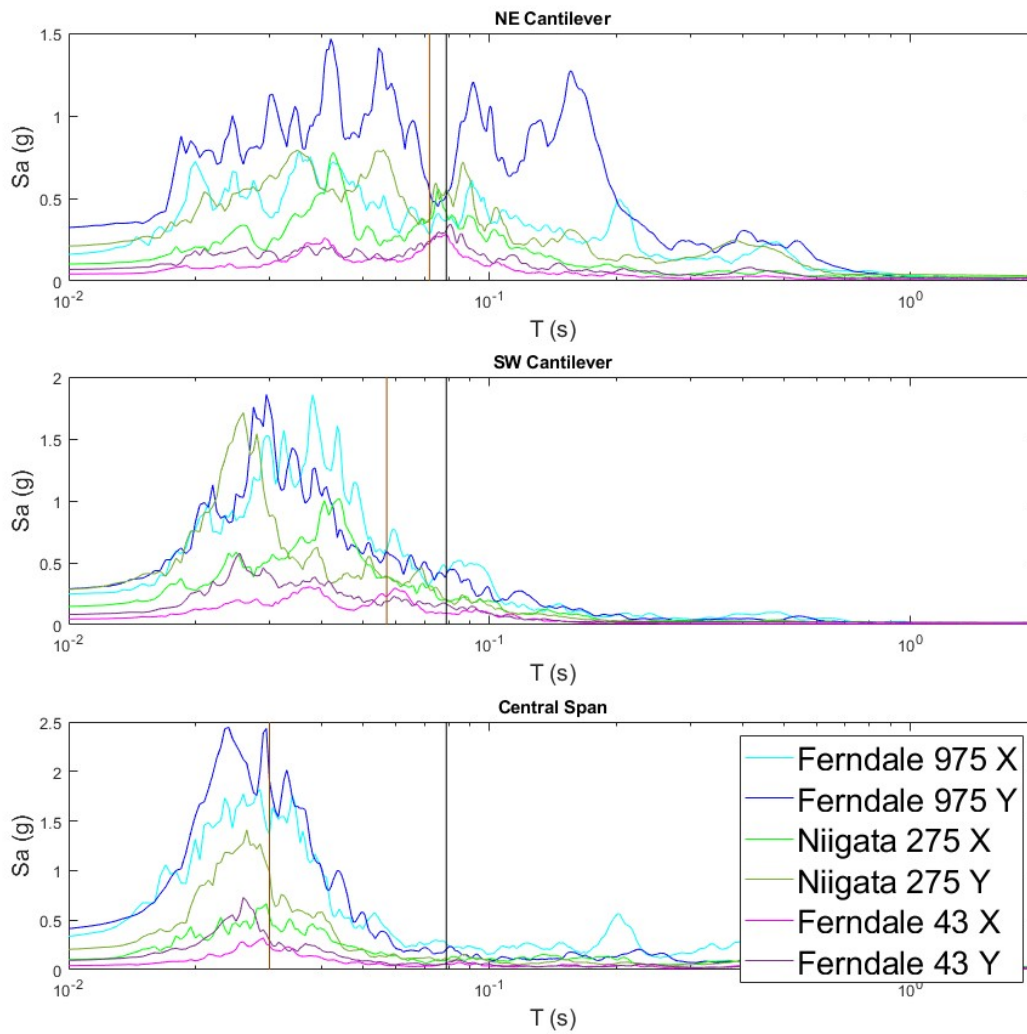


Figure 7.14: Level 4 Vertical Response Spectra for Horizontal-Only Motions of Varying Hazard Levels

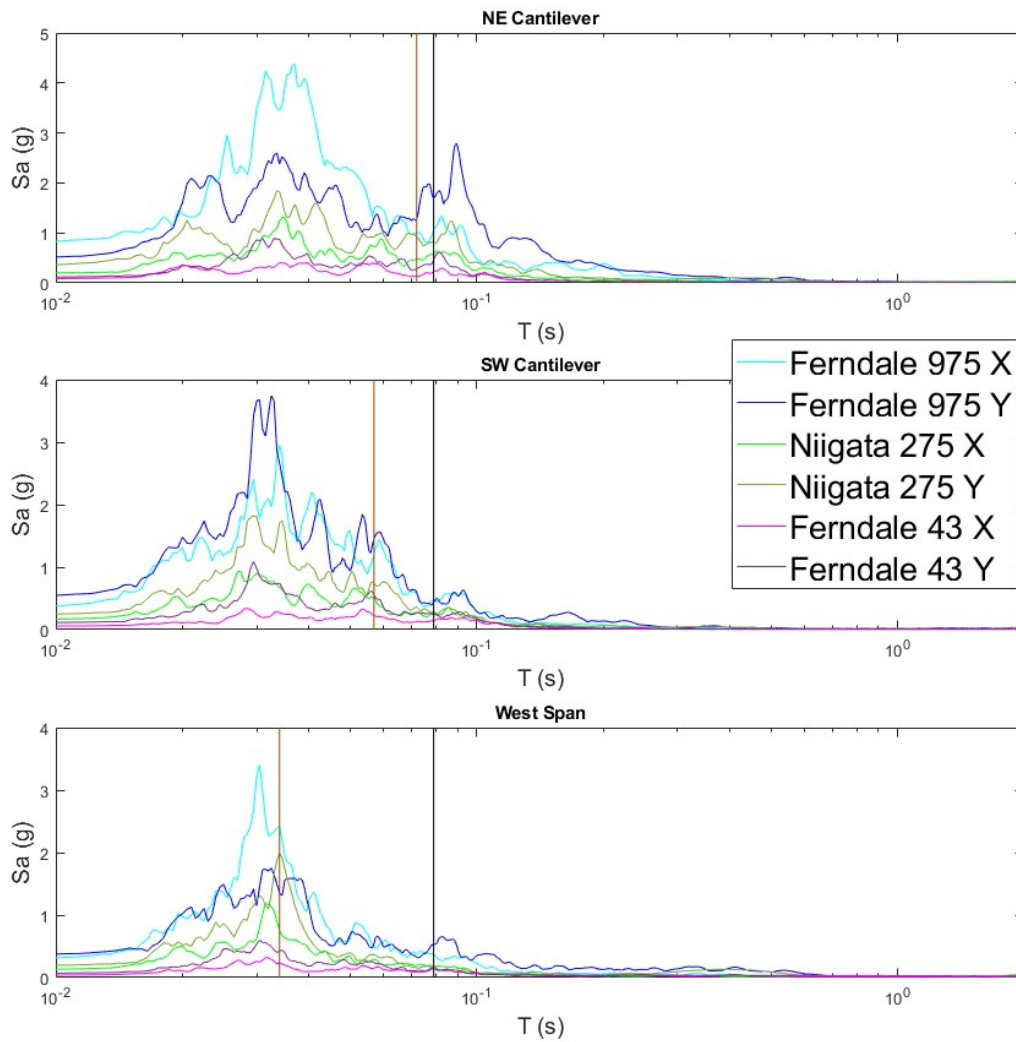


Figure 7.15: Level 8 Vertical Response Spectra for Horizontal-Only Motions of Varying Hazard Levels

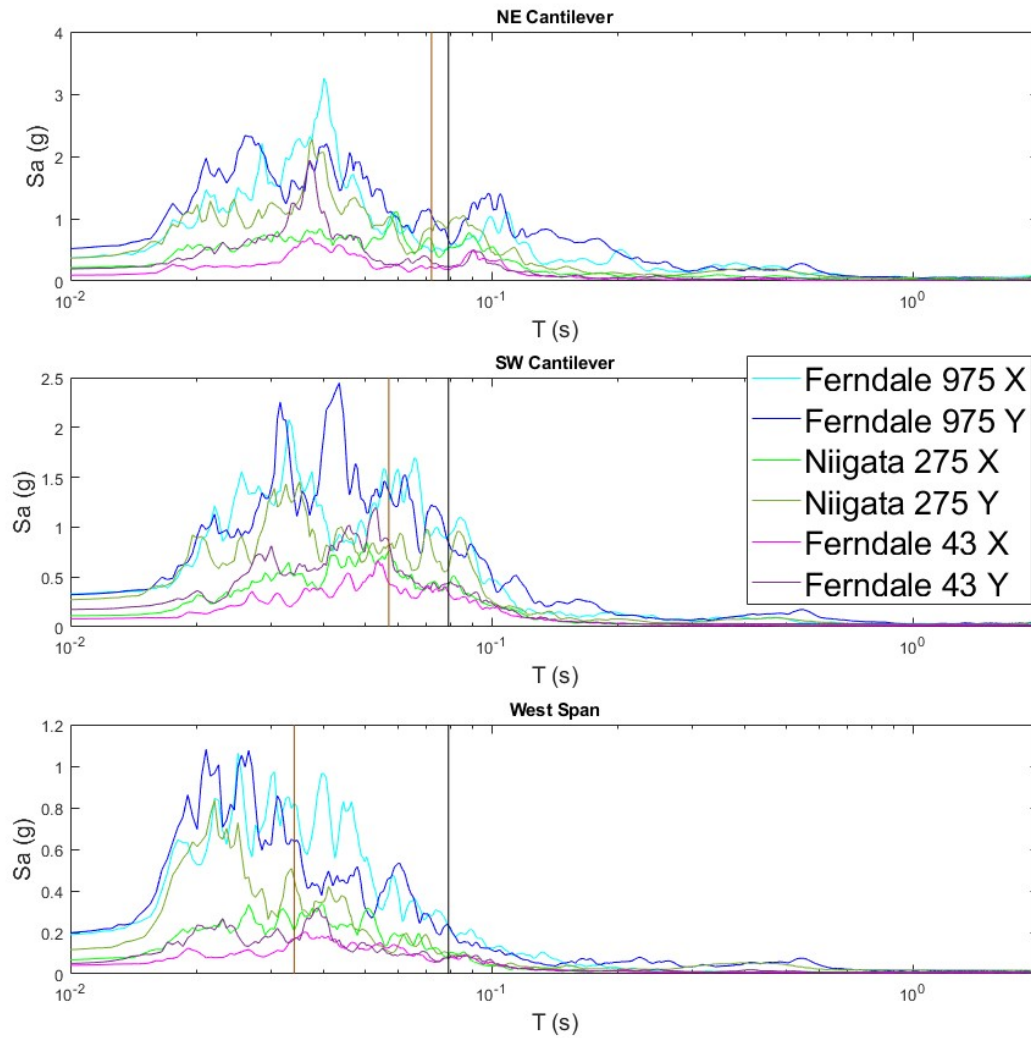


Figure 7.16: Level 11 Vertical Response Spectra for Horizontal-Only Motions of Varying Hazard Levels

7.4.3 Vertical Response Spectra for Horizontal and Vertical Motion of the Same Hazard Level

The vertical response spectra for Ferndale ground motions in the X, Y, and XYZ directions at the 975 hazard level are illustrated in Figures 7.17-7.20. The vertical response of the XYZ motion had a higher amplitude at the table and the floor locations than the X and Y motions since there was intentional vertical motion. However, the Ferndale XYZ motion also had a higher amplitude vertical response than the target Z input; the increase in amplitude could be due to either the presence of input in the X and Y directions or difficulty controlling the vertical input of the table. The X and Y motions may have influenced the vertical response in the XYZ motion, particularly in the high frequency, low period domain.

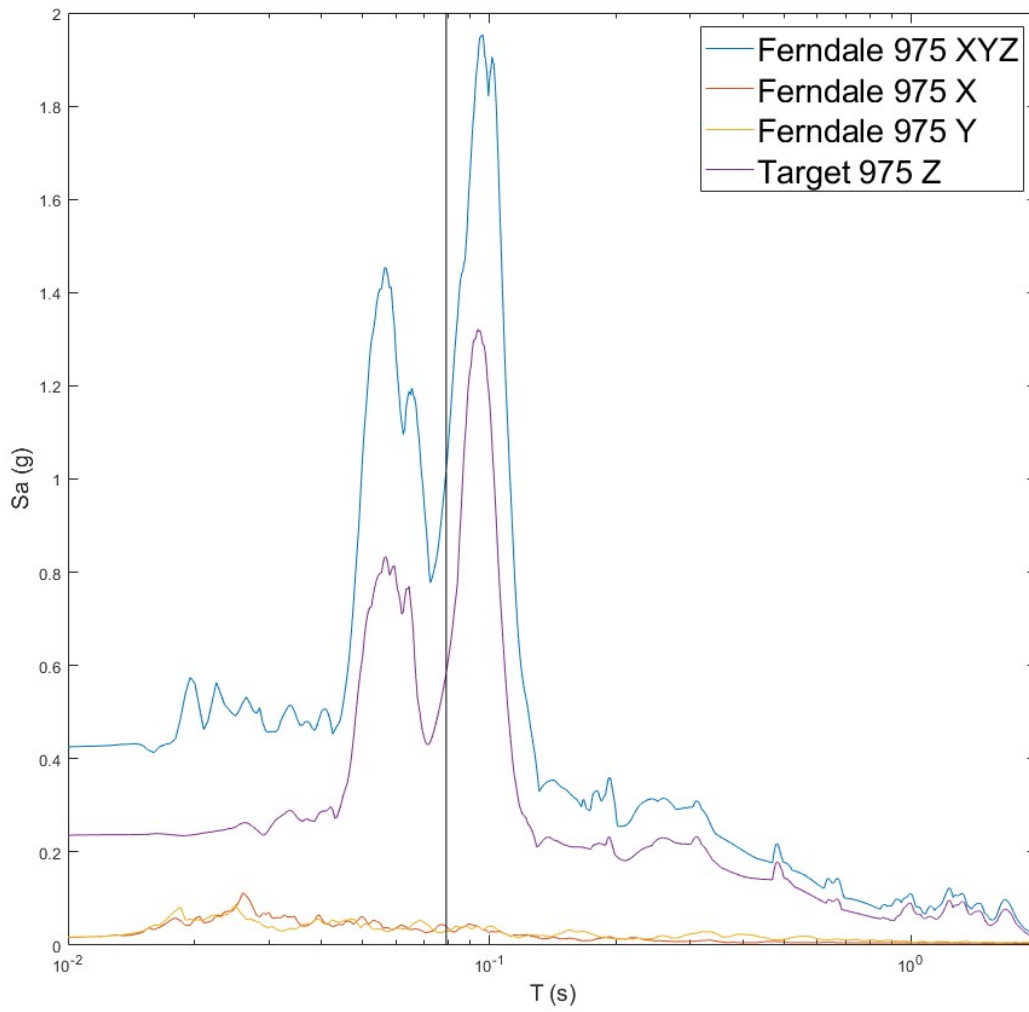


Figure 7.17: Shake Table Vertical Response Spectra for Ferndale 975

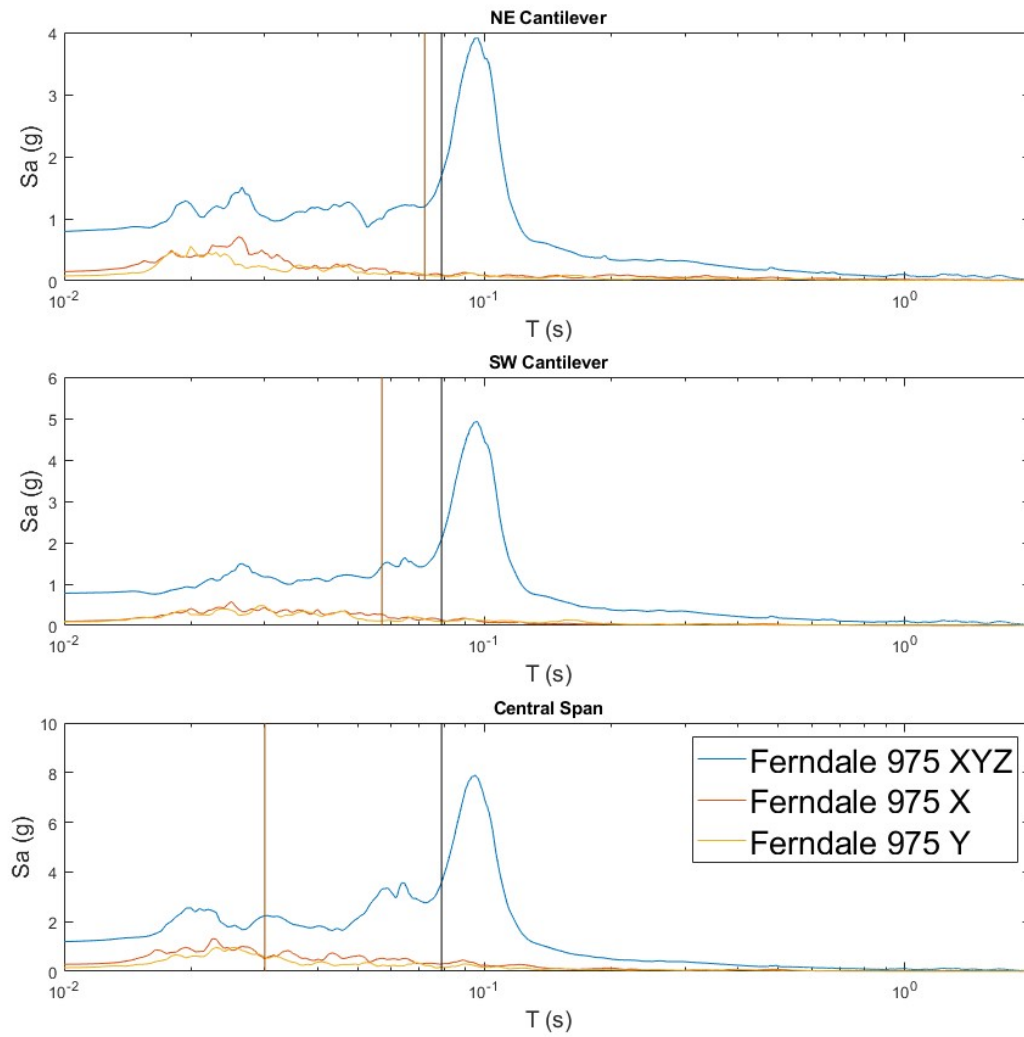


Figure 7.18: Level 4 Vertical Response Spectra for Ferndale 975

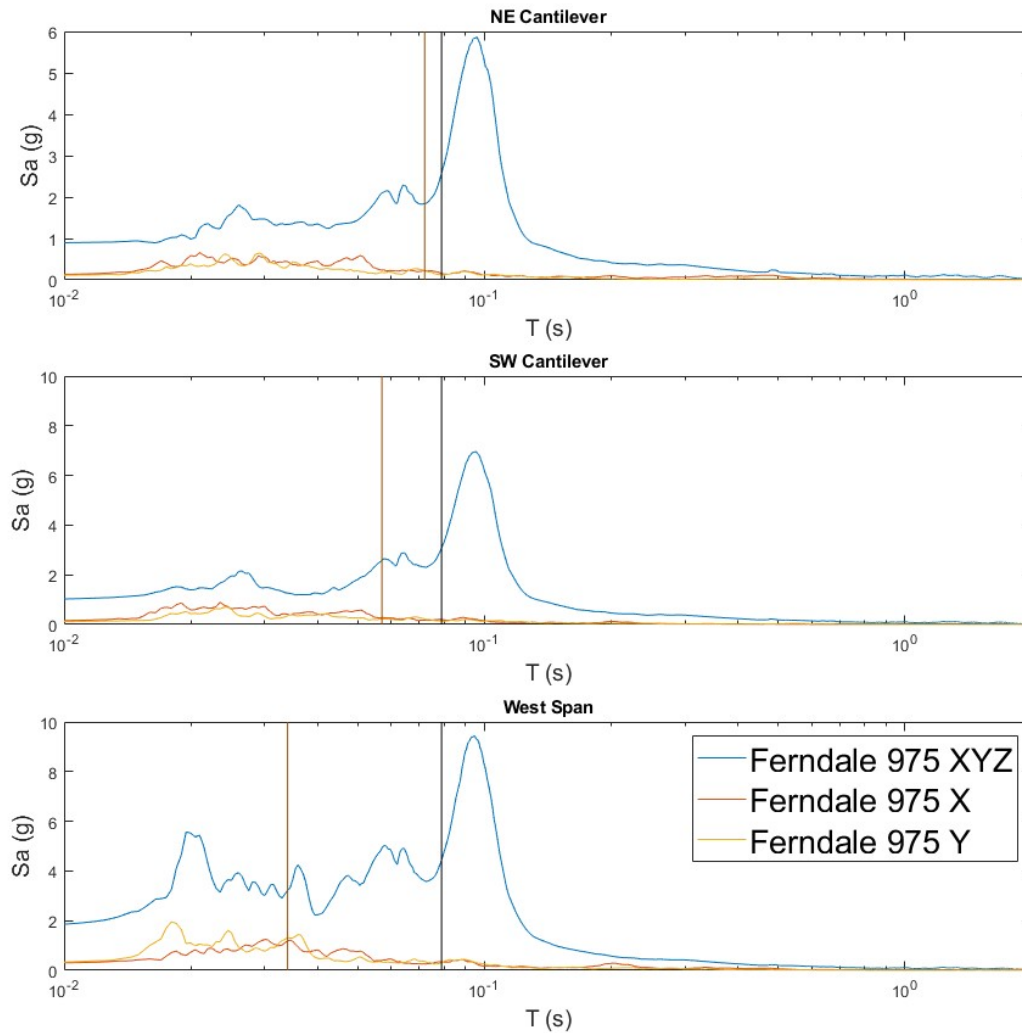


Figure 7.19: Level 8 Vertical Response Spectra for Ferndale 975

Figure 7.17 displays both the target vertical motion and the recorded vertical motion at the table. The recorded motion had a higher amplitude than the target motion. This was due to issues with input controls of the shake table in the vertical direction, as well as contributions from the horizontal motions – particularly in the high frequency domain.

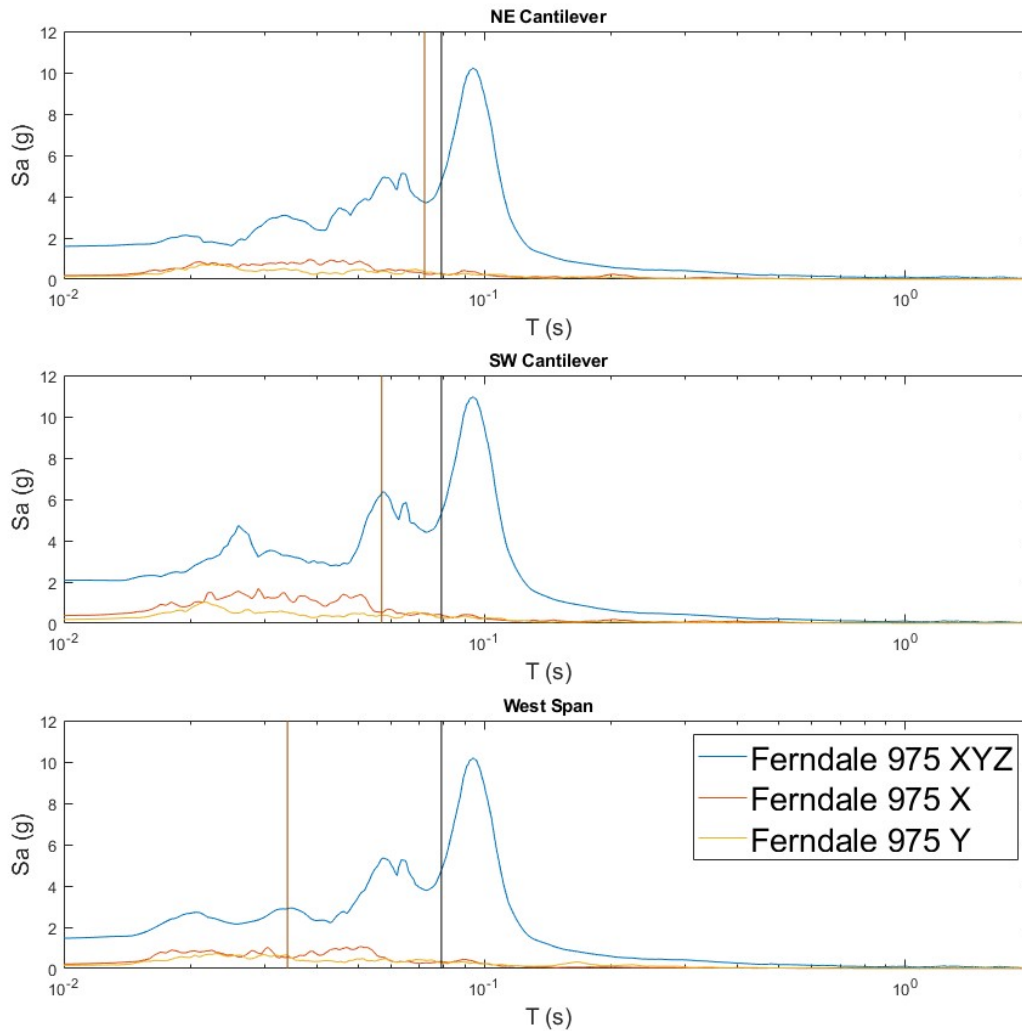


Figure 7.20: Level 11 Vertical Response Spectra for Ferndale 975

7.5 Vertical Response Spectra Ratios

To identify the behavior of the floors as the acceleration travels up the building, ratios of the spectral accelerations between the COM locations and the shake table input were computed. The ratios were computed for the MCE and 975 hazard levels by averaging the vertical

response spectra for the motions at each hazard level. Figures 7.21 and 7.22 illustrate the ratio for the MCE and 975 hazard levels, respectively.

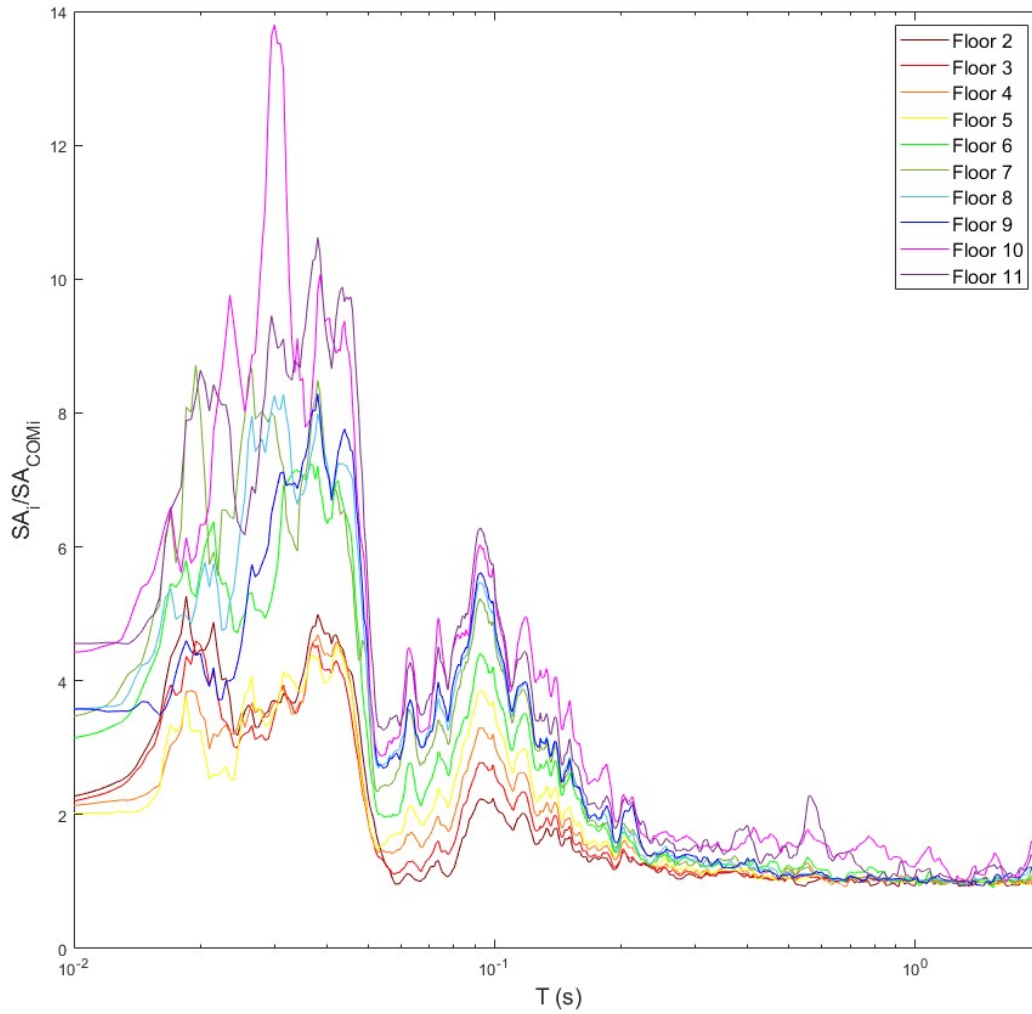


Figure 7.21: Spectral Acceleration Ratios of the COM to the Table Input for MCE Motions

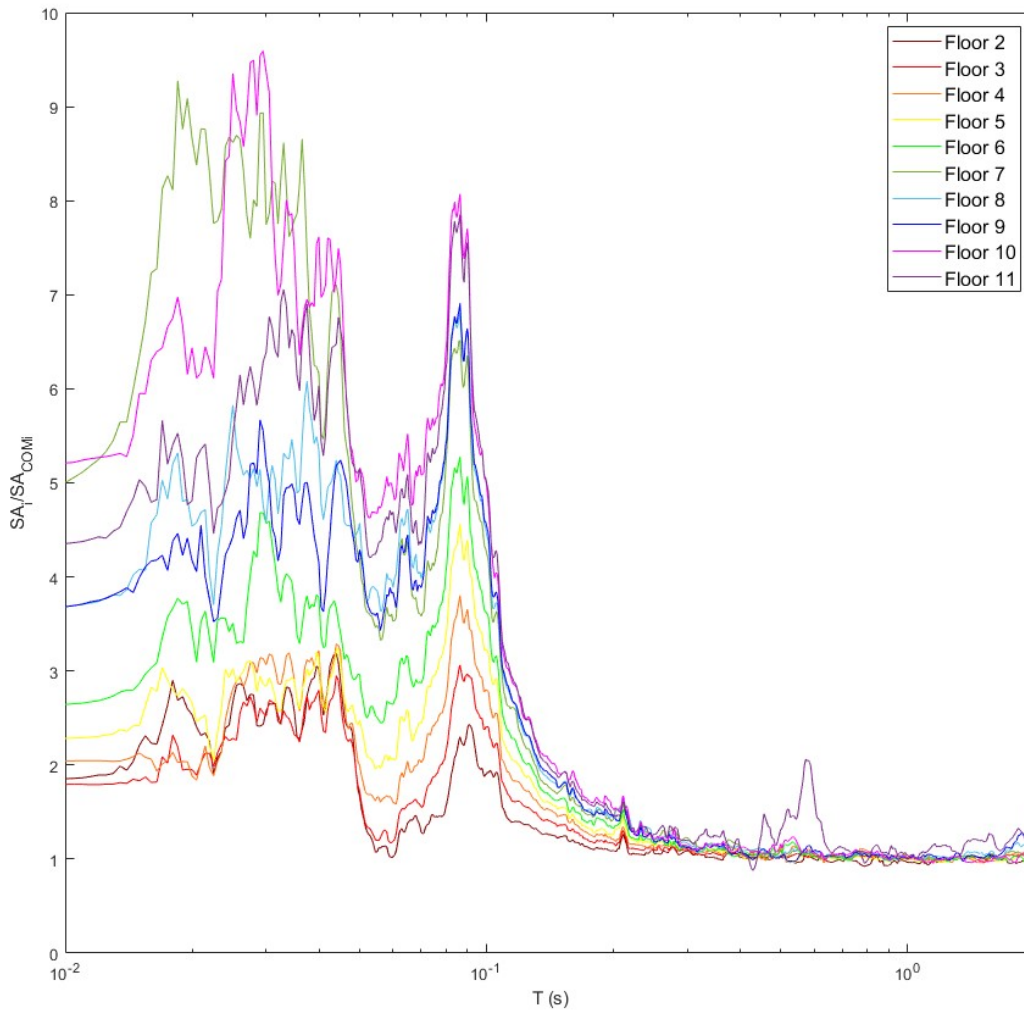


Figure 7.22: Spectral Acceleration Ratios of the COM to the Table Input for 975 Motions

For both the MCE and 975 hazard levels, the accelerations increased at each level, so the accelerations got larger as they traveled up the building. There was also vertical response at two period ranges, both a low and high-period range. The low-period, high frequency response may be linked to vertical period of the shake table. The high-period, low-frequency

response may be linked to the period of the input ground motion and vertical resonance of the structure.

Figure 7.23 contains a plot of the ratios of the response spectra of the floor span locations vs the COM of their respective floor. The initial point at T equals 0 compares the peak accelerations of the floor span location to that levels input motion. Table 7.1 summarizes the average peak acceleration ratio and max peak acceleration ratio for each floor span. Outside of the central spans, the peak accelerations on average hardly increased or decreased when compared that floor's input motion. However, the max peak acceleration increase was 1.51 times higher than that floor's input motion.

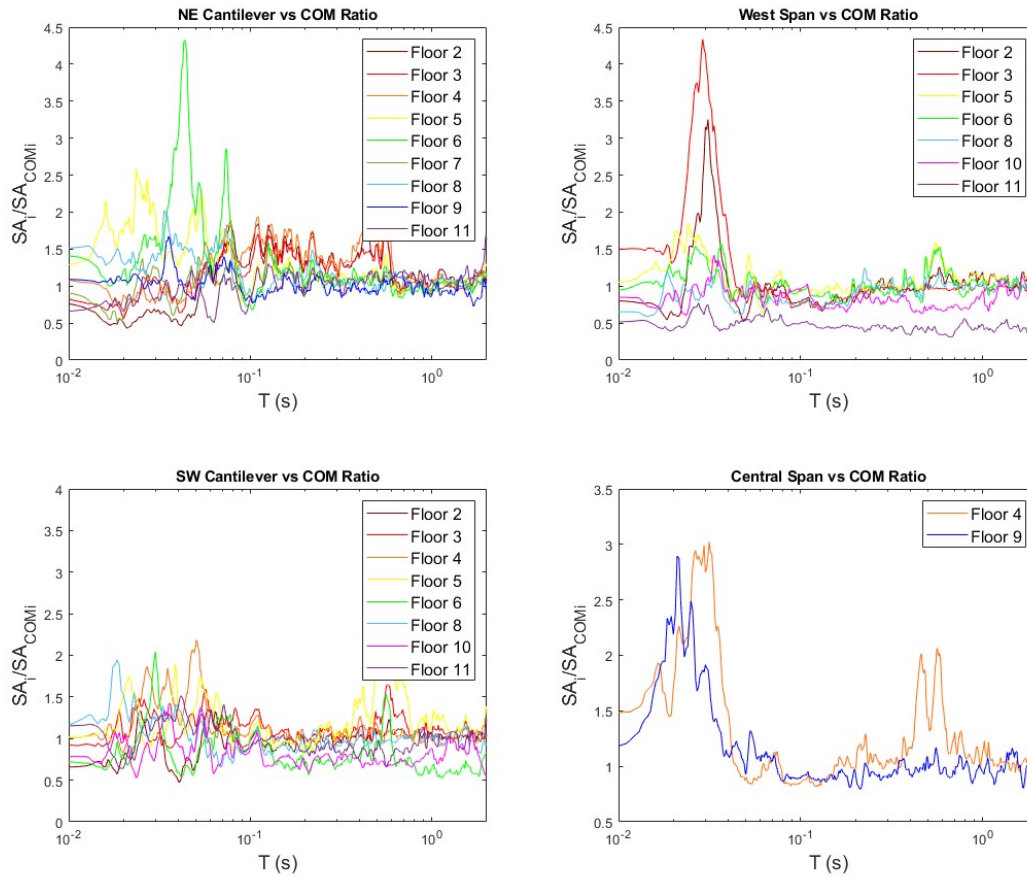


Figure 7.23: Spectral Acceleration Ratios of the Floor Spectra to the COM Spectra for MCE

Table 7.1: Sapn to COM Peak Acceleration Ratios

Floor Span Location	Average Peak Acceleration Ratio	Max Peak Acceleration Ratio
NE Cantilever	1.06	1.51
SW Cantilever	0.91	1.15
West Span	0.9	1.5
Central Span	1.33	1.48

7.6 Fragility Curve Development

Before this project, no fragility curves had been developed for the vertical response of mass timber floors. Using fragility curves, industry professionals can help protect acceleration sensitive equipment and perform loss estimation and performance based design for mass timber floors.

To develop the fragility curves, Method B from [Porter et al. \[2006\]](#) was used. The process included binning the data by the spectral accelerations of the input motions, tracking which floor spans exceeded the damage states, calculating the logarithmic mean and deviation for the data set, and plotting the log normal distribution for the calculated mean and deviation. The logarithmic mean (μ) and the logarithmic deviation (Θ) for each curve are summarized in [Table 7.2](#). [Figure 7.24](#) illustrates the developed fragility curves for input motion periods of 0.05 and 0.1 seconds.

Table 7.2: Logarithmic Mean and Deviation for Fragility Curves

Input Motion Period (s)	Damage State	μ	Θ
0.05	0.5g	-1.36	0.51
	0.75g	-0.81	0.72
	1g	-0.33	0.60
0.1	0.5g	-1.04	0.62
	0.75g	-0.43	0.72
	1g	0.05	0.51

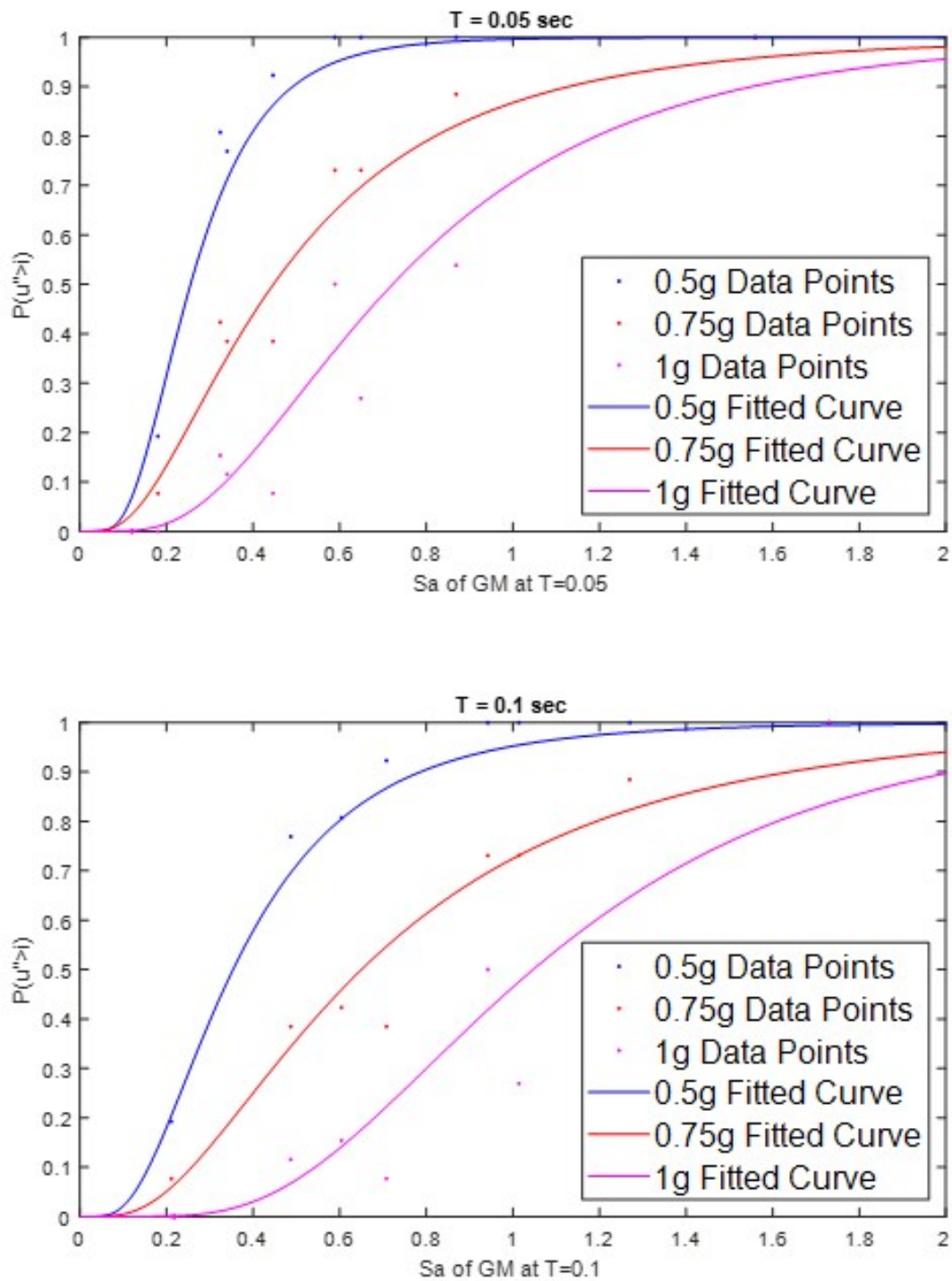


Figure 7.24: Fragility Curves for Mass Timber Floors

The x-axes of the fragility curves plot the spectral acceleration for the given period, and the y-axes plot the probability of the acceleration of a mass timber floor exceeding the damage state. The damage states used were 0.5 g, 0.75 g, and 1 g. The plots include data points of the raw probabilities as well as the fitted fragility curves.

Chapter 8

SUMMARY AND CONCLUSIONS

8.1 Summary

The purpose of this research was to investigate the vertical response of mass timber floors subjected to dynamic vertical ground motions using numerical models and large-scale experiments. There were five different types of mass timber floors that were tested and modeled. The models were developed in SAP2000 with recommendations from the WoodWorks Floor Vibration Design Guide [Breneman et al., 2021]. The physical testing was conducted using the NHERI TallWood Project's 10-Story mass timber building that was constructed on the Shake Table at the University of California, San Diego [Chapter 3]. Heel Drop tests were performed on span locations throughout the building to identify the floor frequencies. The building was subjected to a series of vertical ground motions causing vertical acceleration in the floor spans. This section summarizes the topics discussed in this thesis.

8.1.1 Numerical Model Development

Numerical models were developed in SAP2000 following recommendations from the WoodWorks Floor Vibration Design Guide [Breneman et al., 2021] with modifications. Both isotropic and layered shell elements were used to model the mass timber floors. A model was developed for each floor individually, as well as a model that contained the entire structural vertical system for the test building. A time history of the shake table motion was used as the dynamic load case for the models.

8.1.2 Numerical Model Calibration

Heel drop tests were performed by KPFF on the mass timber floors in the NHERI TallWood Project 10-story building. The heel drop tests identified the floor frequencies of the different floor types and spans. The numerical models were calibrated to these frequencies by discretizing masses, adjusting the stiffness, and modeling the exterior walls using springs.

8.1.3 Dynamic Testing

Nine different vertical ground motions at varying hazard levels were used for the dynamic vertical testing of the 10-story building. Accelerometers were placed at different locations on the floors to record the vertical accelerations during testing.

8.1.4 Analysis of Dynamic Test Data

The mass timber floors were subjected to large vertical ground motions (up to the maximum considered earthquake) without damage. However, the mass timber floors experienced large vertical accelerations during the dynamic tests. There was little differentiation between each floor type.

The peak vertical accelerations were compared to the numerical models as well as vertical response spectra of different spans. The numerical models did not consistently produce accurate results, but the models were significantly more accurate when 7% damping was used rather than 2% damping.

8.2 Conclusions

Mass timber floors were undamaged when subjected to large vertical ground motions and thus can certainly provide high levels of seismic performance when subjected to vertical ground motions. The numerical models were inconsistent at predicting the acceleration response of the mass timber floors, but adjusting a few parameters could make the numerical models viable for predicting seismic vertical response in mass timber floor.

Numerous conclusions can be drawn from the numerical modeling process, the numerical model calibration, and the analysis of the vertical accelerometer testing:

- The damping ratios used in modeling should be higher than the recommended 2% for bare mass timber floors when modeling floors constructed in a building.
- Exterior walls provided less vertical stiffness to floor systems than guidelines suggest.
- The amplitude of the vertical response had a significant peak in both the high and low-frequency range. The vertical floor response spectra increased substantially with increasing elevation.
- Horizontal-only ground motions induced a vertical response in both the table and the mass timber floors.
- The peak vertical floor accelerations were up to 1.5 times larger than the floor's input motion.

8.3 Recommendations for Future Work

Further work is recommended to learn more about mass timber floors subjected to vertical dynamic loads. The following section recommends future research needs for mass timber floors and the numerical modeling process.

8.3.1 10-Story Test Data Analysis

The following research could be performed on the data from the 10-story test:

- Calculating the damping ratios for the different floor types and spans.
- Recalculating the response spectra for each floor span based on a calculated damping ratio.

- Applying different filtering methods to the data.
- Using frequency analyses to identify the frequencies of the floor spans.

8.3.2 Numerical Modeling

The following adjustments to the numerical models could be researched to see if more consistent results could be produced:

- Performing a convergence study on the meshing when applying vertical ground motions.
- Discretizing the masses on the mass timber floors.
- Applying variable damping for each mode.
- A parametric study to assess which parameters most strongly affect the results.

8.3.3 Different Mass Timber Floors

Similar research from this thesis could be applied to the following types of mass timber floors and spans:

- Longer mass timber floor spans that resemble the industry span lengths.
- Mass timber floors with toppings (i.e. composite and non-composite concrete topping).

REFERENCES

- AISC (2017). *Steel Construction Manual*. American Institute of Steel Construction.
- APA (2020). *Standard for Performance Rated Cross-Laminated Timber, ANSI/APA PRG 320-2019*. APA - The Engineered Wood Association.
- APA (2022). *Product Standard for Structural Glued Laminated Timber, ANSI A190.1-2022*. APA - The Engineered Wood Association.
- ASCE (2016). *Minimum Design Loads for Buildings and Other Structures. ASCE 7-16*. American Society of Civil Engineering.
- ATC (2012). “Reducing the risks of nonstructural earthquake damage – a practical guide.” *Report no.*, Federal Emergency Management Agency.
- AWC (2018). *National Design Specification for Wood Construction*. American Wood Council.
- Boise Cascade (2022). “Esr-5157: Boise cascade wood products, llc.” *Report no.*, Boise Cascade Wood Products, LLC.
- Brandner, R., Flatscher, G., Ringhofer, A., Schickhofer, G., and Thiel, A. (2016). “Cross laminated timber (clt): overview and development.” *European Journal of Wood and Wood Products*, 74, 331–351.
- Breneman, S., Zimmerman, R., Gerber, A., Epp, L., Dickof, C., Taylor, A., Loasby, W., McDonnell, E., Slotboom, C., McCutcheon, J., and Visscher, R. (2021). *U.S. Mass Timber Floor Vibration Design Guide*. WoodWorks - Wood Products Council.

- Busch, A. (2023). “Design and construction of tall mass timber buildings with resilient post-tensioned mass timber rocking walls.” Ph.D. thesis, Colorado School of Mines, Golden, Colorado.
- Chopra, A. K. (2014). *Dynamics of Structures*. Pearson.
- CSA O86:19 (2019). “Engineering design in wood.” *Report no.*, CSA Group.
- Cuerrier-Auclair, S. (2020). *Design Guide for Timber-Concrete Composite Floors in Canada*. FPInnovations.
- Dolan, J. D., Murray, T., Johnson, J., Runte, D., and Shue, B. C. (1999). “Preventing annoying wood floor vibrations.” *Journal of Structural Engineering*, 125.
- Epp, L. (2018). “A new mass timber product in north america.” *Wood Design and Building*.
- Forest Products Laboratory (2010). *Wood Handbook*. USDA.
- Hong, K. E. M. (2014). “Structural performance of nail-laminated timber-concrete composite floors.” M.S. thesis, University of Waterloo, Waterloo, Ontario.
- How, S., Sik, H., and Uyup, M. (2016). “An overview of manufacturing process of glued-laminated timber.
- Huang, H., Gao, Y., and Chang, W.-S. (2020). “Human-induced vibration of cross-laminated timber (clt) floor under different boundary conditions.” *Engineering Structures*, 204.
- Irvine, T. (2010). *An Introduction to Shock and Vibration Response Spectra*.
- Jarnerö, K., Brandt, A., and Olsson, A. (2015). “Vibration properties of a timber floor assessed in laboratory and during construction.” *Engineering Structures*, 82, 44–54.
- Ji, Y., Ryan, K., Roser, W., and Hutchinson, T. (2022). “Nheri tallwood 10-story nonstructural, part 3 of 4: Cold-formed steel framed interior walls.

- Karacabeyli, E. and Douglas, B. (2013). *CLT Handbook: Cross-Laminated Timber*. FPInnovations.
- Milojević, M., Racic, V., Marjanović, M., and Nefovska-Danilović, M. (2023). “Influence of inter-panel connections on vibration response of clt floors due to pedestrian-induced loading.” *Engineering Structures*, 277.
- Natterer, J. (2002). “New technologies for engineered timber structures.” *Progress in Structural Engineering and Materials*, 4, 245–263.
- OIB (2020). “European technical assessment.” *Report no.*, Austrian Institute of Construction Engineering.
- Porter, K., Kennedy, R., and Bachman, R. (2006). “Developing fragility functions for building components for atc-58.
- Roser, W., Ryan, K., Ji, Y., and Hutchinson, T. (2022). “Nheri tallwood 10-story non-structural, part 2 of 4: Drift-compatible connections for cold-formed steel framed exterior walls.
- Smulski, S. (1997). *Engineered Wood Products: A Guide for Specifiers, Designers & Users*. Pfs Research Foundation.
- Sorosh, S., Hutchinson, T., and Ryan, K. (2022a). “Nheri tallwood 10-story nonstructural, part 4 of 4: Prefabricated steel stair subassemblies.
- Sorosh, S., Hutchinson, T. C., Ryan, K. L., and Wichman, S. (2022b). “Numerical simulation of prefabricated steel stairs to be implemented in the nheri tallwood building.
- Soti, R., Ho, T. X., and Sinha, A. (2021). “Structural performance characterization of mass plywood panels.” *Materials in Civil Engineering*, 33.
- StructureCraft (2021). *DESIGN AND PROFILE GUIDE: Dowel Laminated Timber*. StructureCraft.

Werner, H. (1997). “Brettstapelbauweise.” *Informationdienst Holz*.

Wichman, S. (2023). “Seismic behavior of tall rocking mass timber walls.” Ph.D. thesis, University of Washington, Seattle, Washington.

Wynn, S., Ryan, K., Roser, W., Ji, S. S., and Hutchinson, T. (2022). “Nheri tallwood 10-story nonstructural, part 1 of 4: Project overview and curtain wall subassembly.

Appendix A

10-STORY TEST DETAILED DRAWINGS

The drawings for the 10-Story test were developed for [Busch \[2023\]](#) and are discussed in more detail throughout that dissertation.

SHEET INDEX			
Sheet Number	Sheet Name	Page Set	Print
1001	CONCRETE WALLS	X	X
1002	CONCRETE SLABS	X	X
1003	CONCRETE BEAMS	X	X
1004	CONCRETE COLUMNS	X	X
1005	CONCRETE JOISTS	X	X
1006	CONCRETE DECKING	X	X
1007	CONCRETE CURBS	X	X
1008	CONCRETE STAIRS	X	X
1009	CONCRETE ELEVATIONS	X	X
1010	CONCRETE SECTION	X	X
1011	CONCRETE DETAIL	X	X
1012	CONCRETE CONNECTION	X	X
1013	CONCRETE REINFORCEMENT	X	X
1014	CONCRETE FINISHES	X	X
1015	CONCRETE PROTECTION	X	X
1016	CONCRETE CURING	X	X
1017	CONCRETE TOLERANCES	X	X
1018	CONCRETE QUALITY CONTROL	X	X
1019	CONCRETE SAFETY	X	X
1020	CONCRETE MAINTENANCE	X	X
1021	CONCRETE REPAIRS	X	X
1022	CONCRETE DEMOLITION	X	X
1023	CONCRETE DISPOSAL	X	X
1024	CONCRETE RECYCLING	X	X
1025	CONCRETE SUSTAINABILITY	X	X
1026	CONCRETE INNOVATION	X	X
1027	CONCRETE RESEARCH	X	X
1028	CONCRETE EDUCATION	X	X
1029	CONCRETE HISTORY	X	X
1030	CONCRETE FUTURE	X	X
1031	CONCRETE INDEX	X	X

LIST OF ABBREVIATIONS

A.B	AMERICAN BUILT
A.C	AMERICAN CONCRETE INSTITUTE
A.C.I.	AMERICAN INSTITUTE OF CONCRETE TECHNOLOGISTS
A.C.I. 308	AMERICAN INSTITUTE OF CONCRETE TECHNOLOGISTS 308
A.C.I. 308.1R	AMERICAN INSTITUTE OF CONCRETE TECHNOLOGISTS 308.1R
A.C.I. 308.2R	AMERICAN INSTITUTE OF CONCRETE TECHNOLOGISTS 308.2R
A.C.I. 308.3R	AMERICAN INSTITUTE OF CONCRETE TECHNOLOGISTS 308.3R
A.C.I. 308.4R	AMERICAN INSTITUTE OF CONCRETE TECHNOLOGISTS 308.4R
A.C.I. 308.5R	AMERICAN INSTITUTE OF CONCRETE TECHNOLOGISTS 308.5R
A.C.I. 308.6R	AMERICAN INSTITUTE OF CONCRETE TECHNOLOGISTS 308.6R
A.C.I. 308.7R	AMERICAN INSTITUTE OF CONCRETE TECHNOLOGISTS 308.7R
A.C.I. 308.8R	AMERICAN INSTITUTE OF CONCRETE TECHNOLOGISTS 308.8R
A.C.I. 308.9R	AMERICAN INSTITUTE OF CONCRETE TECHNOLOGISTS 308.9R
A.C.I. 308.10R	AMERICAN INSTITUTE OF CONCRETE TECHNOLOGISTS 308.10R
A.C.I. 308.11R	AMERICAN INSTITUTE OF CONCRETE TECHNOLOGISTS 308.11R
A.C.I. 308.12R	AMERICAN INSTITUTE OF CONCRETE TECHNOLOGISTS 308.12R
A.C.I. 308.13R	AMERICAN INSTITUTE OF CONCRETE TECHNOLOGISTS 308.13R
A.C.I. 308.14R	AMERICAN INSTITUTE OF CONCRETE TECHNOLOGISTS 308.14R
A.C.I. 308.15R	AMERICAN INSTITUTE OF CONCRETE TECHNOLOGISTS 308.15R
A.C.I. 308.16R	AMERICAN INSTITUTE OF CONCRETE TECHNOLOGISTS 308.16R
A.C.I. 308.17R	AMERICAN INSTITUTE OF CONCRETE TECHNOLOGISTS 308.17R
A.C.I. 308.18R	AMERICAN INSTITUTE OF CONCRETE TECHNOLOGISTS 308.18R
A.C.I. 308.19R	AMERICAN INSTITUTE OF CONCRETE TECHNOLOGISTS 308.19R
A.C.I. 308.20R	AMERICAN INSTITUTE OF CONCRETE TECHNOLOGISTS 308.20R
A.C.I. 308.21R	AMERICAN INSTITUTE OF CONCRETE TECHNOLOGISTS 308.21R
A.C.I. 308.22R	AMERICAN INSTITUTE OF CONCRETE TECHNOLOGISTS 308.22R
A.C.I. 308.23R	AMERICAN INSTITUTE OF CONCRETE TECHNOLOGISTS 308.23R
A.C.I. 308.24R	AMERICAN INSTITUTE OF CONCRETE TECHNOLOGISTS 308.24R
A.C.I. 308.25R	AMERICAN INSTITUTE OF CONCRETE TECHNOLOGISTS 308.25R
A.C.I. 308.26R	AMERICAN INSTITUTE OF CONCRETE TECHNOLOGISTS 308.26R
A.C.I. 308.27R	AMERICAN INSTITUTE OF CONCRETE TECHNOLOGISTS 308.27R
A.C.I. 308.28R	AMERICAN INSTITUTE OF CONCRETE TECHNOLOGISTS 308.28R
A.C.I. 308.29R	AMERICAN INSTITUTE OF CONCRETE TECHNOLOGISTS 308.29R
A.C.I. 308.30R	AMERICAN INSTITUTE OF CONCRETE TECHNOLOGISTS 308.30R
A.C.I. 308.31R	AMERICAN INSTITUTE OF CONCRETE TECHNOLOGISTS 308.31R
A.C.I. 308.32R	AMERICAN INSTITUTE OF CONCRETE TECHNOLOGISTS 308.32R
A.C.I. 308.33R	AMERICAN INSTITUTE OF CONCRETE TECHNOLOGISTS 308.33R
A.C.I. 308.34R	AMERICAN INSTITUTE OF CONCRETE TECHNOLOGISTS 308.34R
A.C.I. 308.35R	AMERICAN INSTITUTE OF CONCRETE TECHNOLOGISTS 308.35R
A.C.I. 308.36R	AMERICAN INSTITUTE OF CONCRETE TECHNOLOGISTS 308.36R
A.C.I. 308.37R	AMERICAN INSTITUTE OF CONCRETE TECHNOLOGISTS 308.37R
A.C.I. 308.38R	AMERICAN INSTITUTE OF CONCRETE TECHNOLOGISTS 308.38R
A.C.I. 308.39R	AMERICAN INSTITUTE OF CONCRETE TECHNOLOGISTS 308.39R
A.C.I. 308.40R	AMERICAN INSTITUTE OF CONCRETE TECHNOLOGISTS 308.40R
A.C.I. 308.41R	AMERICAN INSTITUTE OF CONCRETE TECHNOLOGISTS 308.41R
A.C.I. 308.42R	AMERICAN INSTITUTE OF CONCRETE TECHNOLOGISTS 308.42R
A.C.I. 308.43R	AMERICAN INSTITUTE OF CONCRETE TECHNOLOGISTS 308.43R
A.C.I. 308.44R	AMERICAN INSTITUTE OF CONCRETE TECHNOLOGISTS 308.44R
A.C.I. 308.45R	AMERICAN INSTITUTE OF CONCRETE TECHNOLOGISTS 308.45R
A.C.I. 308.46R	AMERICAN INSTITUTE OF CONCRETE TECHNOLOGISTS 308.46R
A.C.I. 308.47R	AMERICAN INSTITUTE OF CONCRETE TECHNOLOGISTS 308.47R
A.C.I. 308.48R	AMERICAN INSTITUTE OF CONCRETE TECHNOLOGISTS 308.48R
A.C.I. 308.49R	AMERICAN INSTITUTE OF CONCRETE TECHNOLOGISTS 308.49R
A.C.I. 308.50R	AMERICAN INSTITUTE OF CONCRETE TECHNOLOGISTS 308.50R
A.C.I. 308.51R	AMERICAN INSTITUTE OF CONCRETE TECHNOLOGISTS 308.51R
A.C.I. 308.52R	AMERICAN INSTITUTE OF CONCRETE TECHNOLOGISTS 308.52R
A.C.I. 308.53R	AMERICAN INSTITUTE OF CONCRETE TECHNOLOGISTS 308.53R
A.C.I. 308.54R	AMERICAN INSTITUTE OF CONCRETE TECHNOLOGISTS 308.54R
A.C.I. 308.55R	AMERICAN INSTITUTE OF CONCRETE TECHNOLOGISTS 308.55R
A.C.I. 308.56R	AMERICAN INSTITUTE OF CONCRETE TECHNOLOGISTS 308.56R
A.C.I. 308.57R	AMERICAN INSTITUTE OF CONCRETE TECHNOLOGISTS 308.57R
A.C.I. 308.58R	AMERICAN INSTITUTE OF CONCRETE TECHNOLOGISTS 308.58R
A.C.I. 308.59R	AMERICAN INSTITUTE OF CONCRETE TECHNOLOGISTS 308.59R
A.C.I. 308.60R	AMERICAN INSTITUTE OF CONCRETE TECHNOLOGISTS 308.60R
A.C.I. 308.61R	AMERICAN INSTITUTE OF CONCRETE TECHNOLOGISTS 308.61R
A.C.I. 308.62R	AMERICAN INSTITUTE OF CONCRETE TECHNOLOGISTS 308.62R
A.C.I. 308.63R	AMERICAN INSTITUTE OF CONCRETE TECHNOLOGISTS 308.63R
A.C.I. 308.64R	AMERICAN INSTITUTE OF CONCRETE TECHNOLOGISTS 308.64R
A.C.I. 308.65R	AMERICAN INSTITUTE OF CONCRETE TECHNOLOGISTS 308.65R
A.C.I. 308.66R	AMERICAN INSTITUTE OF CONCRETE TECHNOLOGISTS 308.66R
A.C.I. 308.67R	AMERICAN INSTITUTE OF CONCRETE TECHNOLOGISTS 308.67R
A.C.I. 308.68R	AMERICAN INSTITUTE OF CONCRETE TECHNOLOGISTS 308.68R
A.C.I. 308.69R	AMERICAN INSTITUTE OF CONCRETE TECHNOLOGISTS 308.69R
A.C.I. 308.70R	AMERICAN INSTITUTE OF CONCRETE TECHNOLOGISTS 308.70R
A.C.I. 308.71R	AMERICAN INSTITUTE OF CONCRETE TECHNOLOGISTS 308.71R
A.C.I. 308.72R	AMERICAN INSTITUTE OF CONCRETE TECHNOLOGISTS 308.72R
A.C.I. 308.73R	AMERICAN INSTITUTE OF CONCRETE TECHNOLOGISTS 308.73R
A.C.I. 308.74R	AMERICAN INSTITUTE OF CONCRETE TECHNOLOGISTS 308.74R
A.C.I. 308.75R	AMERICAN INSTITUTE OF CONCRETE TECHNOLOGISTS 308.75R
A.C.I. 308.76R	AMERICAN INSTITUTE OF CONCRETE TECHNOLOGISTS 308.76R
A.C.I. 308.77R	AMERICAN INSTITUTE OF CONCRETE TECHNOLOGISTS 308.77R
A.C.I. 308.78R	AMERICAN INSTITUTE OF CONCRETE TECHNOLOGISTS 308.78R
A.C.I. 308.79R	AMERICAN INSTITUTE OF CONCRETE TECHNOLOGISTS 308.79R
A.C.I. 308.80R	AMERICAN INSTITUTE OF CONCRETE TECHNOLOGISTS 308.80R
A.C.I. 308.81R	AMERICAN INSTITUTE OF CONCRETE TECHNOLOGISTS 308.81R
A.C.I. 308.82R	AMERICAN INSTITUTE OF CONCRETE TECHNOLOGISTS 308.82R
A.C.I. 308.83R	AMERICAN INSTITUTE OF CONCRETE TECHNOLOGISTS 308.83R
A.C.I. 308.84R	AMERICAN INSTITUTE OF CONCRETE TECHNOLOGISTS 308.84R
A.C.I. 308.85R	AMERICAN INSTITUTE OF CONCRETE TECHNOLOGISTS 308.85R
A.C.I. 308.86R	AMERICAN INSTITUTE OF CONCRETE TECHNOLOGISTS 308.86R
A.C.I. 308.87R	AMERICAN INSTITUTE OF CONCRETE TECHNOLOGISTS 308.87R
A.C.I. 308.88R	AMERICAN INSTITUTE OF CONCRETE TECHNOLOGISTS 308.88R
A.C.I. 308.89R	AMERICAN INSTITUTE OF CONCRETE TECHNOLOGISTS 308.89R
A.C.I. 308.90R	AMERICAN INSTITUTE OF CONCRETE TECHNOLOGISTS 308.90R
A.C.I. 308.91R	AMERICAN INSTITUTE OF CONCRETE TECHNOLOGISTS 308.91R
A.C.I. 308.92R	AMERICAN INSTITUTE OF CONCRETE TECHNOLOGISTS 308.92R
A.C.I. 308.93R	AMERICAN INSTITUTE OF CONCRETE TECHNOLOGISTS 308.93R
A.C.I. 308.94R	AMERICAN INSTITUTE OF CONCRETE TECHNOLOGISTS 308.94R
A.C.I. 308.95R	AMERICAN INSTITUTE OF CONCRETE TECHNOLOGISTS 308.95R
A.C.I. 308.96R	AMERICAN INSTITUTE OF CONCRETE TECHNOLOGISTS 308.96R
A.C.I. 308.97R	AMERICAN INSTITUTE OF CONCRETE TECHNOLOGISTS 308.97R
A.C.I. 308.98R	AMERICAN INSTITUTE OF CONCRETE TECHNOLOGISTS 308.98R
A.C.I. 308.99R	AMERICAN INSTITUTE OF CONCRETE TECHNOLOGISTS 308.99R
A.C.I. 308.100R	AMERICAN INSTITUTE OF CONCRETE TECHNOLOGISTS 308.100R



1001 Park St
 Oakland, CA 94612
 510.434.1234
 2023 © MPEEREST

PROJECT
 10-Story Test

14201 Parkmead Road
 San Diego, CA 92131

SET INSURANCE
 Revision 1

DATE: 08/08/2023
 TIME: 09:00 AM
 USER: [Name]
 PROJECT: [Name]

Sheet No.	Sheet Name	Page Set	Print
1001	CONCRETE WALLS	X	X
1002	CONCRETE SLABS	X	X
1003	CONCRETE BEAMS	X	X
1004	CONCRETE COLUMNS	X	X
1005	CONCRETE JOISTS	X	X
1006	CONCRETE DECKING	X	X
1007	CONCRETE CURBS	X	X
1008	CONCRETE STAIRS	X	X
1009	CONCRETE ELEVATIONS	X	X
1010	CONCRETE SECTION	X	X
1011	CONCRETE DETAIL	X	X
1012	CONCRETE CONNECTION	X	X
1013	CONCRETE REINFORCEMENT	X	X
1014	CONCRETE FINISHES	X	X
1015	CONCRETE PROTECTION	X	X
1016	CONCRETE CURING	X	X
1017	CONCRETE TOLERANCES	X	X
1018	CONCRETE SAFETY	X	X
1019	CONCRETE MAINTENANCE	X	X
1020	CONCRETE REPAIRS	X	X
1021	CONCRETE DEMOLITION	X	X
1022	CONCRETE DISPOSAL	X	X
1023	CONCRETE RECYCLING	X	X
1024	CONCRETE SUSTAINABILITY	X	X
1025	CONCRETE INNOVATION	X	X
1026	CONCRETE RESEARCH	X	X
1027	CONCRETE EDUCATION	X	X
1028	CONCRETE HISTORY	X	X
1029	CONCRETE FUTURE	X	X
1030	CONCRETE INDEX	X	X

SHEET INDEX
 Drawing Index and List
 of Abbreviations

S001

STRUCTURAL STEEL

TYPE	SYMBOL	DESCRIPTION
WELDED CONNECTION	WELDED CONNECTION	WELDED CONNECTION
STEEL TO CONCRETE CONNECTION	STEEL TO CONCRETE CONNECTION	STEEL TO CONCRETE CONNECTION
STEEL TO STEEL CONNECTION	STEEL TO STEEL CONNECTION	STEEL TO STEEL CONNECTION
STEEL TO WOOD CONNECTION	STEEL TO WOOD CONNECTION	STEEL TO WOOD CONNECTION
STEEL TO MASONRY CONNECTION	STEEL TO MASONRY CONNECTION	STEEL TO MASONRY CONNECTION
STEEL TO GLASS CONNECTION	STEEL TO GLASS CONNECTION	STEEL TO GLASS CONNECTION
STEEL TO OTHER CONNECTION	STEEL TO OTHER CONNECTION	STEEL TO OTHER CONNECTION

CONCRETE REINFORCING STEEL SHALL BE AS FOLLOWS:

1. ALL REINFORCING STEEL SHALL BE SUPPLIED BY A QUALIFIED SUPPLIER WHO SHALL BE RESPONSIBLE FOR OBTAINING ALL NECESSARY APPROVALS AND PERMITS FROM THE LOCAL AUTHORITY.

2. ALL REINFORCING STEEL SHALL BE SUPPLIED IN ACCORDANCE WITH THE REQUIREMENTS OF THE LOCAL AUTHORITY AND THE DESIGNER.

3. ALL REINFORCING STEEL SHALL BE SUPPLIED IN ACCORDANCE WITH THE REQUIREMENTS OF THE LOCAL AUTHORITY AND THE DESIGNER.

4. ALL REINFORCING STEEL SHALL BE SUPPLIED IN ACCORDANCE WITH THE REQUIREMENTS OF THE LOCAL AUTHORITY AND THE DESIGNER.

5. ALL REINFORCING STEEL SHALL BE SUPPLIED IN ACCORDANCE WITH THE REQUIREMENTS OF THE LOCAL AUTHORITY AND THE DESIGNER.

COLD-FORMED METAL FRAMING

COLD-FORMED METAL FRAMING SHALL BE AS FOLLOWS:

1. ALL COLD-FORMED METAL FRAMING SHALL BE SUPPLIED BY A QUALIFIED SUPPLIER WHO SHALL BE RESPONSIBLE FOR OBTAINING ALL NECESSARY APPROVALS AND PERMITS FROM THE LOCAL AUTHORITY.

2. ALL COLD-FORMED METAL FRAMING SHALL BE SUPPLIED IN ACCORDANCE WITH THE REQUIREMENTS OF THE LOCAL AUTHORITY AND THE DESIGNER.

3. ALL COLD-FORMED METAL FRAMING SHALL BE SUPPLIED IN ACCORDANCE WITH THE REQUIREMENTS OF THE LOCAL AUTHORITY AND THE DESIGNER.

4. ALL COLD-FORMED METAL FRAMING SHALL BE SUPPLIED IN ACCORDANCE WITH THE REQUIREMENTS OF THE LOCAL AUTHORITY AND THE DESIGNER.

5. ALL COLD-FORMED METAL FRAMING SHALL BE SUPPLIED IN ACCORDANCE WITH THE REQUIREMENTS OF THE LOCAL AUTHORITY AND THE DESIGNER.

CONCRETE MIX DESIGNS

CONCRETE CLASS	MIN. COMPRESSIVE STRENGTH (MPa)	MIN. COMPRESSIVE STRENGTH (psi)	MIN. SLUMP (mm)	MIN. SLUMP (in.)
CONCRETE CLASS	MIN. COMPRESSIVE STRENGTH (MPa)	MIN. COMPRESSIVE STRENGTH (psi)	MIN. SLUMP (mm)	MIN. SLUMP (in.)

CONCRETE REINFORCING STEEL

REINFORCING STEEL TYPE	DIAMETER (mm)	DIAMETER (in.)	AREA (mm²)	AREA (in²)
REINFORCING STEEL TYPE	DIAMETER (mm)	DIAMETER (in.)	AREA (mm²)	AREA (in²)

CONCRETE EMBEDMENTS

EMBEDMENT TYPE	EMBEDMENT DEPTH (mm)	EMBEDMENT DEPTH (in.)
EMBEDMENT TYPE	EMBEDMENT DEPTH (mm)	EMBEDMENT DEPTH (in.)



1000 Birch St.
Oshkosh, WI 54901
920.233.7262

PROJECT

10-Story Test
14201 Parkwood Road
Sun Prairie, WI 53588

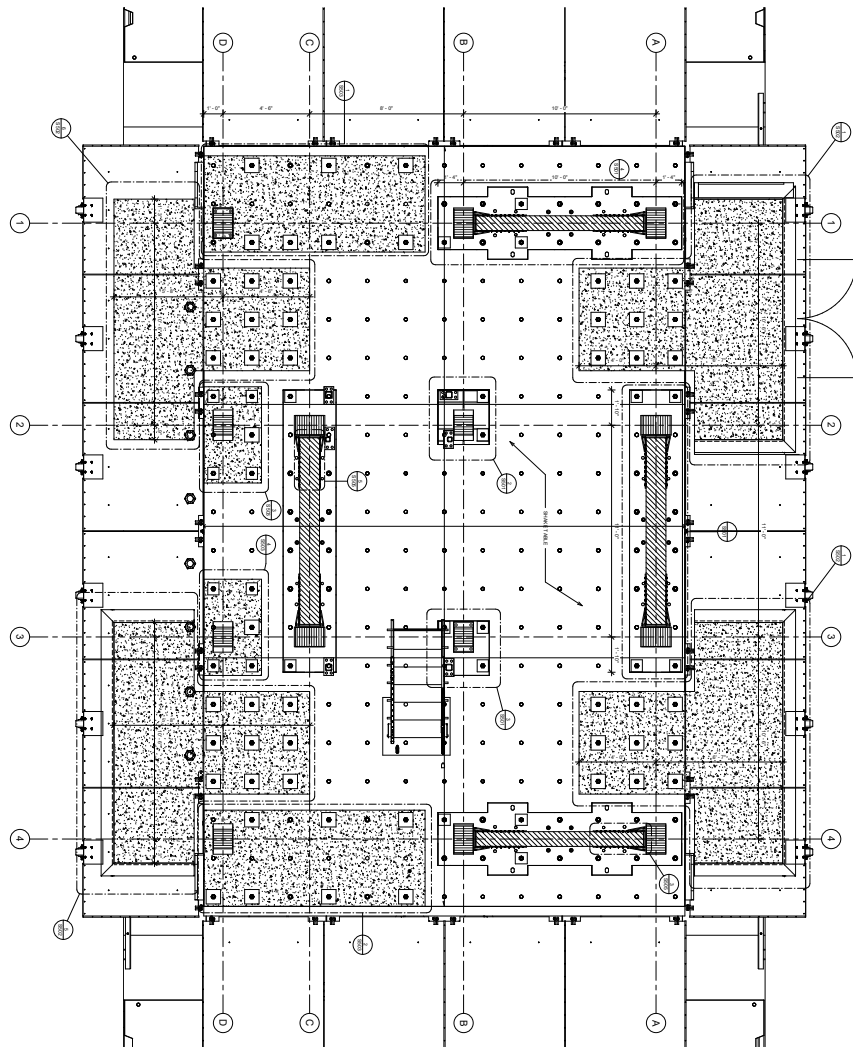
REVISIONS

NO.	DATE	DESCRIPTION
1	03/27/23	ISSUED FOR PERMIT

SHEET SIZE: 30x42
DRAWN: ANB

SHEET

General Structural
Notes
S003





 10-Story Test



1000 Park Dr.
 Oakdale, CT 06047
 203.221.9282

PROJECT: 10-Story Test

10201 Parkers Road
 San Diego, CA 92131

SET ISSUANCE:
 Revision 1

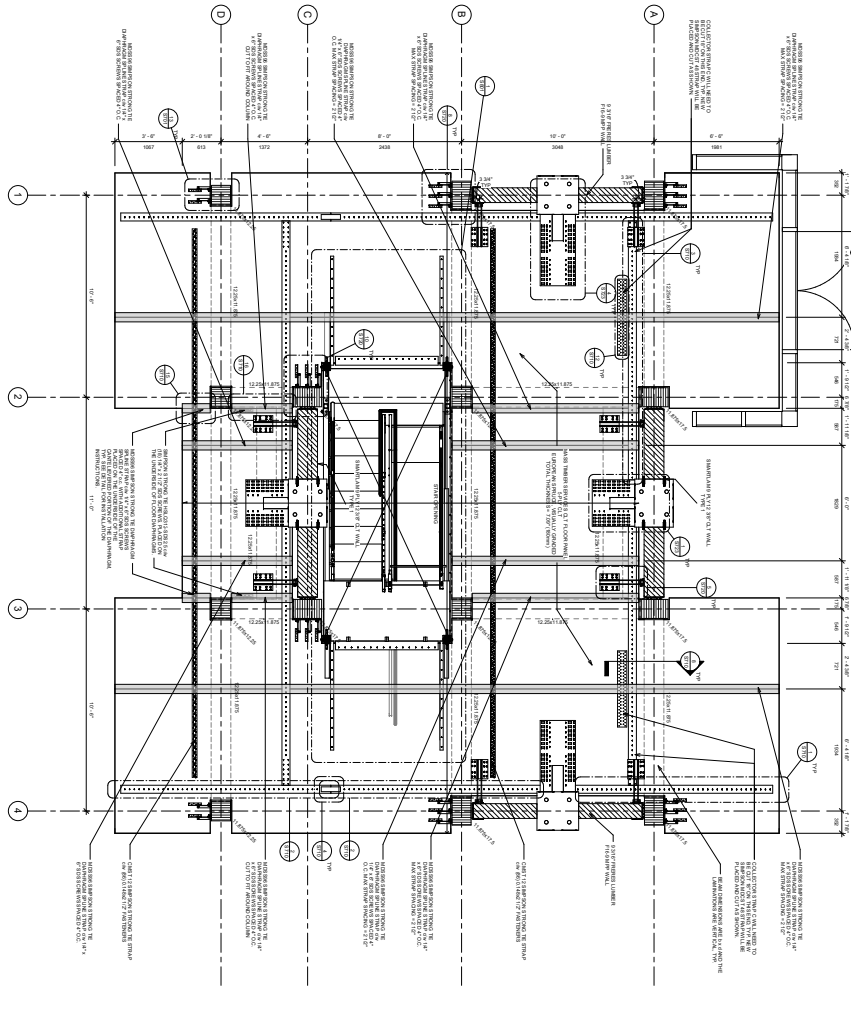
DATE ISSUED: 03/01/23

NO.	REVISION	DATE

SHEET SIZE: 30x42
 DRAWN: ANB

SHEET: 10-Story Test
 Foundation/level 1
 Plan - Structural

S101S



NOTES:
 1. REFER TO SHEET S1025 FOR GENERAL NOTES.
 2. CLT WALLS TO BE INSTALLED IN ACCORDANCE WITH THE MANUFACTURER'S INSTRUCTIONS.
 3. REFER TO SHEET S1025 FOR GENERAL NOTES AND DIMENSIONS.

MPERENT
TRAILWOOD

1020 Park Dr.
 Oakdale, CT 06047
 203.221.1200

PROJECT:
 10-Story Test

1020 Park Drive
 Oakdale, CT 06047
 203.221.1200

SET IN CHARGE:
 Revision 1

DATE: 03/25/2023

BY: [Signature]

FOR: [Signature]

PROJECT: [Signature]

DATE: [Signature]

BY: [Signature]

FOR: [Signature]

PROJECT: [Signature]

DATE: [Signature]

BY: [Signature]

FOR: [Signature]

PROJECT: [Signature]

DATE: [Signature]

BY: [Signature]

FOR: [Signature]

PROJECT: [Signature]

DATE: [Signature]

BY: [Signature]

FOR: [Signature]

PROJECT: [Signature]

DATE: [Signature]

BY: [Signature]

FOR: [Signature]

PROJECT: [Signature]

DATE: [Signature]

BY: [Signature]

FOR: [Signature]

PROJECT: [Signature]

DATE: [Signature]

BY: [Signature]

FOR: [Signature]

PROJECT: [Signature]

DATE: [Signature]

BY: [Signature]

FOR: [Signature]

PROJECT: [Signature]

DATE: [Signature]

BY: [Signature]

FOR: [Signature]

PROJECT: [Signature]

DATE: [Signature]

BY: [Signature]

FOR: [Signature]

PROJECT: [Signature]

DATE: [Signature]

BY: [Signature]

FOR: [Signature]

PROJECT: [Signature]

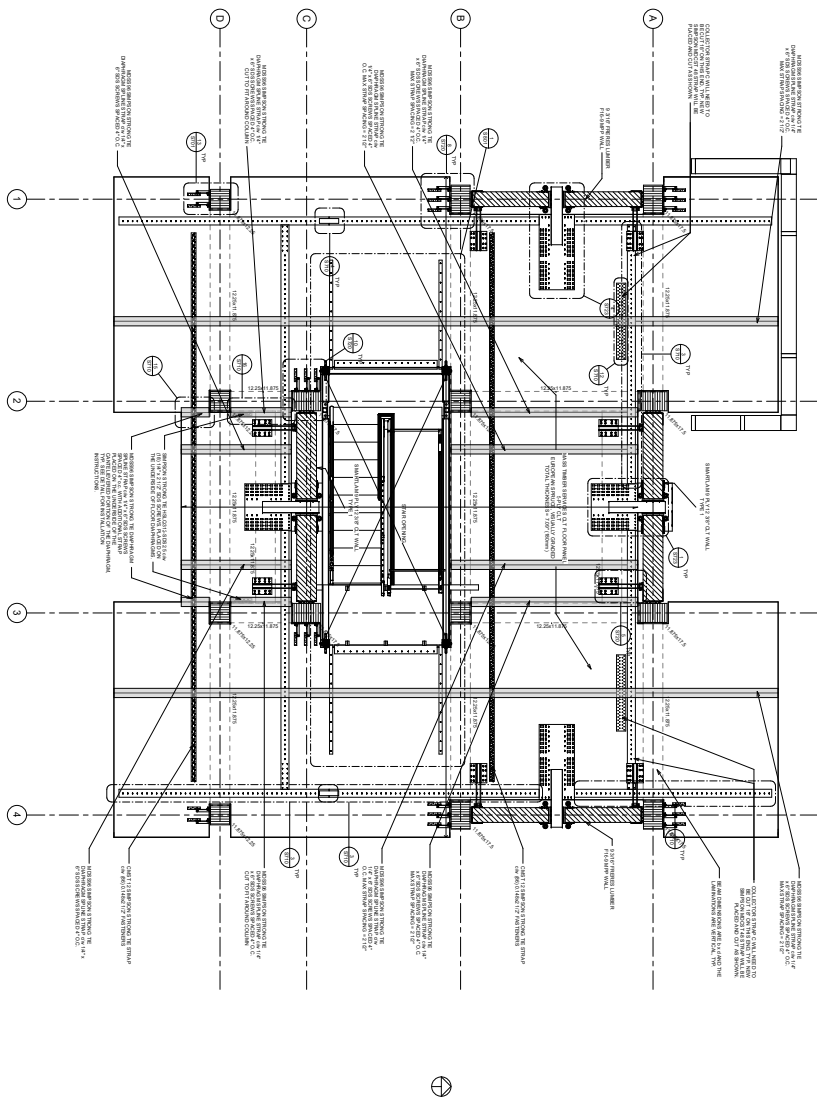
DATE: [Signature]

BY: [Signature]

S1025

SHEET:
 Level 2 Plan -
 Structural
 DRAWN BY: AN

- NOTES
1. MAX. SPS. HANGERS REMOVED IN 1 FLOOR PLAN
 2. HANGERS IN 2ND FLOOR REMOVED IN CONNECTION WITH BOARD EDGES
 3. HANGERS IN 3RD FLOOR REMOVED IN CONNECTION WITH BOARD EDGES



MPERENT
TRAILWOOD

1000 Park Dr
Oakland, CA 94612
510.533.1320

PROJECT:
10-Story Test

14201 Paramo Road
San Diego, CA 92131

SET/ISSUANCE:
Revision 1

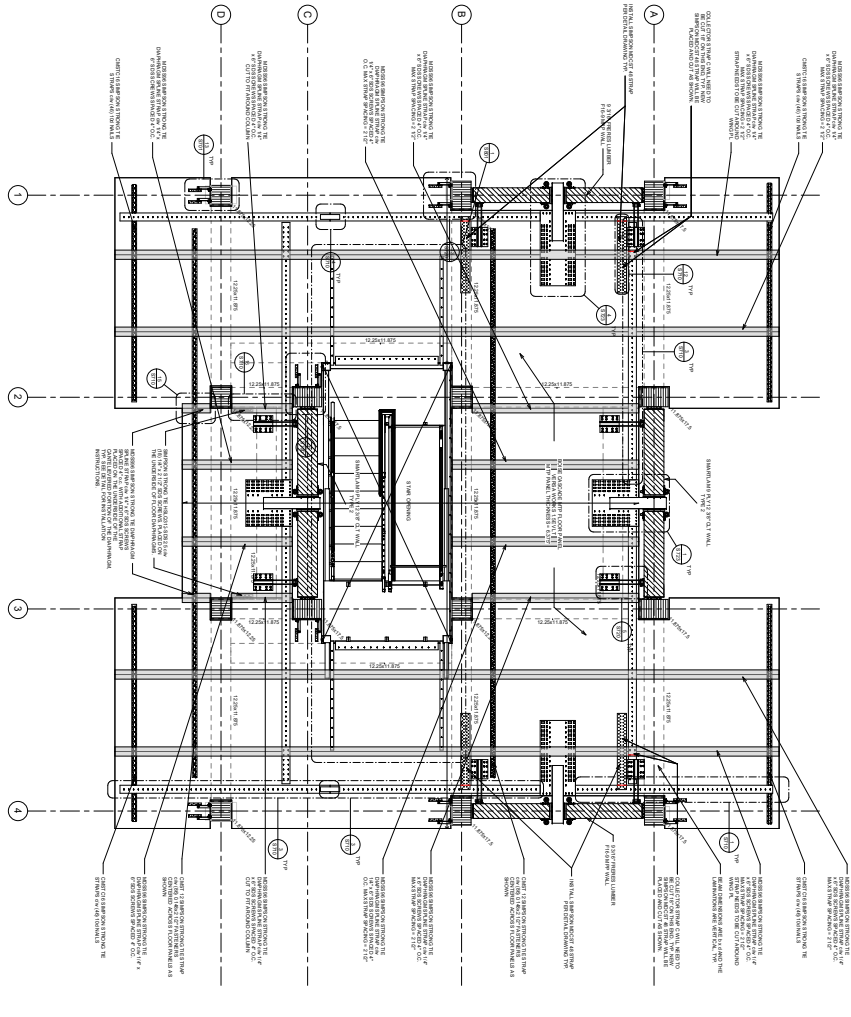
DATE: 03/28/2023

No.	Revision	Description	Date
1			03/28/23

SHEET SIZE: 30x42
DRAWN BY: ANB

SHEET:
Level 3 Plan -
Structural

S103S



- Notes**
1. REFER TO DRAWING 10-100 FOR CLT PANEL CONNECTIONS.
 2. REFER TO DRAWING 10-101 FOR CLT PANEL CONNECTIONS.
 3. REFER TO DRAWING 10-102 FOR CLT PANEL CONNECTIONS.
 4. REFER TO DRAWING 10-103 FOR CLT PANEL CONNECTIONS.



1020 Park Dr
Graham, CO 80431
303.733.9200

PROJECT:
10-Story Test

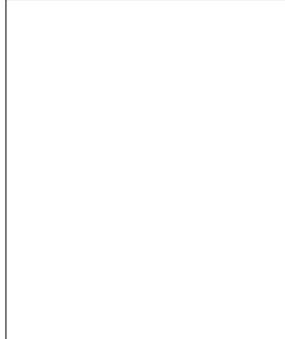
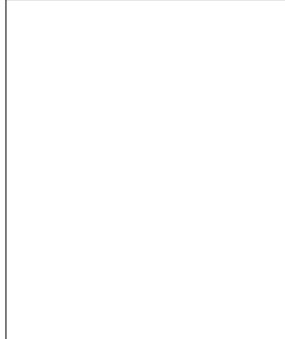
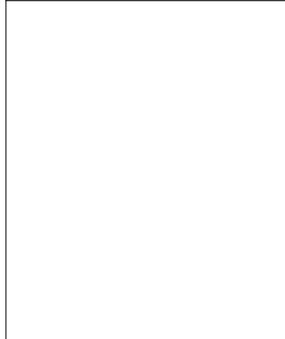
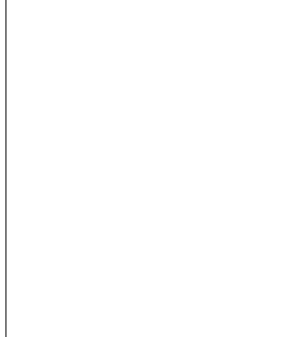
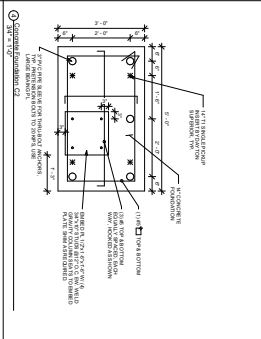
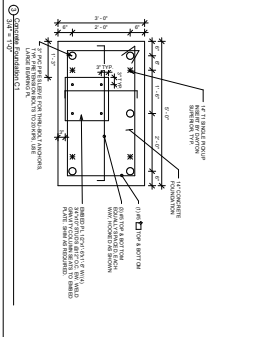
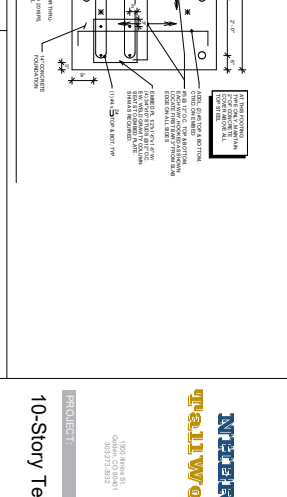
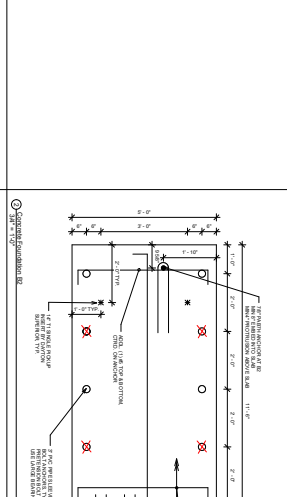
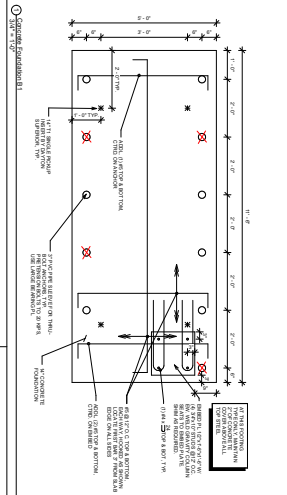
14201 Parkway Road
San Diego, CA 92131

SET ISSUANCE:

DATE	REVISIONS	BY	CHKD

SHEET:
Level 9 Plan - Structural

S109S



PROJECT: 10-Story Test

14201 Parkway Road
San Diego, CA 92131

DATE: 03/25/2023

DESIGNER: ANB

ITEM:

QTY:

SHEET: Concrete Foundation Details

S503

PROJECT:
10-Story Test

14201 Parkway Road
San Diego, CA 92131

DATE: 03/25/2023

DESIGNER: ANB

PROJECT:
10-Story Test

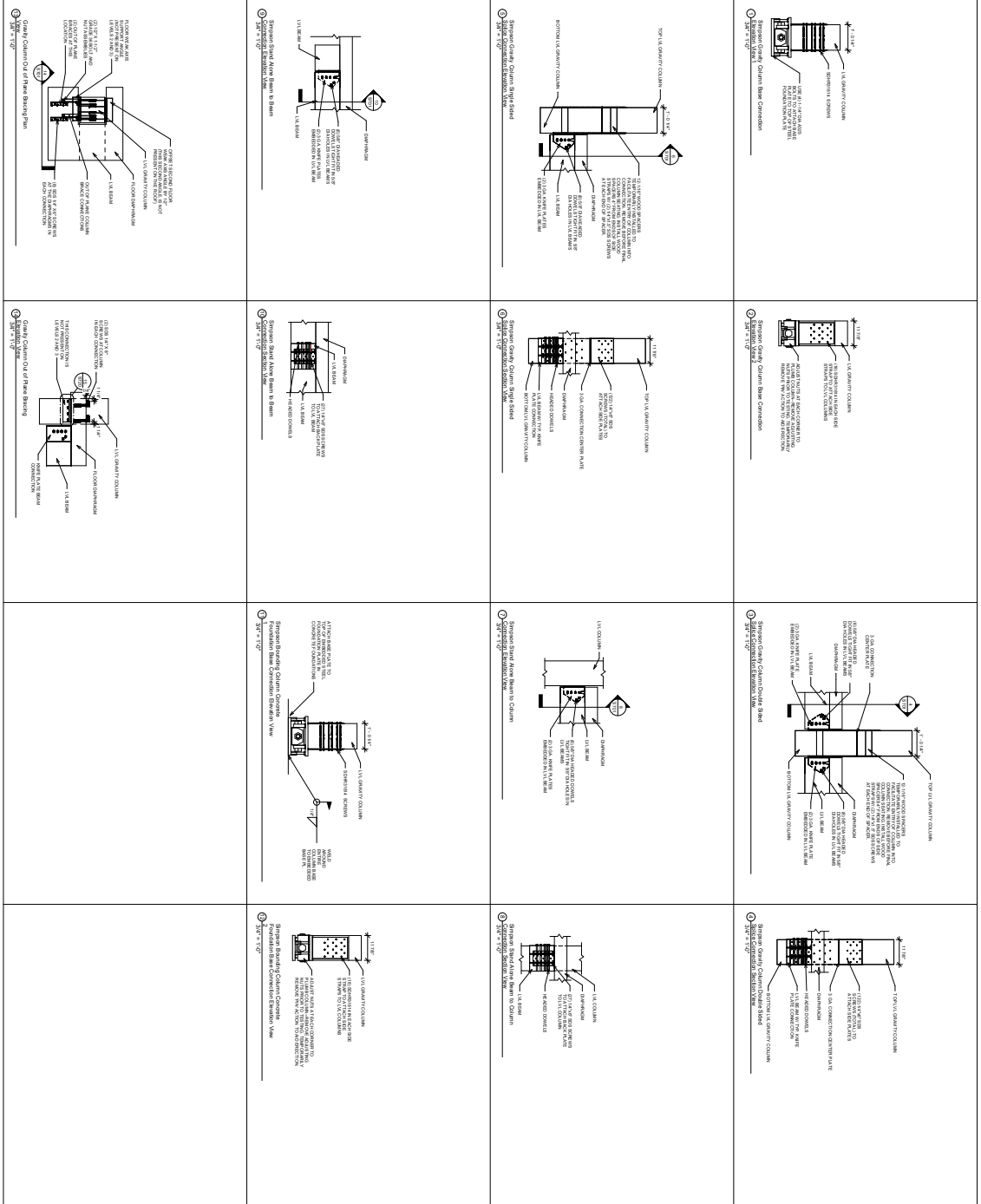
14201 Parkway Road
San Diego, CA 92131

DATE: 03/25/2023

DESIGNER: ANB

SHEET: Foundation Connection Details

S505



PROJECT:

10-Story Test

CLIENT:

1001 Pine St
 Oakland, CA 94612
 510.434.2222

DATE:

03/25/2023

SETBACK:

10211 Panama Road
 San Diego, CA 92131

REVISIONS:

NO.	DESCRIPTION	DATE

SHEET SIZE:

DRAWN BY: AN

SHEET:

Simpson Gravity
 Details

S701

<p>Impact Column A 2# 10 11'-0" MAXIMUM FROM FACE OF BEARING 10'-0" MAXIMUM FROM FACE OF BEARING 2# 10 10'-0" MAXIMUM FROM FACE OF BEARING 2# 10 10'-0" MAXIMUM FROM FACE OF BEARING</p>	<p>Impact Column B 2# 10 10'-0" MAXIMUM FROM FACE OF BEARING 2# 10 10'-0" MAXIMUM FROM FACE OF BEARING 2# 10 10'-0" MAXIMUM FROM FACE OF BEARING</p>	<p>Impact Column C 2# 10 10'-0" MAXIMUM FROM FACE OF BEARING 2# 10 10'-0" MAXIMUM FROM FACE OF BEARING 2# 10 10'-0" MAXIMUM FROM FACE OF BEARING</p>	<p>Impact Column D 2# 10 10'-0" MAXIMUM FROM FACE OF BEARING 2# 10 10'-0" MAXIMUM FROM FACE OF BEARING 2# 10 10'-0" MAXIMUM FROM FACE OF BEARING</p>
<p>Impact Column E 2# 10 10'-0" MAXIMUM FROM FACE OF BEARING 2# 10 10'-0" MAXIMUM FROM FACE OF BEARING 2# 10 10'-0" MAXIMUM FROM FACE OF BEARING</p>	<p>Impact Column F 2# 10 10'-0" MAXIMUM FROM FACE OF BEARING 2# 10 10'-0" MAXIMUM FROM FACE OF BEARING 2# 10 10'-0" MAXIMUM FROM FACE OF BEARING</p>	<p>Impact Column G 2# 10 10'-0" MAXIMUM FROM FACE OF BEARING 2# 10 10'-0" MAXIMUM FROM FACE OF BEARING 2# 10 10'-0" MAXIMUM FROM FACE OF BEARING</p>	<p>Impact Column H 2# 10 10'-0" MAXIMUM FROM FACE OF BEARING 2# 10 10'-0" MAXIMUM FROM FACE OF BEARING 2# 10 10'-0" MAXIMUM FROM FACE OF BEARING</p>
<p>Impact Column I 2# 10 10'-0" MAXIMUM FROM FACE OF BEARING 2# 10 10'-0" MAXIMUM FROM FACE OF BEARING 2# 10 10'-0" MAXIMUM FROM FACE OF BEARING</p>	<p>Impact Column J 2# 10 10'-0" MAXIMUM FROM FACE OF BEARING 2# 10 10'-0" MAXIMUM FROM FACE OF BEARING 2# 10 10'-0" MAXIMUM FROM FACE OF BEARING</p>	<p>Impact Column K 2# 10 10'-0" MAXIMUM FROM FACE OF BEARING 2# 10 10'-0" MAXIMUM FROM FACE OF BEARING 2# 10 10'-0" MAXIMUM FROM FACE OF BEARING</p>	<p>Impact Column L 2# 10 10'-0" MAXIMUM FROM FACE OF BEARING 2# 10 10'-0" MAXIMUM FROM FACE OF BEARING 2# 10 10'-0" MAXIMUM FROM FACE OF BEARING</p>
<p>Impact Column M 2# 10 10'-0" MAXIMUM FROM FACE OF BEARING 2# 10 10'-0" MAXIMUM FROM FACE OF BEARING 2# 10 10'-0" MAXIMUM FROM FACE OF BEARING</p>	<p>Impact Column N 2# 10 10'-0" MAXIMUM FROM FACE OF BEARING 2# 10 10'-0" MAXIMUM FROM FACE OF BEARING 2# 10 10'-0" MAXIMUM FROM FACE OF BEARING</p>	<p>Impact Column O 2# 10 10'-0" MAXIMUM FROM FACE OF BEARING 2# 10 10'-0" MAXIMUM FROM FACE OF BEARING 2# 10 10'-0" MAXIMUM FROM FACE OF BEARING</p>	<p>Impact Column P 2# 10 10'-0" MAXIMUM FROM FACE OF BEARING 2# 10 10'-0" MAXIMUM FROM FACE OF BEARING 2# 10 10'-0" MAXIMUM FROM FACE OF BEARING</p>
<p>Impact Column Q 2# 10 10'-0" MAXIMUM FROM FACE OF BEARING 2# 10 10'-0" MAXIMUM FROM FACE OF BEARING 2# 10 10'-0" MAXIMUM FROM FACE OF BEARING</p>	<p>Impact Column R 2# 10 10'-0" MAXIMUM FROM FACE OF BEARING 2# 10 10'-0" MAXIMUM FROM FACE OF BEARING 2# 10 10'-0" MAXIMUM FROM FACE OF BEARING</p>	<p>Impact Column S 2# 10 10'-0" MAXIMUM FROM FACE OF BEARING 2# 10 10'-0" MAXIMUM FROM FACE OF BEARING 2# 10 10'-0" MAXIMUM FROM FACE OF BEARING</p>	<p>Impact Column T 2# 10 10'-0" MAXIMUM FROM FACE OF BEARING 2# 10 10'-0" MAXIMUM FROM FACE OF BEARING 2# 10 10'-0" MAXIMUM FROM FACE OF BEARING</p>

1020 Park St
Oakland, CA 94612
510.434.2222

PROJECT

10-Story Test

SET INSURANCE

14201 Potrero Road
San Diego, CA 92131

DATE REVISIONS

No.	Description	Date

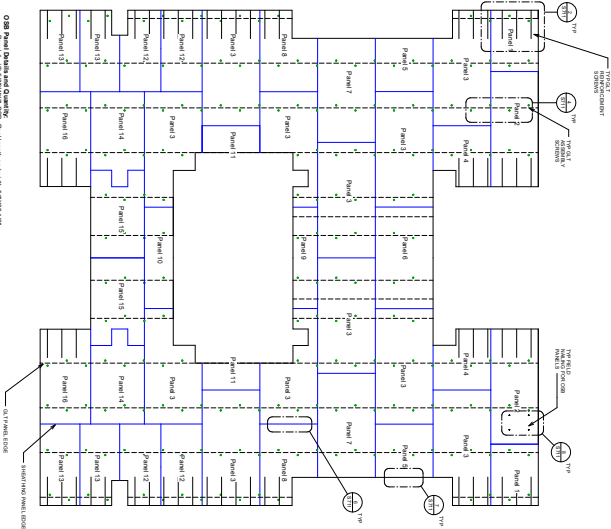
SHEET SIZE: 30x42

DRAWN BY: ANB

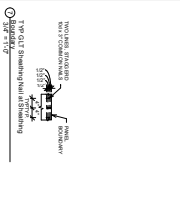
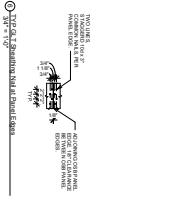
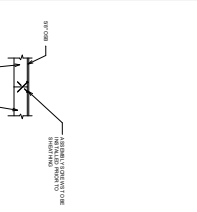
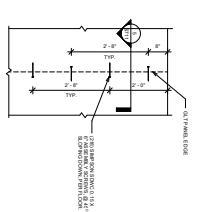
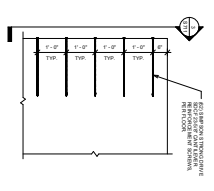
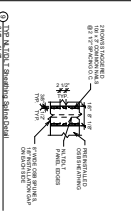
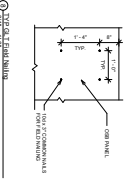
SHEET

Diaphragm Details

S710



- CLT Panel Details and Quantities**
- Panel 1 - (1) 8'0" x 8'0" CLT Panel, Height and width is 8'0" x 8'0"
 - Panel 2 - (1) 8'0" x 8'0" CLT Panel, Height and width is 8'0" x 8'0"
 - Panel 3 - (1) 8'0" x 8'0" CLT Panel, Height and width is 8'0" x 8'0"
 - Panel 4 - (1) 8'0" x 8'0" CLT Panel, Height and width is 8'0" x 8'0"
 - Panel 5 - (1) 8'0" x 8'0" CLT Panel, Height and width is 8'0" x 8'0"
 - Panel 6 - (1) 8'0" x 8'0" CLT Panel, Height and width is 8'0" x 8'0"
 - Panel 7 - (1) 8'0" x 8'0" CLT Panel, Height and width is 8'0" x 8'0"
 - Panel 8 - (1) 8'0" x 8'0" CLT Panel, Height and width is 8'0" x 8'0"
 - Panel 9 - (1) 8'0" x 8'0" CLT Panel, Height and width is 8'0" x 8'0"
 - Panel 10 - (1) 8'0" x 8'0" CLT Panel, Height and width is 8'0" x 8'0"
 - Panel 11 - (1) 8'0" x 8'0" CLT Panel, Height and width is 8'0" x 8'0"
 - Panel 12 - (1) 8'0" x 8'0" CLT Panel, Height and width is 8'0" x 8'0"
 - Panel 13 - (1) 8'0" x 8'0" CLT Panel, Height and width is 8'0" x 8'0"
 - Panel 14 - (1) 8'0" x 8'0" CLT Panel, Height and width is 8'0" x 8'0"
 - Panel 15 - (1) 8'0" x 8'0" CLT Panel, Height and width is 8'0" x 8'0"
 - Panel 16 - (1) 8'0" x 8'0" CLT Panel, Height and width is 8'0" x 8'0"
- The quantity for this list is only for one single CLT Panel. Note



PROJECT: 10-Story Test

14201 Pomeroy Road
San Diego, CA 92131

DATE: 03/25/23

DESIGNER: [Blank]

CHECKER: [Blank]

DATE: [Blank]

DESCRIPTION: [Blank]

DATE: [Blank]

ITEM: [Blank]

QTY: [Blank]

SHEET: [Blank]

Sheathing Details

ITEM: [Blank]

QTY: [Blank]

SHEET: [Blank]

Sheathing Details

S711

<p>10-Story Slab Edge Section Scale: 1/4" = 1'-0"</p>	<p>10-Story Slab Edge Section Scale: 1/4" = 1'-0"</p>	<p>10-Story Slab Edge Section Scale: 1/4" = 1'-0"</p>	<p>10-Story Slab Edge Section Scale: 1/4" = 1'-0"</p>
<p>10-Story Slab Edge Section Scale: 1/4" = 1'-0"</p>	<p>10-Story Slab Edge Section Scale: 1/4" = 1'-0"</p>	<p>10-Story Slab Edge Section Scale: 1/4" = 1'-0"</p>	<p>10-Story Slab Edge Section Scale: 1/4" = 1'-0"</p>
<p>10-Story Slab Edge Section Scale: 1/4" = 1'-0"</p>	<p>10-Story Slab Edge Section Scale: 1/4" = 1'-0"</p>	<p>10-Story Slab Edge Section Scale: 1/4" = 1'-0"</p>	<p>10-Story Slab Edge Section Scale: 1/4" = 1'-0"</p>
<p>10-Story Slab Edge Section Scale: 1/4" = 1'-0"</p>	<p>10-Story Slab Edge Section Scale: 1/4" = 1'-0"</p>	<p>10-Story Slab Edge Section Scale: 1/4" = 1'-0"</p>	<p>10-Story Slab Edge Section Scale: 1/4" = 1'-0"</p>

PROJECT: 10-Story Test

10201 Perimeter Road
San Diego, CA 92131

DATE: 03/25/2023

SCALE: 1/4" = 1'-0"

10201 Perimeter Road
San Diego, CA 92131
360.551.1200

ITEM: _____

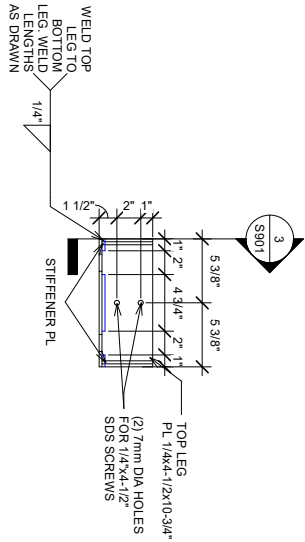
QTY: _____

SHEET: _____

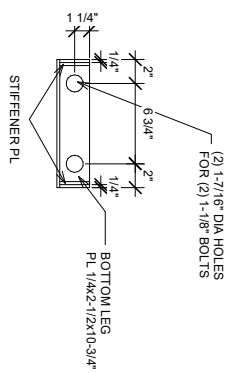
Notes:

1. Lateral Details

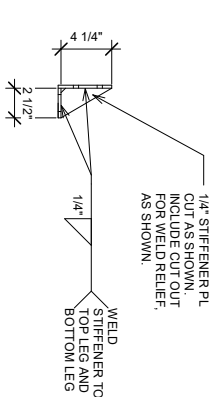
ST22



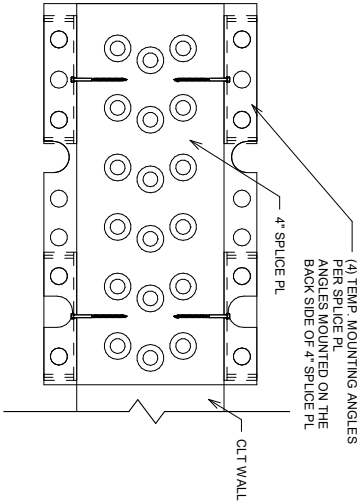
1 CLT Temp. Mounting Angle Elevation
1 1/2" = 1'-0"



2 CLT Temp. Mounting Angle Plan
1 1/2" = 1'-0"



3 CLT Temp. Mounting Angle Section
1 1/2" = 1'-0"



4 CLT Installation View of Temp. Splice
1 1/2" = 1'-0"

INSTALLATION NOTES:
 - THE ANGLES SHOULD BE PLACED ON THE BACK SIDE (OPPOSITE SIDE OF THE COUNTERSUNK HOLES) OF THE SPICE PL.
 - LINE THE 1-7/16" DIA HOLES IN THE BOTTOM LEG OF THE ANGLE WITH THE EXISTING 1-7/16" DIA HOLES IN THE 4" SPICE PLATE. THE EDGE OF THE BOTTOM LEG SHOULD BE FLUSH WITH THE EDGE OF THE SPICE PL (AS SHOWN). MEASUREMENTS WILL BE MADE THE DAY OF INSTALLATION TO ENSURE THE WALL WIDTH MATCHES THE DISTANCE BETWEEN THE TWO ANGLES.
 - IF AN ADJUSTMENT NEEDS TO BE MADE DUE TO PANEL SWELLING, THE ANGLES CAN BE MOVED TO MATCH THE AS BUILT PANEL WIDTH.
 - THE ANGLES ARE MOVED AT LEAST 1/4" FROM THE EDGE OF THE SPICE PL.
 - ONCE PLACEMENT IS CONFIRMED THE ANGLES CAN BE BOLTED TO THE FRONT SIDE OF THE SPICE PL.
 - ONCE THE ANGLES ARE ATTACHED TO THE SPICE PLATE, THE SPICE PLATE CAN BE PLACED ON THE WALL. WHEN THE CORRECT PLACEMENT IS DETERMINED THE (2) SDS SCREWS IN EACH OF THE ANGLES CAN BE INSTALLED TO KEEP THE SPICE PLATE IN PLACE.
 - ONCE THE SCREWS ARE IN PLACE THE EPOXY ROD PROCESS CAN BEGIN.
 - ONCE THE EPOXY PROCESS IS OVER AND FULLY CURED THE TEMPORARY ANGLES CAN BE UNBOLTED AND REUSED ON OTHER PLATES FOLLOWING THE SAME PROCESSES.

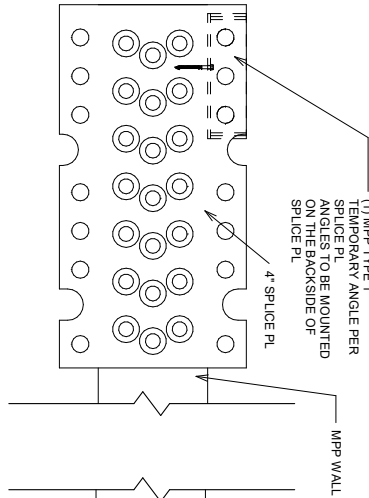
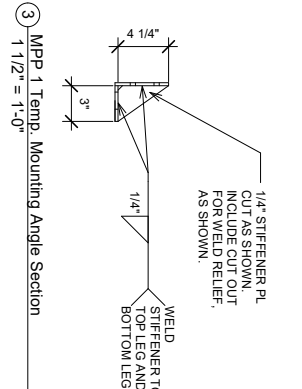
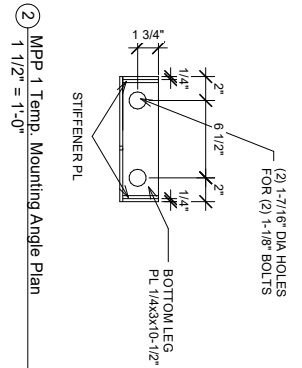
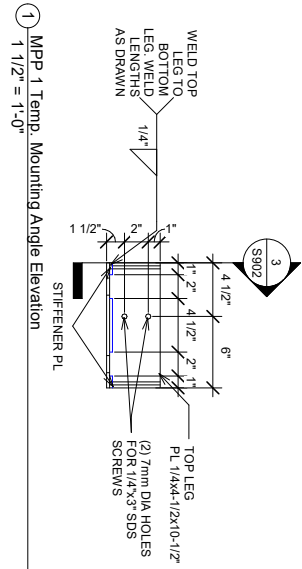
TOTAL QUANTITY: 8

NHERI
TailWood

NHERI TailWood
 10-Story Test

No.	Description	Date

CLT Temp. Mounting Angles
 Project Number: **S901**
 Date: 9/15/2022
 Drawn by: ANB
 Checked by:
 Scale: 1 1/2" = 1'-0"



INSTALLATION NOTES:

- THE ANGLES SHOULD BE PLACED ON THE BACK SIDE (OPPOSITE SIDE OF THE EXISTING WALL) OF THE SPLICE PL.
- LINE THE 1-7/16" DIA HOLES IN THE BOTTOM LEG OF THE ANGLE WITH THE EXISTING 1-7/16" DIA HOLES IN THE 4" SPLICE PLATE. THE EDGE OF THE BOTTOM LEG SHOULD BE FLUSH WITH THE EDGE OF THE SPLICE PL (AS SHOWN). MEASUREMENTS WILL BE MADE THE DAY OF INSTALLATION TO ENSURE THE WALL WIDTH MATCHES THE DISTANCE BETWEEN THE TWO ANGLES.
- IF AN ADJUSTMENT NEEDS TO BE MADE DUE TO PANEL SWELLING, THE ANGLES CAN BE MOVED TO MATCH THE AS-BUILT PANEL WIDTH.
- IF THE ANGLES ARE MOVED A LEVEL WILL NEED TO BE USED TO ENSURE THE ANGLES ARE SET PLING STRAIGHT BEFORE BOLTING.
- AFTER THE ANGLES ARE BOLTED TO THE 4" SPLICE PL, THE SPLICE PL SHOULD BE TIGHTENED TO THE CORRECT TORQUE.
- USING 1-3/8" BOLTS, TIGHTENING OF THE BOLTS NEEDS TO OCCUR ON THE FRONT SIDE OF THE SPLICE PL.
- ONCE THE ANGLES ARE ATTACHED TO THE SPLICE PLATE, THE SPLICE PLATE CAN BE PLACED ON THE WALL, WHEN THE CORRECT PLACEMENT IS DETERMINED THE (2) SDS SCREWS IN EACH OF THE ANGLES CAN BE INSTALLED TO KEEP THE SPLICE PLATE IN PLACE.
- ONCE THE SCREWS ARE IN PLACE THE EPOXY ROD PROCESS CAN BEGIN.
- ONCE THE EPOXY PROCESS IS OVER AND FULLY CURED, THE TEMPORARY ANGLES CAN BE UNBOLTED AND REUSED ON OTHER PLATES FOLLOWING THE SAME PROCESS.

TOTAL QUANTITY: 2

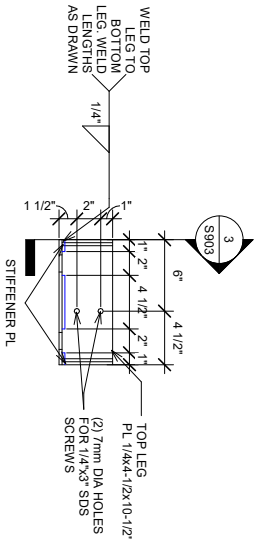
④ MPP 1 Installation View of Temp. Angles
1 1/2" = 1'-0"

NIHERI
TailWood

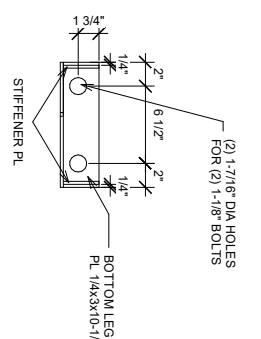
NIHERI TailWood
10-Story Test

No.	Description	Date

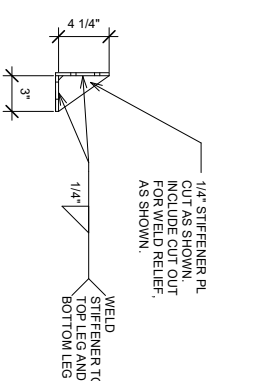
MPP 1 Temp. Mounting Angle		S902
Project Number	Project Number	
Date	9/15/2022	Scale 1 1/2" = 1'-0"
Drawn by	ANB	
Checked by	Checker	



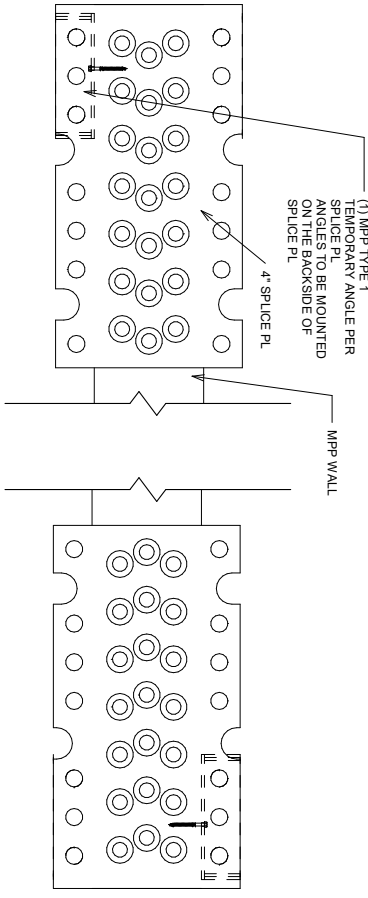
1 MPP 2 Temp. Mounting Angle Elevation
1 1/2" = 1'-0"



2 MPP 2 Temp. Mounting Angle Plan
1 1/2" = 1'-0"



3 MPP 2 Temp. Mounting Angle Section
1 1/2" = 1'-0"



4 MPP 2 Installation View of Temp. Angles
1 1/2" = 1'-0"

INSTALLATION NOTES:

- THE ANGLES SHOULD BE PLACED ON THE BACK SIDE (OPPOSITE SIDE OF THE COUNTERSUNK HOLES) OF THE SPLICE PL.
- LINE THE 1-7/16" DIA HOLES IN THE BOTTOM LEG OF THE ANGLE WITH THE EXISTING 1-7/16" DIA HOLES IN THE TOP LEG. THE SPACING OF THE ANGLES SHOULD BE FLUSH WITH THE EDGES OF THE SPLICE PL. THIS SHOWS THE SPACING TO BE THE DAY OF INSTALLATION TO ENSURE THE WALL WIDTH MATCHES THE DISTANCE BETWEEN THE TWO ANGLES.
- IF AN ADJUSTMENT NEEDS TO BE MADE DUE TO PANEL SWELLING, THE ANGLES CAN BE MOVED TO MATCH THE AS-BUILT PANEL WIDTH.
- IF THE ANGLES ARE MOVED, A LEVEL WILL NEED TO BE USED TO ENSURE THE ANGLES ARE SITTING STRAIGHT BEFORE BOLT TIGHTENING.
- ONCE PLACEMENT IS CONFIRMED THE ANGLES CAN BE BOLTED TO THE 4" SPLICE PL USING 1-3/8" BOLTS. TIGHTENING OF THE BOLTS NEEDS TO OCCUR ON THE FRONT SIDE OF THE SPLICE PL.
- ONCE THE ANGLES ARE ATTACHED TO THE SPLICE PLATE, THE SPLICE PLATE CAN BE PLACED ON THE WALL WHEN THE CORRECT PLACEMENT IS DETERMINED. THE (2) SDS SCREWS IN EACH OF THE ANGLES CAN BE INSTALLED TO KEEP THE SPLICE PLATE IN PLACE.
- ONCE THE SCREWS ARE IN PLACE THE EPOXY ROD PROCESS CAN BEGIN.
- ONCE THE EPOXY PROCESS IS OVER AND FULLY CURED, THE TEMPORARY ANGLES CAN BE UNBOLTED AND REUSED ON OTHER PLATES FOLLOWING THE SAME PROCESS.

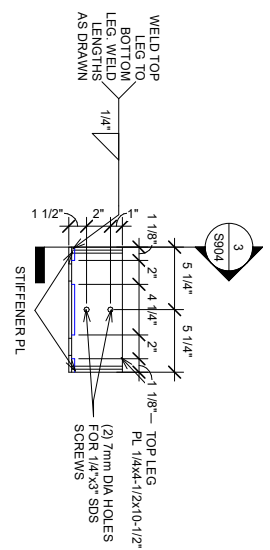
TOTAL QUANTITY: 2



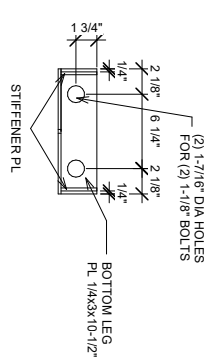
NHERI TallWood
10-Story Test

No.	Description	Date

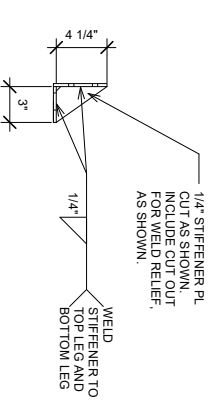
MPP 2 Temp. Mounting Angle	
Project Number	Project Number
Date	9/15/2022
Drawn by	ANB
Checked by	Checker
S903	
Scale 1 1/2" = 1'-0"	



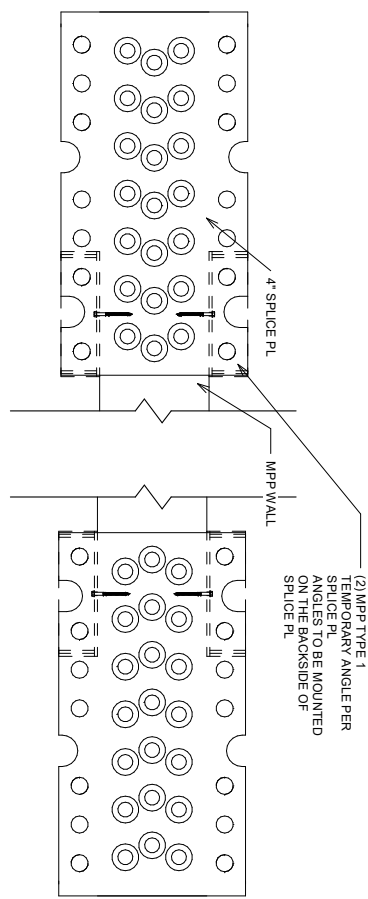
① MPP 3 Temp. Mounting Angle Elevation
 1 1/2" = 1'-0"



② MPP 3 Temp. Mounting Angle Plan
 1 1/2" = 1'-0"



③ MPP 3 Temp. Mounting Angle Section
 1 1/2" = 1'-0"



④ MPP 3 Installation View of Temp. Angles
 1 1/2" = 1'-0"

INSTALLATION NOTES:
 - THE ANGLE SHOULD BE PLACED ON THE BACK SIDE (OPPOSITE SIDE OF THE COUNTERSUNK HOLES) OF THE SPLICE PL.
 - LINE THE 1/2" DIA HOLES IN THE BOTTOM LEG OF THE ANGLE WITH THE EXISTING 1-7/16" DIA HOLES IN THE 4" SPLICE PL. THE EDGE OF THE BOTTOM LEG SHOULD BE FLUSH WITH THE EDGE OF THE SPLICE PL (AS SHOWN). MEASUREMENTS WILL BE MADE THE DAY OF INSTALLATION TO ENSURE THE WALL WIDTH MATCHES THE DISTANCE BETWEEN THE TWO ANGLES.
 - IF AN ADJUSTMENT NEEDS TO BE MADE DUE TO PANEL SWELLING, THE ANGLES CAN BE MOVED TO MATCH THE AS-BUILT PANEL WIDTH.
 - IF THE ANGLES ARE MOVED, A LEVEL WILL NEED TO BE USED TO ENSURE THE ANGLES ARE PLACED AT THE SAME LEVEL.
 - ONCE PLACEMENT IS CONFIRMED, THE ANGLES CAN BE BOLTED TO THE 4" SPLICE PL USING 1-3/8" BOLTS. TIGHTENING OF THE BOLTS NEEDS TO OCCUR ON THE FRONT SIDE OF THE SPLICE PL.
 - ONCE THE ANGLES ARE ATTACHED TO THE SPLICE PLATE, THE SPLICE PLATE CAN BE PLACED ON THE WALL. WHEN THE CORRECT PLACEMENT IS DETERMINED, THE (2) SDS SCREWS IN EACH OF THE ANGLES CAN BE INSTALLED TO KEEP THE SPLICE PLATE IN PLACE.
 - ONCE THE SCREWS ARE IN PLACE, THE EPOXY ROD PROCESS CAN BEGIN.
 - ONCE THE EPOXY PROCESS IS OVER AND FULLY CURED, THE TEMPORARY ANGLES CAN BE UNBOLTED AND REUSED ON OTHER PLATES FOLLOWING THE SAME PROCESS.

TOTAL QUANTITY: 4



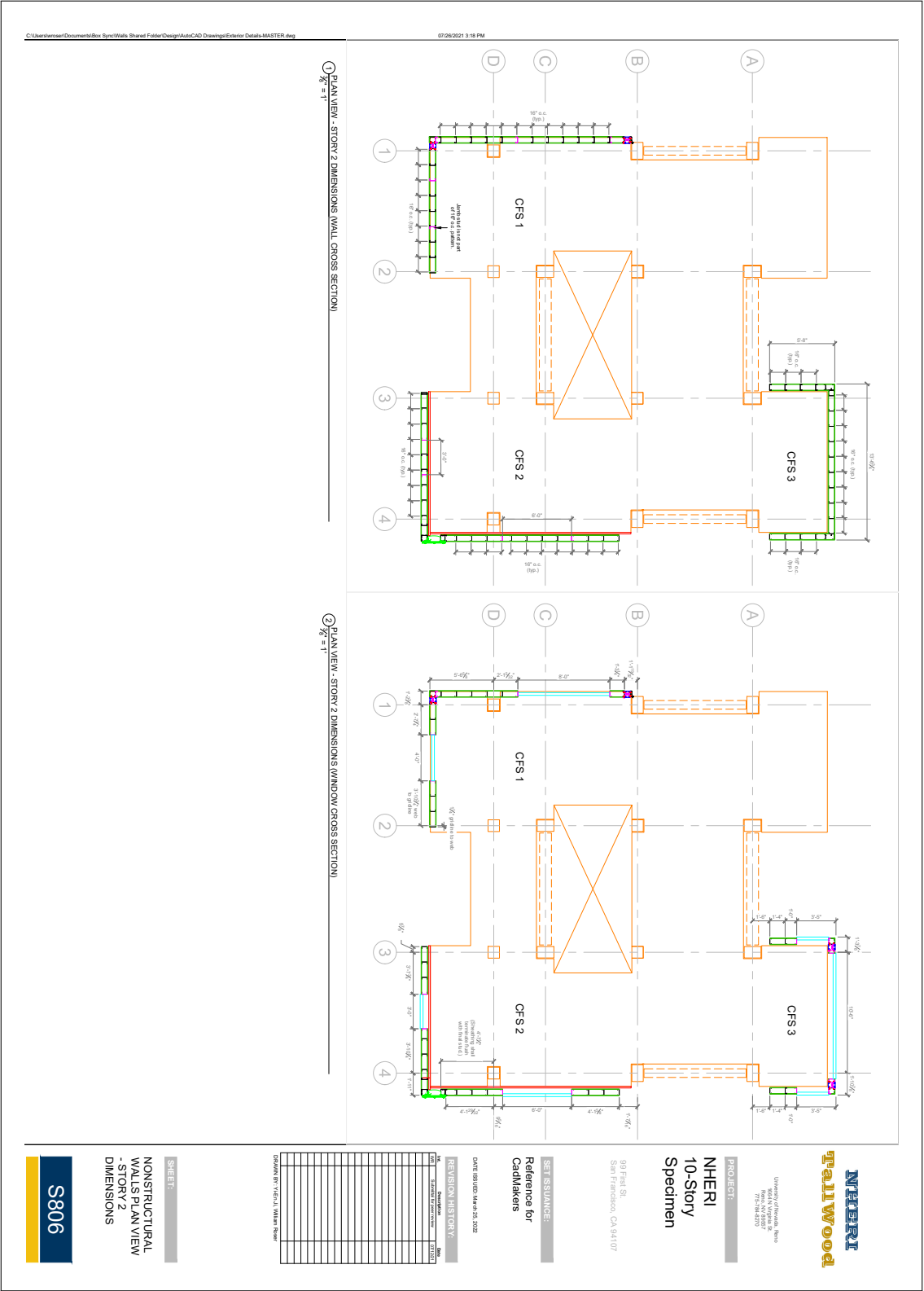
NHERI TallWood
 10-Story Test

No.	Description	Date

MPP 3 Temp. Mounting Angle		S904
Project Number	Project Number	
Date	9/15/2022	
Drawn by	ANB	
Checked by	Checker	Scale 1 1/2" = 1'-0"

Appendix B

NONSTRUCTURAL WALL LOCATION DRAWINGS



C:\Users\mcc\Documents\Box Sync\Walls Sheet\Folder\Design\AutoCAD Drawings\Exterior Details-MASTER.dwg

07/26/2021 3:18 PM

① PLAN VIEW - STORY 2 DIMENSIONS (WALL CROSS SECTION)
Scale: 1/8\"

② PLAN VIEW - STORY 2 DIMENSIONS (WINDOW CROSS SECTION)
Scale: 1/8\"



University of Nevada, Reno
624 S. Virginia St.
Reno, NV 89502
775-784-8770

PROJECT:
**NHERI
10-Story
Specimen**

99 First St.
San Francisco, CA 94107

SET ISSUANCE:
Reference for
CastInlakers

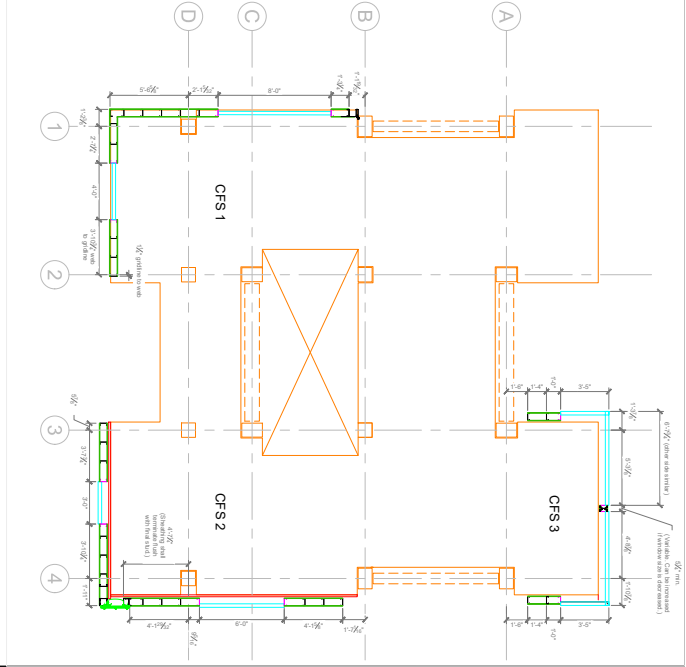
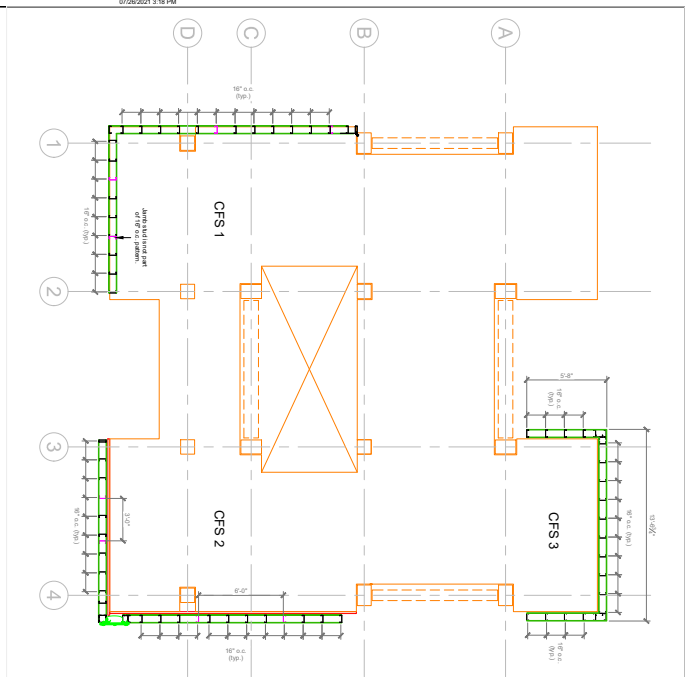
DATE SET ISSUED: 11/14/2018

NO.	DATE	DESCRIPTION	BY
1	11/14/2018	ISSUED FOR SET	WJ
2	11/14/2018	ISSUED FOR SET	WJ
3	11/14/2018	ISSUED FOR SET	WJ
4	11/14/2018	ISSUED FOR SET	WJ
5	11/14/2018	ISSUED FOR SET	WJ
6	11/14/2018	ISSUED FOR SET	WJ
7	11/14/2018	ISSUED FOR SET	WJ
8	11/14/2018	ISSUED FOR SET	WJ
9	11/14/2018	ISSUED FOR SET	WJ
10	11/14/2018	ISSUED FOR SET	WJ
11	11/14/2018	ISSUED FOR SET	WJ
12	11/14/2018	ISSUED FOR SET	WJ
13	11/14/2018	ISSUED FOR SET	WJ
14	11/14/2018	ISSUED FOR SET	WJ
15	11/14/2018	ISSUED FOR SET	WJ
16	11/14/2018	ISSUED FOR SET	WJ
17	11/14/2018	ISSUED FOR SET	WJ
18	11/14/2018	ISSUED FOR SET	WJ
19	11/14/2018	ISSUED FOR SET	WJ
20	11/14/2018	ISSUED FOR SET	WJ
21	11/14/2018	ISSUED FOR SET	WJ
22	11/14/2018	ISSUED FOR SET	WJ
23	11/14/2018	ISSUED FOR SET	WJ
24	11/14/2018	ISSUED FOR SET	WJ
25	11/14/2018	ISSUED FOR SET	WJ
26	11/14/2018	ISSUED FOR SET	WJ
27	11/14/2018	ISSUED FOR SET	WJ
28	11/14/2018	ISSUED FOR SET	WJ
29	11/14/2018	ISSUED FOR SET	WJ
30	11/14/2018	ISSUED FOR SET	WJ
31	11/14/2018	ISSUED FOR SET	WJ
32	11/14/2018	ISSUED FOR SET	WJ
33	11/14/2018	ISSUED FOR SET	WJ
34	11/14/2018	ISSUED FOR SET	WJ
35	11/14/2018	ISSUED FOR SET	WJ
36	11/14/2018	ISSUED FOR SET	WJ
37	11/14/2018	ISSUED FOR SET	WJ
38	11/14/2018	ISSUED FOR SET	WJ
39	11/14/2018	ISSUED FOR SET	WJ
40	11/14/2018	ISSUED FOR SET	WJ
41	11/14/2018	ISSUED FOR SET	WJ
42	11/14/2018	ISSUED FOR SET	WJ
43	11/14/2018	ISSUED FOR SET	WJ
44	11/14/2018	ISSUED FOR SET	WJ
45	11/14/2018	ISSUED FOR SET	WJ
46	11/14/2018	ISSUED FOR SET	WJ
47	11/14/2018	ISSUED FOR SET	WJ
48	11/14/2018	ISSUED FOR SET	WJ
49	11/14/2018	ISSUED FOR SET	WJ
50	11/14/2018	ISSUED FOR SET	WJ

DRAWN BY: TIEBIL WILSON

SHEET:
NONSTRUCTURAL
WALLS PLAN VIEW
- STORY 2
DIMENSIONS

S806



© Usernames\Documents\Box Sync\Walls Sheet Fabric\Design\AutoCAD Drawings\Exterior Details-MASTER.dwg

PROJECT: NHERI 10-Story Specimen
 99 First St.
 San Francisco, CA 94107

SET ISSUANCE: Reference for Castmakers

DATE SET ISSUED: 14-04-2022

NO.	DESCRIPTION	DATE
1	ISSUED FOR REVIEW	12/22/21
2	ISSUED FOR REVIEW	12/22/21
3	ISSUED FOR REVIEW	12/22/21
4	ISSUED FOR REVIEW	12/22/21
5	ISSUED FOR REVIEW	12/22/21
6	ISSUED FOR REVIEW	12/22/21
7	ISSUED FOR REVIEW	12/22/21
8	ISSUED FOR REVIEW	12/22/21
9	ISSUED FOR REVIEW	12/22/21
10	ISSUED FOR REVIEW	12/22/21
11	ISSUED FOR REVIEW	12/22/21
12	ISSUED FOR REVIEW	12/22/21
13	ISSUED FOR REVIEW	12/22/21
14	ISSUED FOR REVIEW	12/22/21
15	ISSUED FOR REVIEW	12/22/21
16	ISSUED FOR REVIEW	12/22/21
17	ISSUED FOR REVIEW	12/22/21
18	ISSUED FOR REVIEW	12/22/21
19	ISSUED FOR REVIEW	12/22/21
20	ISSUED FOR REVIEW	12/22/21
21	ISSUED FOR REVIEW	12/22/21
22	ISSUED FOR REVIEW	12/22/21
23	ISSUED FOR REVIEW	12/22/21
24	ISSUED FOR REVIEW	12/22/21
25	ISSUED FOR REVIEW	12/22/21
26	ISSUED FOR REVIEW	12/22/21
27	ISSUED FOR REVIEW	12/22/21
28	ISSUED FOR REVIEW	12/22/21
29	ISSUED FOR REVIEW	12/22/21
30	ISSUED FOR REVIEW	12/22/21
31	ISSUED FOR REVIEW	12/22/21
32	ISSUED FOR REVIEW	12/22/21
33	ISSUED FOR REVIEW	12/22/21
34	ISSUED FOR REVIEW	12/22/21
35	ISSUED FOR REVIEW	12/22/21
36	ISSUED FOR REVIEW	12/22/21
37	ISSUED FOR REVIEW	12/22/21
38	ISSUED FOR REVIEW	12/22/21
39	ISSUED FOR REVIEW	12/22/21
40	ISSUED FOR REVIEW	12/22/21
41	ISSUED FOR REVIEW	12/22/21
42	ISSUED FOR REVIEW	12/22/21
43	ISSUED FOR REVIEW	12/22/21
44	ISSUED FOR REVIEW	12/22/21
45	ISSUED FOR REVIEW	12/22/21
46	ISSUED FOR REVIEW	12/22/21
47	ISSUED FOR REVIEW	12/22/21
48	ISSUED FOR REVIEW	12/22/21
49	ISSUED FOR REVIEW	12/22/21
50	ISSUED FOR REVIEW	12/22/21
51	ISSUED FOR REVIEW	12/22/21
52	ISSUED FOR REVIEW	12/22/21
53	ISSUED FOR REVIEW	12/22/21
54	ISSUED FOR REVIEW	12/22/21
55	ISSUED FOR REVIEW	12/22/21
56	ISSUED FOR REVIEW	12/22/21
57	ISSUED FOR REVIEW	12/22/21
58	ISSUED FOR REVIEW	12/22/21
59	ISSUED FOR REVIEW	12/22/21
60	ISSUED FOR REVIEW	12/22/21
61	ISSUED FOR REVIEW	12/22/21
62	ISSUED FOR REVIEW	12/22/21
63	ISSUED FOR REVIEW	12/22/21
64	ISSUED FOR REVIEW	12/22/21
65	ISSUED FOR REVIEW	12/22/21
66	ISSUED FOR REVIEW	12/22/21
67	ISSUED FOR REVIEW	12/22/21
68	ISSUED FOR REVIEW	12/22/21
69	ISSUED FOR REVIEW	12/22/21
70	ISSUED FOR REVIEW	12/22/21
71	ISSUED FOR REVIEW	12/22/21
72	ISSUED FOR REVIEW	12/22/21
73	ISSUED FOR REVIEW	12/22/21
74	ISSUED FOR REVIEW	12/22/21
75	ISSUED FOR REVIEW	12/22/21
76	ISSUED FOR REVIEW	12/22/21
77	ISSUED FOR REVIEW	12/22/21
78	ISSUED FOR REVIEW	12/22/21
79	ISSUED FOR REVIEW	12/22/21
80	ISSUED FOR REVIEW	12/22/21
81	ISSUED FOR REVIEW	12/22/21
82	ISSUED FOR REVIEW	12/22/21
83	ISSUED FOR REVIEW	12/22/21
84	ISSUED FOR REVIEW	12/22/21
85	ISSUED FOR REVIEW	12/22/21
86	ISSUED FOR REVIEW	12/22/21
87	ISSUED FOR REVIEW	12/22/21
88	ISSUED FOR REVIEW	12/22/21
89	ISSUED FOR REVIEW	12/22/21
90	ISSUED FOR REVIEW	12/22/21
91	ISSUED FOR REVIEW	12/22/21
92	ISSUED FOR REVIEW	12/22/21
93	ISSUED FOR REVIEW	12/22/21
94	ISSUED FOR REVIEW	12/22/21
95	ISSUED FOR REVIEW	12/22/21
96	ISSUED FOR REVIEW	12/22/21
97	ISSUED FOR REVIEW	12/22/21
98	ISSUED FOR REVIEW	12/22/21
99	ISSUED FOR REVIEW	12/22/21
100	ISSUED FOR REVIEW	12/22/21

DRAWN BY: TIEBIL WILSON

NHERI TallWood
 University of Nevada, Reno
 624 S. Virginia St.
 Reno, NV 89502
 775-784-8770

PROJECT: NHERI 10-Story Specimen

SET ISSUANCE: Reference for Castmakers

DATE SET ISSUED: 14-04-2022

REVISION HISTORY:

NO.	DESCRIPTION	DATE
1	ISSUED FOR REVIEW	12/22/21
2	ISSUED FOR REVIEW	12/22/21
3	ISSUED FOR REVIEW	12/22/21
4	ISSUED FOR REVIEW	12/22/21
5	ISSUED FOR REVIEW	12/22/21
6	ISSUED FOR REVIEW	12/22/21
7	ISSUED FOR REVIEW	12/22/21
8	ISSUED FOR REVIEW	12/22/21
9	ISSUED FOR REVIEW	12/22/21
10	ISSUED FOR REVIEW	12/22/21
11	ISSUED FOR REVIEW	12/22/21
12	ISSUED FOR REVIEW	12/22/21
13	ISSUED FOR REVIEW	12/22/21
14	ISSUED FOR REVIEW	12/22/21
15	ISSUED FOR REVIEW	12/22/21
16	ISSUED FOR REVIEW	12/22/21
17	ISSUED FOR REVIEW	12/22/21
18	ISSUED FOR REVIEW	12/22/21
19	ISSUED FOR REVIEW	12/22/21
20	ISSUED FOR REVIEW	12/22/21
21	ISSUED FOR REVIEW	12/22/21
22	ISSUED FOR REVIEW	12/22/21
23	ISSUED FOR REVIEW	12/22/21
24	ISSUED FOR REVIEW	12/22/21
25	ISSUED FOR REVIEW	12/22/21
26	ISSUED FOR REVIEW	12/22/21
27	ISSUED FOR REVIEW	12/22/21
28	ISSUED FOR REVIEW	12/22/21
29	ISSUED FOR REVIEW	12/22/21
30	ISSUED FOR REVIEW	12/22/21
31	ISSUED FOR REVIEW	12/22/21
32	ISSUED FOR REVIEW	12/22/21
33	ISSUED FOR REVIEW	12/22/21
34	ISSUED FOR REVIEW	12/22/21
35	ISSUED FOR REVIEW	12/22/21
36	ISSUED FOR REVIEW	12/22/21
37	ISSUED FOR REVIEW	12/22/21
38	ISSUED FOR REVIEW	12/22/21
39	ISSUED FOR REVIEW	12/22/21
40	ISSUED FOR REVIEW	12/22/21
41	ISSUED FOR REVIEW	12/22/21
42	ISSUED FOR REVIEW	12/22/21
43	ISSUED FOR REVIEW	12/22/21
44	ISSUED FOR REVIEW	12/22/21
45	ISSUED FOR REVIEW	12/22/21
46	ISSUED FOR REVIEW	12/22/21
47	ISSUED FOR REVIEW	12/22/21
48	ISSUED FOR REVIEW	12/22/21
49	ISSUED FOR REVIEW	12/22/21
50	ISSUED FOR REVIEW	12/22/21
51	ISSUED FOR REVIEW	12/22/21
52	ISSUED FOR REVIEW	12/22/21
53	ISSUED FOR REVIEW	12/22/21
54	ISSUED FOR REVIEW	12/22/21
55	ISSUED FOR REVIEW	12/22/21
56	ISSUED FOR REVIEW	12/22/21
57	ISSUED FOR REVIEW	12/22/21
58	ISSUED FOR REVIEW	12/22/21
59	ISSUED FOR REVIEW	12/22/21
60	ISSUED FOR REVIEW	12/22/21
61	ISSUED FOR REVIEW	12/22/21
62	ISSUED FOR REVIEW	12/22/21
63	ISSUED FOR REVIEW	12/22/21
64	ISSUED FOR REVIEW	12/22/21
65	ISSUED FOR REVIEW	12/22/21
66	ISSUED FOR REVIEW	12/22/21
67	ISSUED FOR REVIEW	12/22/21
68	ISSUED FOR REVIEW	12/22/21
69	ISSUED FOR REVIEW	12/22/21
70	ISSUED FOR REVIEW	12/22/21
71	ISSUED FOR REVIEW	12/22/21
72	ISSUED FOR REVIEW	12/22/21
73	ISSUED FOR REVIEW	12/22/21
74	ISSUED FOR REVIEW	12/22/21
75	ISSUED FOR REVIEW	12/22/21
76	ISSUED FOR REVIEW	12/22/21
77	ISSUED FOR REVIEW	12/22/21
78	ISSUED FOR REVIEW	12/22/21
79	ISSUED FOR REVIEW	12/22/21
80	ISSUED FOR REVIEW	12/22/21
81	ISSUED FOR REVIEW	12/22/21
82	ISSUED FOR REVIEW	12/22/21
83	ISSUED FOR REVIEW	12/22/21
84	ISSUED FOR REVIEW	12/22/21
85	ISSUED FOR REVIEW	12/22/21
86	ISSUED FOR REVIEW	12/22/21
87	ISSUED FOR REVIEW	12/22/21
88	ISSUED FOR REVIEW	12/22/21
89	ISSUED FOR REVIEW	12/22/21
90	ISSUED FOR REVIEW	12/22/21
91	ISSUED FOR REVIEW	12/22/21
92	ISSUED FOR REVIEW	12/22/21
93	ISSUED FOR REVIEW	12/22/21
94	ISSUED FOR REVIEW	12/22/21
95	ISSUED FOR REVIEW	12/22/21
96	ISSUED FOR REVIEW	12/22/21
97	ISSUED FOR REVIEW	12/22/21
98	ISSUED FOR REVIEW	12/22/21
99	ISSUED FOR REVIEW	12/22/21
100	ISSUED FOR REVIEW	12/22/21

DRAWN BY: TIEBIL WILSON

SHEET: NONSTRUCTURAL WALLS PLAN VIEW - STORY 3 DIMENSIONS

S808

Appendix C

45° PLOTS

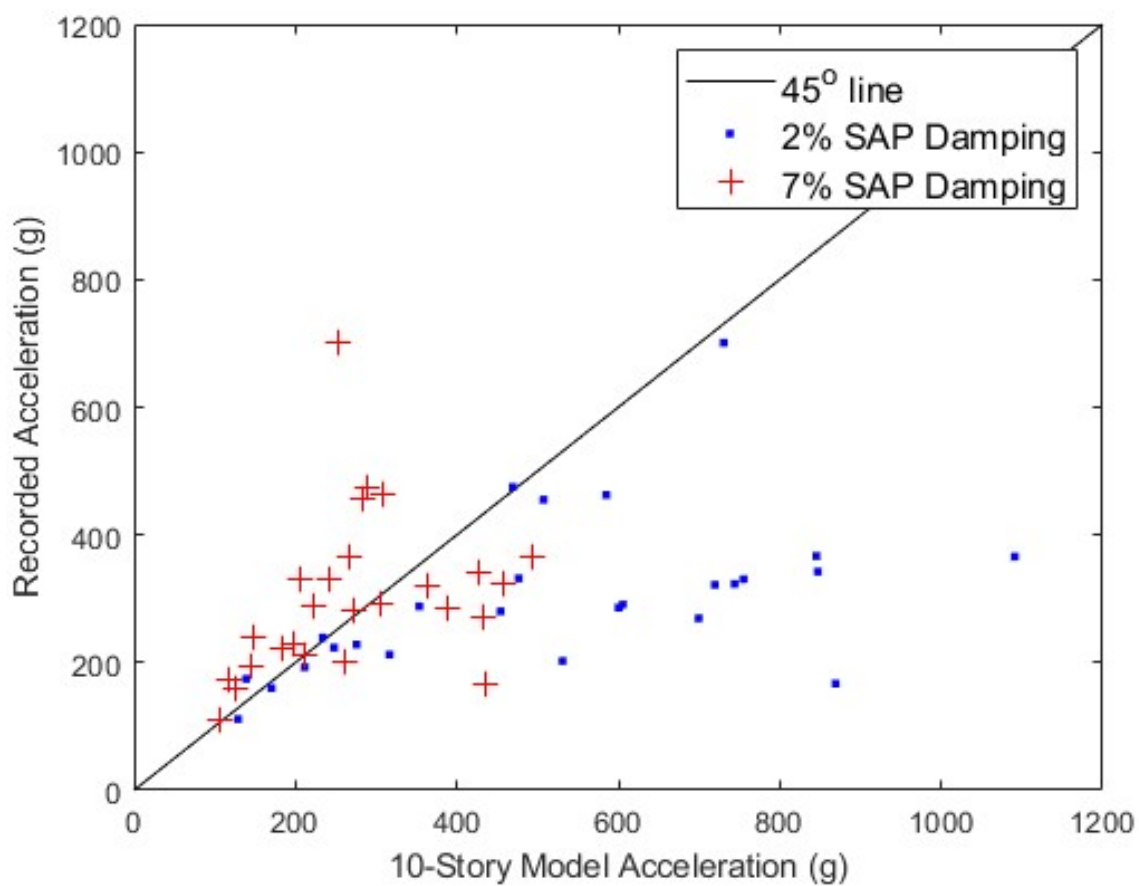


Figure C.1: Peak Acceleration Comparison for Loma Prieta MCE: 10-Story SAP Model vs Measured Data

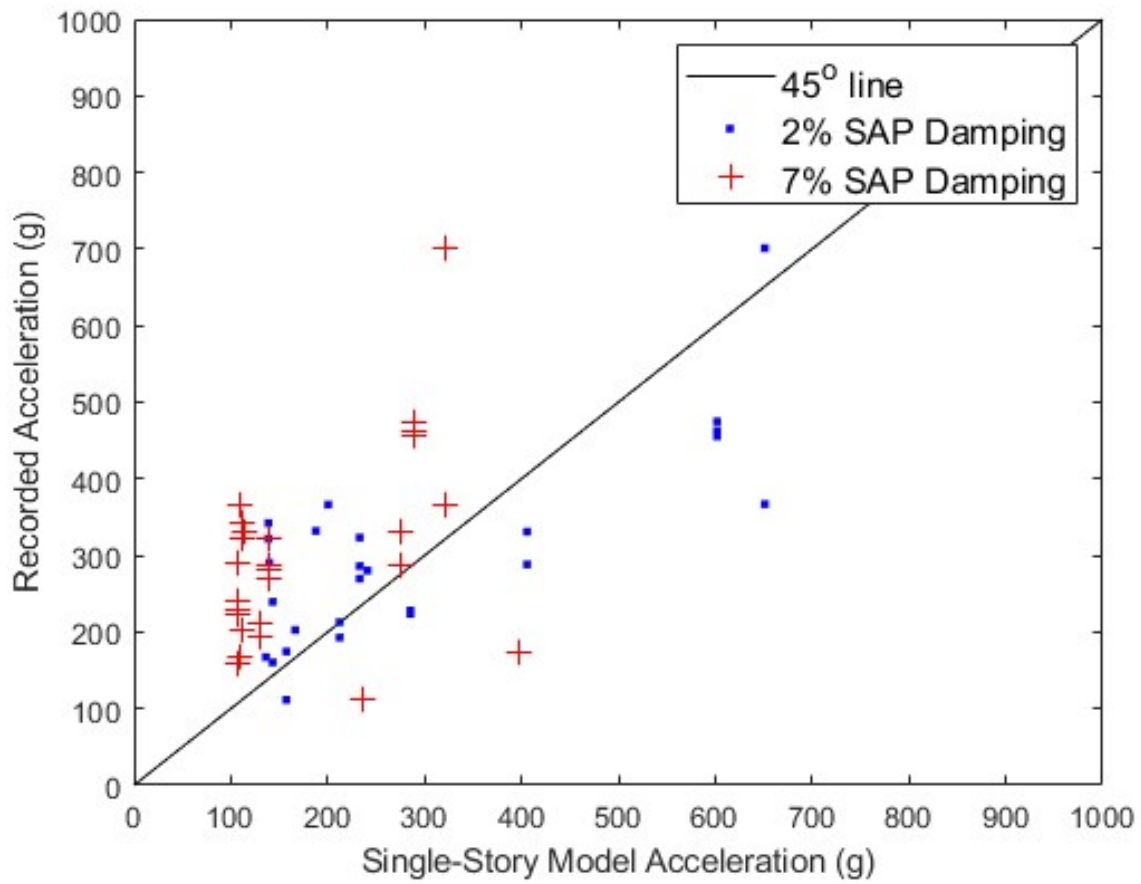


Figure C.2: Peak Acceleration Comparison for Loma Prieta MCE: Single-Story SAP Model vs Measured Data